CHARACTERIZATION OF A ROBOTIC MANIPULATOR FOR DYNAMIC WIND TUNNEL APPLICATIONS

THESIS

James C. Lancaster, Captain, USAF

AFIT-ENY-MS-15-M-227

DEPARTMENT OF THE AIR FORCE
AIR UNIVERSITY

AIR FORCE INSTITUTE OF TECHNOLOGY

Wright-Patterson Air Force Base, Ohio

CHARACTERIZATION OF A ROBOTIC MANIPULATOR

FOR DYNAMIC WIND TUNNEL APPLICATIONS

THESIS

Presented to the Faculty

Department of Aeronautical Engineering

Graduate School of Engineering and Management

Air Force Institute of Technology

Air University

Air Education and Training Command

in Partial Fulfillment of the Requirements for the

Degree of Master of Science in Aeronautical Engineering

James C. Lancaster, B.S.A.E.

Captain, USAF

March 19, 2015

AFIT-ENY-MS-15-M-227

CHARACTERIZATION OF A ROBOTIC MANIPULATOR

FOR DYNAMIC WIND TUNNEL APPLICATIONS

THESIS

James C. Lancaster, B.S.A.E.
Captain, USAF

Committee Membership:

Dr. Mark Reeder
Chair

Dr. Richard Cobb
Member

Dr. Donald Kunz
Member

AFIT-ENY-MS-15-M-227

Abstract

The newly acquired 6-DOF Motion Test Apparatus (MTA) was installed to perform dynamic wind tunnel testing in the AFIT Low Speed Wind Tunnel. Several complex trajectories revealed that the overall performance of the test rig needed improvement especially during small motions. The resultant motion exposed that further enhancements would need to be performed individually for each joint. This research effort focused on the improvement of the MTA wrist roll motor and controller when performing a pitch oscillation. The controller software was improved using angular position feedback. With the properly tuned proportional gain, the new closed-loop system exhibited reduced signal bias up to 95% and reduced amplitude attenuation in some cases up to 10%. The enhanced system was then utilized for wind tunnel experiments along with supporting systems. A secondary position and orientation sensor, an Inertial Measurement Unit (IMU), was used to validate the Euler angle output calculated by the MTA Computer using forward kinematics. Additionally, fast-response pressure transducers were flush-mounted to the wing of the model in order to record aerodynamic data during pitch oscillations. The acquired pressure signals revealed evidence of unsteady vortex shedding. The MTA performed equally well under aerodynamic loads at tunnel speeds of 60 mph, when compared to tests performed with zero freestream velocity.

I dedicate my thesis to my loving wife, who has supported my career and my education throughout our lives together. She has burdened herself with most of the household load while she too actively pursues her advanced degree. Thank you for motivating me when I was worn down. I love you and hope that one day I can show you as much love and support as you have given me.

Acknowledgements

Table of Contents

List of Figures

List of Tables

CHARACTERIZATION OF A ROBOTIC MANIPULATOR

FOR DYNAMIC WIND TUNNEL APPLICATIONS

I. Introduction

1.1 Motivation

Early development and basic research can benefit from dynamic wind tunnel research. The dynamic aspect of the experiment refers to the fact that the Item Under Test (IUT) is intentionally moved in a predictable trajectory while measuring force and moments. One way to perform dynamic wind tunnel experiments is to utilize a robust motion test rig that is capable of replicating actions performed during flight. For example, Micro Air Vehicles (MAVs) require an in-depth understanding of aerodynamic qualities enabling them to be agile and to maintain reliable flying qualities. Much progress has been made towards understanding unsteady aerodynamic phenomenons of biological fliers for bio-inspired MAVs. There have been advances in computational methods and numerical modeling, but these advances alone do not yet fully characterize Micro Air Vehicles. Experimental investigations are still a necessary element of MAV design.
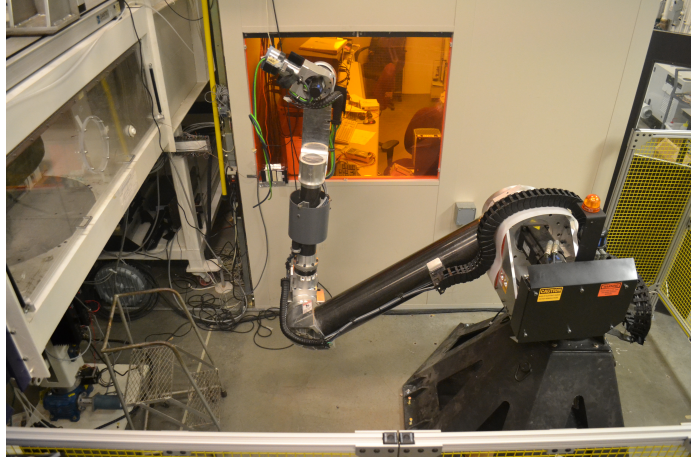
Figure 1. MTA setup perpendicular to the AFIT Low Speed Wind Tunnel.

Combining a new 6-DOF Motion Test Apparatus (MTA) in conjunction with the AFIT Low Speed Wind Tunnel, shown in Figure 1, will enable a broad range of aerodynamic experiments to be conducted. These experiments encompass basic research of unsteady aerodynamics, store separation, study of MAV dynamics in the presence of wind gusts and ground effects, "flexible weapon" development, and many other possibilities. The envisioned flexible weapon system presents challenges to the traditional required wind tunnel tests [22]. Basic research has been aimed at decreasing the burden of testing through intelligent application of Design of Experiments (DOE). Analysis such as simulation, stability and control, and performance estimations require wind tunnel generated maps of aerodynamic loads data. The various configurations of the Flexible Weapon greatly increase the workload and cost of performing wind tunnel testing. The 6-DOF MTA will be used to create a map of the DOE for a given model. The generated maps will then be used to schedule gains and control behaviors. In turn, the wind tunnel models will have servo-controlled surfaces with control systems in-the-loop. Using surrogate mapping techniques developed at the University of Florida-Research and Engineering Education Faciility (REEF), the resulting effectiveness of the model's controllability will be assessed. Furthermore,

these techniques can apply to the design of MAVs through wind tunnel flight testing using closed-loop control.

The first phase of this endeavor required the installation and characterization of the MTA and supporting systems in the AFIT Low Speed Wind Tunnel. Additionally, the MTA was found to require improvements, including implementation of a position feedback controller. This research project also used a pitch oscillation about the quarter-chord of a low aspect ratio, NACA-0012 wing to observe and enhance the capabilities of the MTA wrist roll motor and controller. An Inertial Measurement Unit (IMU) independently measured IUT orientation and was utilized to compare to the MTA encoder output. Preliminary unsteady aerodynamic data was collected using pressure transducers and a data acquisition system.

1.2 Problem Statement

The overarching goal of the project was to install and characterize the MTA. Since the apparatus was originally design for the UF-REEF Aerodynamic Characterization Facility (ACF), careful consideration was given to placement and installation of the MTA relative to the AFIT Low Speed Wind Tunnel. The MTA performance was assessed by commanding complex trajectories, such as a pitch-plunge of a wing and an arc within the horizontal plane mimicking a store separation. While the motions were, by and large, close to the commanded input, significant position and orientation errors were encountered. In order to perform more complex motions, the performance and limitations of the MTA needed to be characterized. The goal of this research was simplified to analyze a kinematic motion that only required a single-Degree-of-Freedom (DOF) and a single joint to execute. The problem statement of this thesis is as follows:

*Quantify the performance of the MTA wrist roll motor and controller us-
ing a pitch oscillation (single-DOF motion). Implement feedback con-
trol, if needed, to enhance the performance of the wrist roll motor/con-
troller. Quantify the performance of the new closed-loop system using
both the MTA's Cartesian position output and a secondary, independent
position/orientation sensor. Finally collect limited unsteady aerodynamic
data for dynamic wind tunnel experiments using a pitch oscillation.*

1.3   Document Organization

The remainder of this thesis is organized in following manner. *Chapter II* dis-
cusses: *i.*) the reference frames and coordinate transformations used with the MTA
and wind tunnel; *ii.*) the robotic kinematics necessary to understand how the 6-DOF
motion test rig is applied to position the model; *iii.*) background information and
studies performed in dynamic wind tunnel testing; *iv.*) the general operation of pres-
sure transducers and IMU devices; *v.*) procedures for characterizing and controlling
a nonlinear system.

Chapter III details: *i.*) the design, operation, and control system specifications of
the MTA; *ii.*) the installation and adjustments made for integrating the MTA with
the AFIT Low Speed Wind Tunnel; *iii.*) the methodology of experiments conducted
to evaluate and improve the MTA wrist roll motor and controller; *iv.*) the specific
data acquisition system and senors used as well as the design of the model and sting,
and the setup and measurement of aerodynamic forces during dynamic testing.

Chapter IV entails the results from: *i.*) determining the number of outputs aver-
aged to achieve a stationary process; *ii.*) characterizing the MTA's wrist roll motor
and controller's, open loop system, performance; *iii.*) tuning the proportional gain
for position feedback; *iv.*) characterizing the closed-loop system's performance; *v.*)
IMU's validation of the MTA's calculated Euler angles; *vi.*) conducting dynamic wind
tunnel experiments to study the pressure signals from a pitch oscillation at various
amplitudes and evaluate the performance of the IMU and MTA under aerodynamic

loads.

Finally, *Chapter V* discusses the conclusions about: *i.*) the performance and limitations of the open and closed-loop MTA wrist roll system; *ii.*) the performance and limitations of the IMU and pressure transducers; *iii.*) future work necessary for the advancement of this research effort.

II. Background

This chapter presents an overview of the reference frames and coordinate transformations necessary for dynamic wind tunnel experiments. It also details the kinematics necessary to describe the motion of the robotic manipulator. A brief background covers the extensive literature on dynamic wind tunnel testing and unsteady aerodynamics. Finally systems specific to data acquisition and control of the AFIT MTA are presented.

2.1 Reference Frames

There are four important reference frames, shown in Figure 2, used when discussing dynamic wind tunnel testing with a robotic manipulator. In Section **??**, seven more reference frames are associated with each DOF of the MTA and will only be used to kinematic transformations. Each reference frame is necessary to describe kinematic motion with respect to either the velocity, body, MTA's control point, or MTA's fixed frame. First is the wind reference frame which is subscripted with a "w." This reference frame is centered in the test section of the wind tunnel with z_w down, x_w in the direction of model's instantaneous velocity, and y_w out the far side of the tunnel. For most wind tunnel testing the wind axes are fixed for all time.
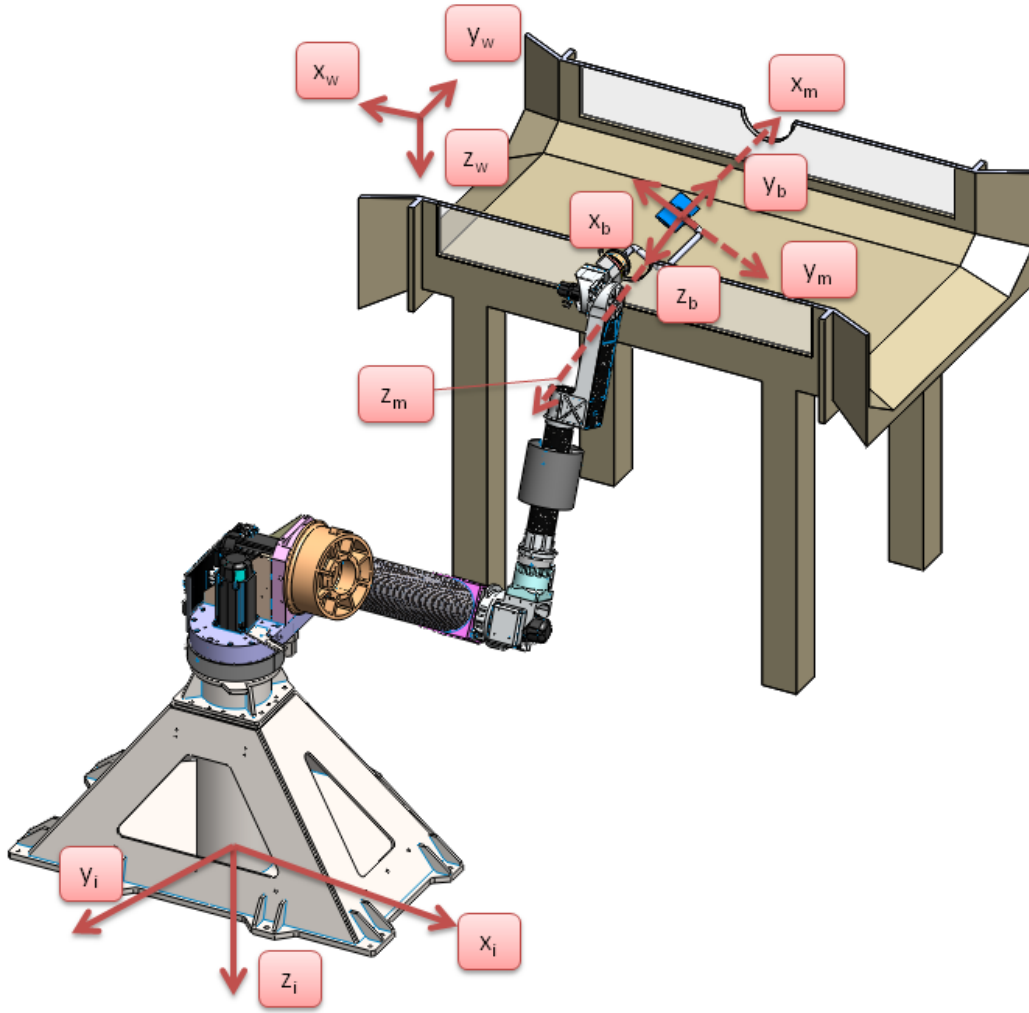
Figure 2. The sectioned view of the wind tunnel reveals the four reference frames of the system

The body-fixed reference frame, subscripted with "b," is centered at a reference point on the IUT. In many situations, including most situations described herein, this reference point corresponds to the quarter-chord of the model's wing. It is oriented similarly to the wind reference frame: z_b down, x_b pointing out the front, and y_b out the right wing.

Coincident to the body-fixed frame is the MTA-model reference frame, subscripted

with "m." This system's origin is referred to as the model control point and is the point about which the trajectories are executed. The MTA-model reference frame is fixed to the body as well, but is rotated 90° about the z_b-axis.

Finally the MTA has an "inertial" reference frame centered under the torso yaw joint, on the floor, at the base of the manipulator, usually referred to with the subscript "i." This coordinate system is referred to as the "inertial frame" because for the purposes of dynamic wind tunnel testing with the MTA, it is fixed for all time. Trajectory files are written to describe the motion of the model with respect to the MTA-inertial reference frame.

2.2   Coordinate Transformations
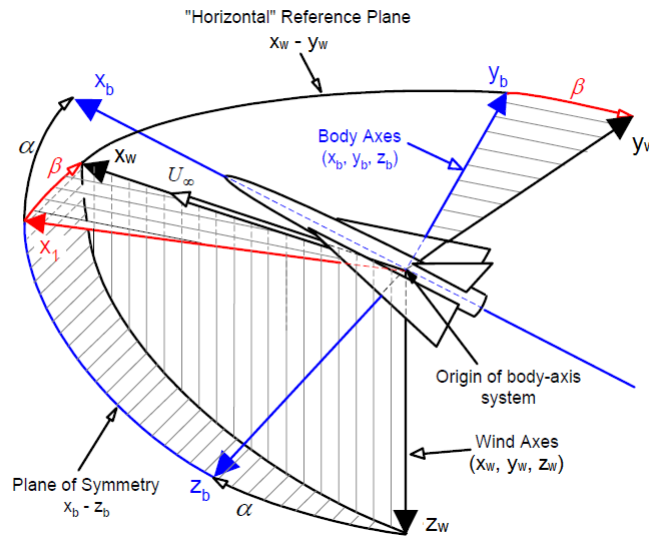
Figure 3. Orientation of the model's body-fixed reference frame with respect to the wind reference frame for flight. [18]

Two aerodynamic angles, angle of attack (α) and sideslip (β), specify the orientation of the model with respect to the freestream velocity. As in the generic representation shown in Figure 3, the angle of attack and sideslip are measured from the projection of the x_w axis onto the x_b-z_b plane. Angle of attack is the angle between

the freestream velocity (U_∞) and x_b. Sideslip is the angle between the projection of x_b onto the x_w-y_w plane and the freestream velocity. It should also be noted that in wind tunnel testing, the freestream velocity is oriented in the opposite direction of Figure 3. The freestream velocity moving towards the model is referred to as the relative wind as opposed to the latter which is referred to as the body's forward velocity. These two concepts can be interchanged between flight and wind tunnel experiments. For the analysis in this thesis, the force and moments will be discussed with respect to the body-fixed reference frame. However, when it becomes necessary to express the forces and moments with respect to the wind axes system, the following transformation is used:

$$
\begin{bmatrix} F_x \\ F_y \\ F_z \end{bmatrix}_w = \begin{bmatrix} \cos\alpha\cos\beta & -\cos\alpha\sin\beta & -\sin\alpha \\ \sin\beta & \cos\beta & 0 \\ \sin\alpha\cos\beta & -\sin\alpha\sin\beta & \cos\alpha \end{bmatrix} \begin{bmatrix} F_x \\ F_y \\ F_z \end{bmatrix}_b
\tag{1}
$$

The transformation in equation (1) is valid for any vector (linear or angular velocity) expressed in the body-fixed axes system. The model's rotations about the x_b, y_b, and z_b axes are referred to as roll, pitch, and yaw, respectively. Three Euler angles describing the orientation of the model as it rotates are: ϕ (x_b), θ (y_b), and ψ (z_b). It is important to note that this naming convention applies to other reference frames described above. For trajectory files the position and orientation of the model are declared with respect to the MTA-inertial reference frame. The rotation between the MTA-inertial and MTA-model reference frames follows a standard 3-2-1 rotation scheme. However the pertinent information for dynamic wind tunnel testing is typically reported with respect to the body or wind axes systems. In order to express the coordinates from MTA-inertial reference frame as body-fixed coordinates, the first transformation must be from the MTA-inertial reference frame to MTA-model ref-

9

erence frame. The position and orientation of the MTA-model coordinate system, subscript "m", with respect to the MTA-inertial coordinate system, subscript "i", must be determined. At each time step in the trajectory or output file, this offset must be removed. Once the two coordinate systems are coincident and their axes are collinear, the Cartesian positions are transformed from the MTA-model reference frame to the body-fixed reference frame, subscript "b", using equation (2).

$$
\begin{bmatrix} x \\ y \\ z \\ \phi \\ \theta \\ \psi \end{bmatrix}_b = \begin{bmatrix} 0 & -1 & 0 & 0 & 0 & 0 \\ 1 & 0 & 0 & 0 & 0 & 0 \\ 0 & 0 & 1 & 0 & 0 & 0 \\ 0 & 0 & 0 & 0 & -1 & 0 \\ 0 & 0 & 0 & -1 & 0 & 0 \\ 0 & 0 & 0 & 0 & 0 & 1 \end{bmatrix}^{-1} \begin{bmatrix} x \\ y \\ z \\ \phi \\ \theta \\ \psi \end{bmatrix}_m
\tag{2}
$$

2.3 Robot Kinematics

A 6-state Cartesian position (x, y, z, ϕ, θ, and ψ), used in the MTA trajectory file, describes the location of the MTA-model reference frame relative to the MTA-inertial reference frame. Using forward kinematics, the model's Cartesian position can be calculated from the six MTA joint angles and the model's offset. The model's offset is the distance between the model's control point and the center of the end of the MTA. Similarly, using inverse kinematics the model's Cartesian position can be transformed into the six joint angles for the MTA. The methods of solving the forward and inverse kinematics, described below, were utilized by the manufacturer of the MTA, RE2, Inc [31]. To effectively operate the MTA, it is important to understand the procedures used to determine model position and joint angles. This section describes in detail the math involved with the forward and inverse kinematics specific to the MTA.

10

Kinematics Reference Frames and Notation.

The six-joints angles are torso yaw (θ_{tr}), shoulder pitch (θ_{sp}), elbow pitch (θ_{ep}), elbow roll (θ_{er}), wrist pitch (θ_{wp}), and wrist roll (θ_{wr}). Figure 4 shows the physical location of each coordinate system that is used in the kinematic transformations. Reference frame 0, seen in Figure 4, is the MTA-inertial reference frame. Reference frames 1 and 2 lie on the axis of rotation for the torso yaw and shoulder pitch degrees-of-freedom respectively. Continuing to the end of the first link, reference frame 3 lies on the axis of rotation for the elbow pitch degree-of-freedom. The fourth reference frame lies on the axis of rotation of the elbow roll. At the end of the second link lies the fifth reference frame on the wrist pitch axis of rotation. At the end of link 3, reference frame 6 lies on the axis of rotation of the wrist roll. Finally the origin of the seventh reference frame is coincident with the model offset, which can be relocated per experiment. Reference frame 7 is also known as the MTA-model reference frame.
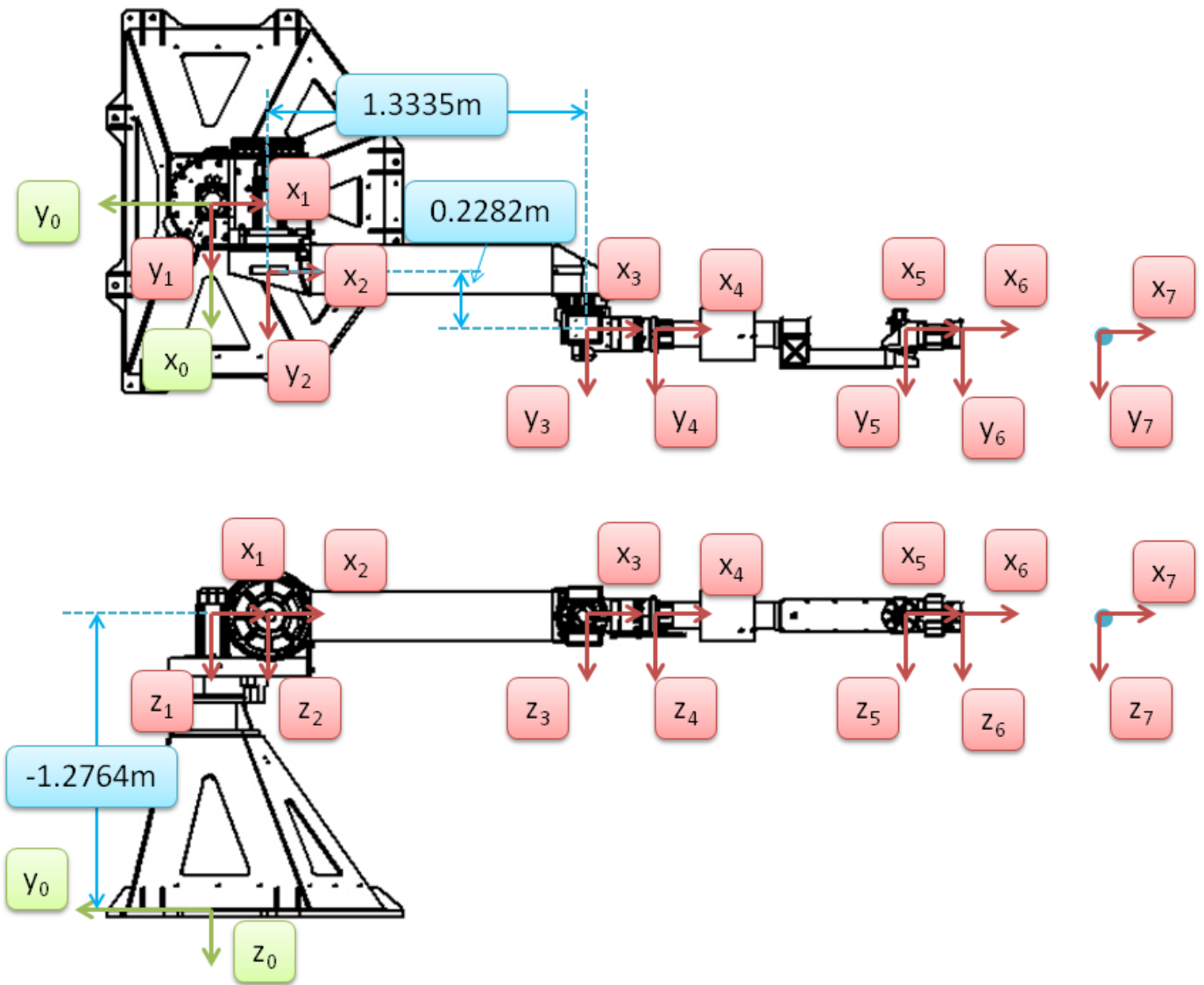
Figure 4. The reference frames labeled 0–7 necessary for robotic kinematics. The blue sphere represents the model's control point. All angles are zero as shown in the diagram. Examples of distances between reference frames are shown; adapted from [31].

Forward Kinematics.

Equations (3)–(9) are the seven rotation/position matrices required for the homogeneous transform between the MTA-inertial frame (Ref. frame 0) and the MTA-model frame (Ref. frame 7). For the purposes of the forward and inverse kinematic calculations all links are assumed to be infinitely stiff. The units applicable to these equations are degrees for the first three columns and meters for the fourth column. The first 3-by-3 matrix in each equation is the necessary rotation about the respective axis aligning the k-coordinate system with the $(k+1)$-coordinate system. Positive rotation is defined by right-hand rule and the angle is between the k-reference frame and the $(k+1)$-reference frame. For example the shoulder pitch angle, θ_{sp}, is the angle between the x_1 and x_2 axes. Therefore if the link between reference frames 2 and 3 is pointing down, by the right-hand rule, the shoulder pitch angle is negative. The additional fourth row and column describes the translation to move the k-coordinate system coincident to the $(k+1)$-coordinate system. The vector in the fourth column being transformed is $[x, y, z, 1]_{k+1}^T$, which is the location of reference frame $k+1$ with respect to the k reference frame. For example, using Figure 4 and equation (3), reference frame 1 is 1.2764 m directly above the origin of reference frame 0. The fourth row is always $[0, 0, 0, 1]$ in order to maintain a square matrix. These values are specific to the AFIT MTA and are displayed with the same significant figures used for the kinematics in the source code.

$$
{}_1^0T = \begin{bmatrix} \cos(\theta_{tr} - 90°) & -\sin(\theta_{tr} - 90°) & 0 & 0 \\ \sin(\theta_{tr} - 90°) & -\cos(\theta_{tr} - 90°) & 0 & 0 \\ 0 & 0 & 1 & -1.2764 \\ 0 & 0 & 0 & 1 \end{bmatrix} \tag{3}
$$

$$
{}_2^1T = \begin{bmatrix} \cos(\theta_{sp}) & 0 & \sin(\theta_{sp}) & 0.2413 \\ 0 & 1 & 0 & 0.2539 \\ -\sin(\theta_{sp}) & 0 & \cos(\theta_{sp}) & 0 \\ 0 & 0 & 0 & 1 \end{bmatrix} \tag{4}
$$

$$
{}_3^2T = \begin{bmatrix} \cos(\theta_{ep}) & 0 & \sin(\theta_{ep}) & 1.3335 \\ 0 & 1 & 0 & 0.2282 \\ -\sin(\theta_{ep}) & 0 & \cos(\theta_{ep} & 0 \\ 0 & 0 & 0 & 1 \end{bmatrix} \tag{5}
$$

$$
{}_4^3T = \begin{bmatrix} 1 & 0 & 0 & 0.2889 \\ 0 & \cos(\theta_{er}) & -\sin(\theta_{er}) & 0 \\ 0 & \sin(\theta_{er}) & \cos(\theta_{er}) & 0 \\ 0 & 0 & 0 & 1 \end{bmatrix} \tag{6}
$$

$$
{}_5^4T = \begin{bmatrix} \cos(\theta_{wp}) & 0 & \sin(\theta_{wp})1.0572 \\ 0 & 1 & 0 & 0 \\ -\sin(\theta_{wp}) & 0 & \cos(\theta_{wp}) & 0 \\ 0 & 0 & 0 & 1 \end{bmatrix} \tag{7}
$$

$$
{}_6^5T = \begin{bmatrix} 1 & 0 & 0 & 0.2683 \\ 0 & \cos(\theta_{wr}) & -\sin(\theta_{wr}) & 0 \\ 0 & \sin(\theta_{wr}) & \cos(\theta_{wr}) & 0 \\ 0 & 0 & 0 & 1 \end{bmatrix} \tag{8}
$$

$$
{}_7^6T = \begin{bmatrix} 1 & 0 & 0 & model_x \\ 0 & 1 & 0 & model_y \\ 0 & 0 & 1 & model_z \\ 0 & 0 & 0 & 1 \end{bmatrix} \tag{9}
$$

The multiplication of the seven matrices together, equation (10), computes the model's position and orientation, otherwise known as the MTA-model coordinate system, relative to the MTA-inertial reference frame [31]. The model's x-y-z location, found in equation (9), must be specified by the user prior to operation.

$$
{}^0_7T = {}^0_1T * {}^1_2T * {}^2_3T * {}^3_4T * {}^4_5T * {}^5_6T * {}^6_7T \tag{10}
$$

In practice it is more advantageous to specify the values of the model's Cartesian coordinates (x, y, z) and the orientation in the wind tunnel (ϕ_m, θ_m, ψ_m). The MTA designer, Re2 Inc., provided the means to compute the respective joint angles using inverse kinematics.

Inverse Kinematics.

In order to transform the Cartesian position, or location of reference frame 7 with respect to reference frame 0, back to the six joint angles, equation (11) converts each Cartesian position into a homogeneous transform. Here, ϕ, θ, and ψ are between the MTA-model reference frame and the MTA-inertial reference frame. However, there can be more than one closed-form solution due to the multiple degrees-of-freedom of the MTA. For example, some solutions can be solved with the elbow pitched up or rather pitched down. For safety the elbow down solution was set within the source code, when possible, to compute the remaining angles.

$$
{}^0_7T = \begin{bmatrix}
\cos\psi\cos\theta & \cos\psi\sin\theta\sin\phi - \sin\psi\cos\phi & \cos\psi\sin\theta\cos\phi + \sin\psi\sin\phi & x \\
\sin\psi\cos\theta & \sin\psi\sin\theta\sin\phi + \cos\psi\cos\phi & \sin\psi\sin\theta\cos\phi - \cos\psi\sin\phi & y \\
-\sin\theta & \cos\theta\sin\phi & \cos\theta\cos\phi & z \\
0 & 0 & 0 & 1
\end{bmatrix} \tag{11}
$$

15

First the model offsets and translational component of the transformation between the wrist pitch (Ref frame 5) and the wrist roll (Ref frame 6) are separated. Equation (12) shows how $_6^5T$ is separated into its rotational ($_{5'}^5R$) and translational ($_6^{5'}P$) portions. Reference frame 5' corresponds to a reference frame with the same orientation as the wrist roll reference frame (Ref. frame 6) but located at the wrist pitch origin (Ref frame 5).

$$_6^5T = {}_{5'}^5R *{}_6^{5'}P = \begin{bmatrix} 1 & 0 & 0 & 0 \\ 0 & \cos(\theta_{wr}) & -\sin(\theta_{wr}) & 0 \\ 0 & \sin(\theta_{wr}) & \cos(\theta_{wr}) & 0 \\ 0 & 0 & 0 & 1 \end{bmatrix} \begin{bmatrix} 1 & 0 & 0 & 0.2683 \\ 0 & 1 & 0 & 0 \\ 0 & 0 & 1 & 0 \\ 0 & 0 & 0 & 1 \end{bmatrix} \tag{12}$$

In equation (10), $_6^5T$ is replaced with $(_{5'}^5R *_6^{5'}P)$, creating equation (13). Multiplying both sides by the inverse of $_7^6T$ and $_6^{5'}P$ results in equation (14). Since the model offset and the distance between the wrist pitch reference frame and the wrist roll reference frame are fixed for all time, equation (14) places the model at the origin of the wrist pitch reference frame but maintains its orientation.

$$_7^0T = {}_1^0T *{}_2^1T *{}_3^2T *{}_4^3T *{}_5^4T * ({}_{5'}^5R *{}_6^{5'}P) *{}_7^6T \tag{13}$$

$$_5^0T' = {}_1^0T *{}_2^1T *{}_3^2T *{}_4^3T *{}_5^4T *{}_{5'}^5R \tag{14}$$

The $_5^0T'$ accounts for the homogeneous transformation representing the wrist pitch reference frame (Ref. frame 5) at the final prescribed orientation of the model. Pieper proved that if three consecutive joint axes are intersecting, there is a closed-form solution to the inverse kinematics [38]. Re2 Inc. employed Pieper's solution for inverse kinematics to solve for a closed-form solution [31].

For the MTA the elbow roll, wrist pitch, and wrist roll (Ref. frames 4, 5, and 6

respectively) have intersecting axes and can be solved using the model's orientation. The other three joints, torso yaw, shoulder pitch, and elbow pitch (Ref. frames 1, 2, and 3 respectively), are computed using the model's position. Because the shoulder pitch reference frame is offset in both the x and y-directions from the torso reference frame, shown in Figure 5, the geometry of the first two links must be considered.
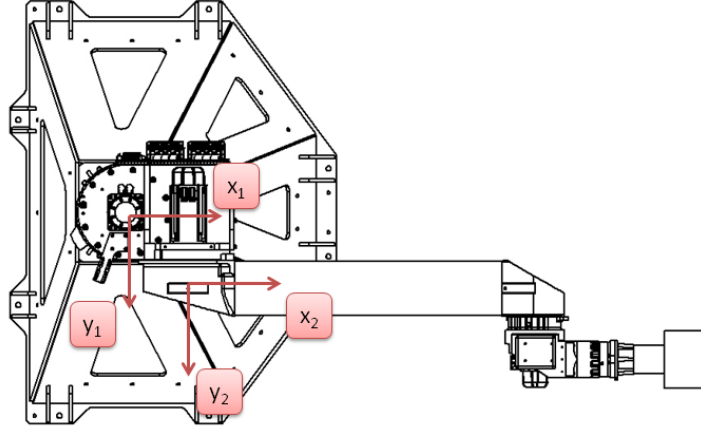
Figure 5. Reference frame 2 is offset in both the x and y-direction from reference frame 1.

Torso Yaw, Shoulder Pitch, and Elbow Pitch Angles.

Figure 6 shows a representation of the three joints: torso yaw (Ref frame 1), shoulder pitch (Ref frame 2), and wrist pitch (Ref frame 5). Elbow pitch is not shown; however, the length of side b is determined by the combination of the shoulder pitch and elbow pitch angles. Length a in equation (15) is the hypotenuse of the triangle with sides corresponding to the x-distance between the torso yaw joint origin and the shoulder pitch joint origin. The y-distance of this triangle is the distance between the torso yaw joint origin and the wrist pitch joint origin. The y-distance is determined by assuming that the wrist pitch x-axis is now collinear with the x-axis of the shoulder pitch joint. In reality the x-axes are not in line in order to give the elbow pitch more

17

mobility. However, this shift does not effect the inverse kinematics.
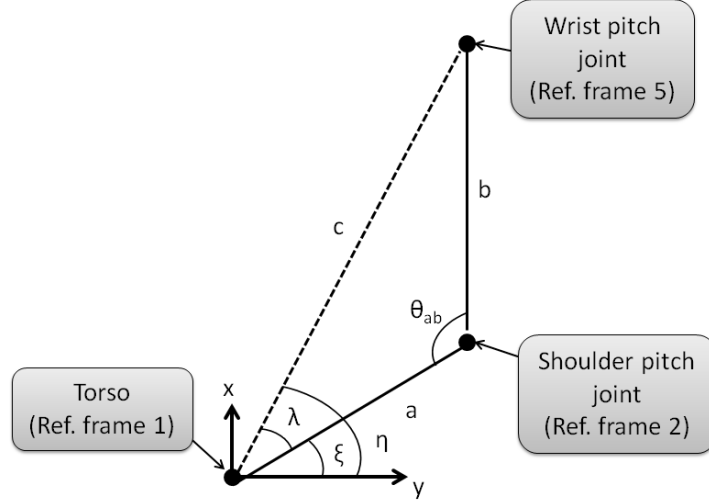
Figure 6. This drawing depicts the geometry of the torso-shoulder-wrist pitch system.

$$a = \sqrt{0.2413^2 + (0.2539 + 0.2282)^2} = 0.5391 \tag{15}$$

$$x_{wp} = x_m - (model_x + 0.2683)$$
$$\tag{16}$$
$$y_{wp} = y_m - model_y$$

$$c = \sqrt{x_{wp}^2 + y_{wp}^2} \tag{17}$$

The length c is calculated using the x and y-location of the wrist pitch which is calculated using equation (16), where $0.2683\,\mathrm{m}$ is the x-distance between the wrist pitch origin and the wrist roll origin. The obtuse angle (θ_{ab}) of the triangle a-b-c is calculated using the supplemental angle relationship shown in equation (18). The law of cosines, equation (19), is rearranged to determine b. Equation (20) has known coefficients and is solved using the quadratic formula, equation (21). Since the *-b* solution is always outside the limitations of the MTA, only the positive solution is calculated.

18

$$\theta_{ab} = 180° - \tan^{-1}\left(\frac{0.2539 + 0.282}{0.2413}\right) = 116.589° \tag{18}$$

$$c^2 = a^2 + b^2 - 2ab\cos(\theta_{ab}) \tag{19}$$

$$b^2 + (2a\cos(\theta_{ab}))b + (a^2 - c^2) = 0 \tag{20}$$

$$b = \frac{-(2a\cos(\theta_{ab})) + \sqrt{4a^2\cos(\theta_{ab})^2 - 4(a^2 - c^2)}}{2} \tag{21}$$

Prior to finding the joint angles for the torso yaw, shoulder pitch, and elbow pitch, the angles between the origins (η, ξ, and λ) must be calculated. Using trigonometry, the three geometric angles are computed in equations (22), (23), and (24). The right triangle with hypotenuse a and angle ξ are used to calculate the position of the shoulder pitch joint with respect to the torso.

$$\eta = \tan^{-1}\left(\frac{y_{wp}}{x_{wp}}\right) \tag{22}$$

$$\lambda = \cos^{-1}\left(\frac{a^2 + c^2 - b^2}{2ac}\right) \tag{23}$$

$$\xi = \eta - \lambda \tag{24}$$

$$x_{sp} = a\cos(\xi)$$
$$\tag{25}$$
$$y_{sp} = a\sin(\xi)$$

Finally the torso yaw angle can be calculated using the angle between b and the x-axis using equation (26).

$$\theta_{tr} = -\tan^{-1}\left(\frac{y_{sp} - y_{wp}}{x_{sp} - x_{wp}}\right) \tag{26}$$

Next the shoulder pitch and elbow pitch angles are calculated using inverse kinematics for a 2-DOF, two-dimensional robotic manipulator [31]. The z-offset between

19

the inertial frame and the shoulder pitch frame is removed from $^0_5T'$. The matrix subtracted is a four-by-four matrix with zeros in all the elements except for the distance, 1.2764 m, in the (3,4) element. The elbow pitch angle is calculated using equation (27), where $L_1 = 1.3335$ and $L_2 = (0.2889 + 1.0572)$.

$$\theta_{ep} = \cos^{-1}\left(\frac{b^2 + z_{sp}^2 + L_1^2 + L_2^2}{2L_1L_2}\right) \tag{27}$$

Since the inverse cosine function results in both a positive and negative solution, both solutions are tracked. The positive solution is used because it represents the elbow down solution. However, there are possible scenarios where the elbow up solution is optimal. For example, if the model was located near the floor close to the MTA, then the elbow down solution would violate the shoulder pitch limits because it would result in the elbow impacting the base. Therefore the elbow up (or negative) solution must be used. Next the shoulder pitch angle is found using equation (28).

$$\theta_{sp} = -\tan^{-1}\left(\frac{-z_{wp}}{b}\right) - \tan^{-1}\left(\frac{L_2\sin(\theta_{ep})}{L_1 + L_2\cos(\theta_{ep})}\right) \tag{28}$$

Elbow Roll and Wrist Angles.

Calculating the torso yaw, shoulder pitch, and elbow pitch angles satisfies the position of the model and the final three joint angles can be computed. The elbow roll, wrist pitch, and wrist roll are used to properly orient the model. The three evaluated angles (θ_{tr}, θ_{sp}, and θ_{ep}) are inserted into equations (3), (4), and (5) solving for ^0_3T. The $^0_5T'$ transformation is condensed as follows:

$$^3_5T' = {}^0_3T^{-1} * {}^0_5T' \tag{29}$$

There are three variables remaining in $^3_5T'$, θ_{er}, θ_{wp}, and θ_{wr}. Using the elements

(e) of $^3_5T'$, the wrist pitch angle is calculated with equation (30).

$$\theta_{wp} = -\tan^{-1}\left(\frac{-\sqrt{e^2_{(2,1)} + e^2_{(3,1)}}}{e_{(1,1)}}\right) \tag{30}$$

If the wrist pitch angle is equal to zero, then the elbow roll is set to zero and the wrist roll angle is calculated as follows:

$$\theta_{wr} = \tan^{-1}\left(\frac{e_{(2,3)}}{-e_{(2,2)}}\right) \tag{31}$$

However, if the wrist pitch is not equal to zero, the two angles are determined using equations (32) and (33).

$$\theta_{er} = \tan^{-1}\left(\frac{e_{(2,1)}/\sin(\theta_{wp})}{-e_{(3,1)}/\sin(\theta_{wp})}\right) \tag{32}$$

$$\theta_{wr} = \tan^{-1}\left(\frac{e_{(1,2)}/\sin(\theta_{wp})}{e_{(1,3)}/\sin(\theta_{wp})}\right) \tag{33}$$

Now that the forward and reverse kinematics have been established, the model's Cartesian position can be calculated by the six joint angles and vice-versa. This allows the user to conduct dynamic wind tunnel experiments by describing the model's movement using the six joint angles as a function of time.

2.4 Dynamic Wind Tunnel Testing

Dynamic wind tunnel testing involves the measurement of forces and moments in a non-static environment. It also involves flowfield characterization of the time-dependent, unsteady aerodynamics occurring during the motion. In order to conduct these experiments the model must be able to move either freely or along a predetermined path. A properly tuned motion test rig allows for the study of certain phenomena that are particular to unsteady aerodynamics.

Motion Test Rigs.

Motion test rigs can be classified into three categories: free-flying wind tunnel models, free motion rigs, and forced-motion rigs [27] . Each of these categories can have varying unconstrained degrees-of-freedom. Free-flying models are useful for investigations on dynamic forces. However free-flying models typically must provide their own propulsion, and the rates of motion increase as the scale of the model decreases. Alternatively, motion can be fixed in varying degrees of freedom using a free-motion rig.

One example of a free-motion rig was used to examine laminar boundary-layer separation during self-sustained, pitch and pitch-heave oscillations [28] [29]. Contrary to free-motion rigs, forced-motion rigs are used to guide the model along a precomputed path. One example of a forced-motion rig is the High Intensity Pitch-Plunge Oscillator designed to oscillate a finite wing in a water tunnel [26]. The rig, shown in Figure 7, consisted of two linear-electric motors used to actuate two, independent plunging rods thus enabling two degrees of freedom. At the Aerodynamic Characterization Facility (ACF) at the University of Florida's REEF, a single degree of freedom, forced-motion rig was developed to study leading edge vortex (LEV) development on a pitching, flat plate [17]. The synchronous movement of two linear motors maneuver the sting shown in Figure 7 to the desired pitching angles. The front linear motor is pin-connected to the sting, while the back linear motor uses a pin-roller connection.
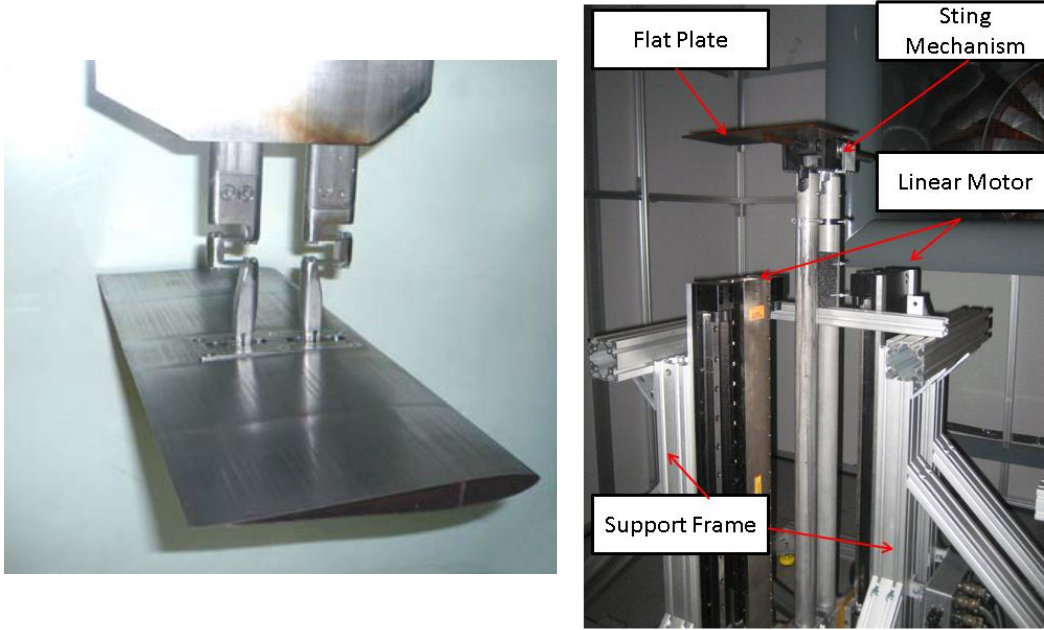
Figure 7. Examples of two motion test rigs. Ol, Dong, and Webb (left) used two linear motors attached by rods directly to the airfoil to perform pitch-plunge [26]. Hart and Ukeiley (right) used two linear motors attached to a sting to perform pitch-up maneuvers [17].

The AFIT MTA is a unique 6-DOF forced-motion rig used for wind tunnel experiments. The MTA may lead to applications such as studying dynamic forces applied to conventional aircraft during gusts or studying interactions between unsteady aerodynamics and flexible wing structures. Using the MTA, trajectories could be restricted to single-DOF or could, ideally, incorporate all 6-DOF depending on the nature of the research. One intended purpose of the MTA is to replicate the movements of a small Micro Air Vehicle (MAV) in flight test conditions through accurate 6-DOF motions with position and force/moment feedback [33].

Unsteady Aerodynamics.

Quasi-steady models are often used as an engineering-level prediction of the flight behavior of small biological fliers and biometric micro air vehicles. The quasi-steady models assume that steady-state forces, which are only a function of wing geome-

23

try, fluid velocity, and angle of attack, are produced at each instantaneous position through a kinematic motion [19] [37]. However experimental investigations by Ellington proved that the quasi-steady model was an inaccurate assumption for many situations [11]. Ellington further proved that hovering flight was only possible through the use of unsteady aerodynamic mechanisms [12]. Not only do unsteady aerodynamics affect the flight behavior of small biological fliers, experiments have demonstrated that the aerodynamic coefficients are also time-dependent. Dickinson and Gotz proved that an accelerating wing at a fixed angle of attack experienced 80% greater lift at the startup of the motion. They showed that in some cases development of vortex regions over the upper surface of the wing led to the sudden increase in lift and remained intact until the LEV traveled 2-2.5 chord lengths downstream [8].

In harmonic oscillations, results are rarely analyzed with respect to the time-domain. Typically the results are a function of the frequency at which they occur. In most aeroelastic and unsteady aerodynamic studies, the research was based on reduced frequency, equation (34), where $2\pi f$ is the frequency (f units of Hz) in rad/s [40]. Like Reynolds number, the reduced frequency is a function of the chord length and freestream velocity.

$$k = \frac{(2\pi f)c}{2U_\infty} \tag{34}$$

$$St = \frac{2kh}{\pi} \tag{35}$$

The reduced frequency in conjunction with a non-dimensional amplitude, such as a non-dimensional plunge length, h, form the Strouhal number, equation (35). For example in a pure pitch motion, 'h' may represent the vertical distance traversed by the leading edge normalized by the chord. The Strouhal number provides insight into

the unsteadiness of flow brought on by the shedding vortices.

Numerous mechanisms have been identified as affecting the aerodynamic performance of flapping wings of small biological fliers, such as dynamic stall, rotational lift, and wake capture. Stall, by definition, is the the angle of attack at which lift rapidly decreases and drag increases. For steady flow, this angle of attack is fixed for a given airfoil geometry and Reynolds number. For a pitching airfoil with a swiftly changing angle of attack, stall can be delayed to incidences which exceed the static stall angle [3]. Dynamic stall is defined as an unsteady aerodynamic phenomenon and is associated with dramatic and persistent loss of lift, typically more substantial than static stall, as well as the persistence of increasing lift past the static stall angle. Because of the time required to build the LEV, the resulting aerodynamic forces and moments exhibit a large lag in response, known as hysteresis [21]. Numerical investigations have shown that this phenomenon is characterized by the development of the LEV over the wing at approximately 22.4° angle of attack which remained attached until 40° [10]. Figure 8 shows an example of how the LEV has not been swept downstream and can still exert appreciable force on the airfoil.

Figure 8. Flow visualization of a pitching airfoil in quiescent water shows the leading edge vortex attached to the upper surface [18].

For the case of cyclic pitch, the airfoil or wing may also start in a post-stall environment and return toward the zero-lift angle of attack during its stroke. Then the

flow reattaches at the leading edge and readjusts to the linear regime of the airfoil at its current angle of attack. Another unsteady aerodynamic mechanism for improved performance is rotational lift. Rotational lift is the aerodynamic consequence of rapid changes in the wing's angle of attack that occur at the downstroke-to-upstroke transition. Dickinson found that the additional lift production in the subsequent stroke was highly susceptible to small changes in duration, the angle of attack of the downstroke, and the angular velocity of the stroke reversal [7]. The mean lift coefficient decreased an average of 25% when the amount of time to flip the angle of attack of the wing from the upstroke to downstroke and vice versa was outside of 5% of the optimal flip time [16]. As the next stroke begins, the wing intercepts the vorticity shed by the previous stroke. This is referred to as wake capture. However, this not only increases aerodynamic lift, but also elevates the drag production [32].

Single Degree-of-Freedom Motions.

Single-DOF motions such as pitch oscillations have been studied for numerous applications. An early example is the study of aeroelastic effects. Empirical solutions were gathered from pitch oscillating experiments to improve helicopter aerodynamic prediction methods [20] [14] [39]. More recently, pitch oscillations were used to prove that reduced frequency, Reynolds number, and angle of attack limits were not the governing parameters for aerodynamic loads time history and evolution of vortex shedding. Using four, single-DOF dynamic profiles, Ol, Dong, and Webb demonstrated that matching reduced frequency, angle of attacks, and Reynolds number was insufficient to obtain the same loads time history or wake geometry [26].

$$\theta(t) = \theta_a \sin(2\pi f_\theta t) + \theta_o \tag{36}$$

Equation (36) is the governing equation for the kinematic motion of a pitch os-

cillation. θ_a is the amplitude of the pitch oscillation about the mean pitch angle, θ_o. The frequency of oscillation, f_θ, has units of Hertz in equation (36) corresponding the number of cycles per second. For basic unsteady aerodynamic research most experiments have placed the axis of rotation at the quarter-chord. However Dickinson found that placing the rotational axis near the trailing edge greatly increased the aerodynamic lift of the wing by capturing the vorticity generated by the rotation [7]. During a pure plunge motion the kinematics are governed by equation (37) where H_o is the normalized heave amplitude, $H_o = h/c$. Okamoto and Azuma demonstrated that the lift coefficient increases with an increasing static pitch angle up to 20° [25].

$$h(t) = H_o \sin(2\pi f_h t) \tag{37}$$

Two Degree-of-Freedom Motions.

One example of a motion, which has been predominantly studied, that requires 2-DOF is a pitch-plunge. Equations (38) and (39) are the equations that describe pitch-plunge kinematics. There are several parameters used to tune this movement. As previously mentioned, mean pitch angle and each DOF's frequency and amplitude can be set. Two new parameters, ϕ_h and ϕ_θ, tune the phase shift between the two motions. According to Ellenrieder, the phase shift affects the timing of the shedding vortices [36].

$$h(t) = H_o \sin(2\pi f_h t + \varphi_h) \tag{38}$$

$$\theta(t) = \theta_o + \theta_a \sin(2\pi f_\theta t + \varphi_\theta) \tag{39}$$

Performing a pitch-plunge maneuver with a a flat plate, Hart and Ukeiley showed that as the phase lags between the motions began to differ, the LEV crucially alters the

lift profile. The creation and convection of the LEV was shown to delay or speed up as the phase shift was varied between motions [16]. There is also a multitude of other pitch-plunge combinations which have been documented in literature [7] [26] [29] [32].

2.5 Measurements

In order to quantify the aerodynamic performance of these single- and muli-DOF motions, the results must be measured using the appropriate technique. A variety of techniques have been used to study the affects of unsteady aerodynamics. Particle Image Velocimetry (PIV) is a non-intrusive optical measurement system used to study the flowfield around an airfoil or wing. This technique has been used numerous times in literature to study the development of LEV and von Karman streets during kinematic motions [17] [26]. Alternatively, a force balance can be used to measure the dynamic force and moments in order to quantify the kinematic motion's affect on the aerodynamic performance [6] [7] [32].

Force and Moment.

Compared to static wind tunnel testing, sampling rate is particularly important to force and moment measurements during dynamic wind tunnel testing. In most static testing, the sampling rate only has to be fast enough to capture the time-invariant data of interest. However in dynamic testing, most data is time-dependent and the dynamic phenomenons may occur on different time scales. Measurement systems must be selected to accommodate the time-rate of change of the aerodynamic forces it is measuring. The Nyquist criteria states that samples should be acquired at least twice as fast as the fastest phenomenon the experiments are trying to capture. The sensitivity of a force balance was crucial to the flapping wing experiments meant to imitate insect wings [6]. Using models and simulations, engineers are able to predict

the magnitude of the expected loads and use a force balance with proper sensitivity.

$$L(t) = \frac{1}{2}\rho_\infty U_\infty^2 S C_L(t) \tag{40}$$

$$D(t) = \frac{1}{2}\rho_\infty U_\infty^2 S C_D(t) \tag{41}$$

In most studies performed with a load cell, only lift and drag, equations (40) and (41), were measured. The forces are both functions of time due to the time-varying effective angle of attack. Effective angle of attack in its simplest form is the angle between the freestream velocity and the chordline of the airfoil form the reference frame of the airfoil. This measurement is complicated by dynamic motions occurring. For example, during a plunge oscillation the effective angle of attack is numerically solved using equation (42), where $\frac{dh(t)}{dt}$ is the instantaneous velocity of the airfoils plunging motion.

$$\alpha(t) = \theta_o + \tan^{-1}\left(-\frac{1}{U_\infty}\frac{dh(t)}{dt}\right) \tag{42}$$

Before capturing these aerodynamic forces, the system must be tared. Taring is a method of removing the inertial forces acting on a system. When acquiring aerodynamic loads, it is important to isolate them from the inertial loads in order to draw proper conclusions. For best results, taring is conducted in a vacuum where the trajectory is executed isolating a time-history of the dynamic-inertial loads and ensuring that no forces due to air resistance are present. However, depending on the size of the model, trajectory, and motion test rig, it can be difficult to create a vacuum in which to test. During Hart and Ukeiley's experiments on a pitching-plunging flat plate, the flat plate was replaced with a steel rod with equivalent mass and moment properties [16]. The trajectories were executed and the dynamic-tare data was collected. Alternative methods have been attempted such as quasi-static
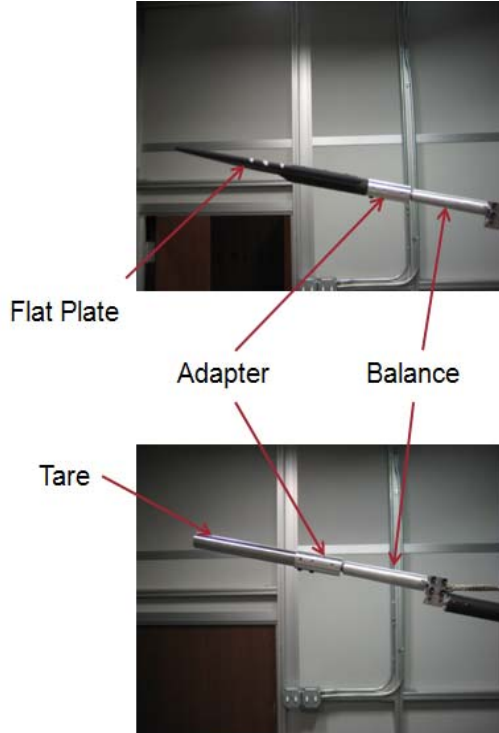
Figure 9. The flat plate model was replaced with a steel rod with the same mass and moments for taring [16].

taring. Quasi-static taring involves calculating the inertial forces at static angles of attack and interpolating the information acquired [34]. Another method is to conduct the dynamic tare inside helium gas rich environment instead of a vacuum.

Time-Dependent Pressure Measurements.

Although dynamic force data can often provide a representation of the net affects on a body, it is also helpful to know local properties, such as surface pressure. It is important for the surface pressure sensor to be as non-intrusive as possible. Micro-electronic sensors are constructed from materials such as piezoresistive materials. Piezoresistive sensors are semi-conductive materials that exhibit a change in resistance due to an applied pressure or force. By adjusting the type and concentration of impurities found in the semiconductor, the resistivity can be greatly increased [5]. This is crucial to the design of micro-sensors that respond to small mechanical inputs

30

with large electrical outputs.

Piezoresistive pressure transducers are typically constructed from a Wheatstone bridge attached to a diaphragm [13]. When there is a pressure difference between the two sides of the diaphragm, the diaphragm will deflect causing a change in the resistance, thus changing the output voltage. These sensors have been used for decades to collect time-accurate pressure data for many applications.

Position and Orientation Measurements.

Accurate location and orientation measurements typically require multiple sources of information. For example photogrammetry requires up to three cameras, depending on the number of DOF, to calculate the position and orientation of a model in motion. However an Inertial Measurement Unit (IMU) is often comprised of three different types of sensors: gyroscopes, magnetometers, and DC accelerometers. Each sensor utilizes a specific technique to estimate the Euler angles of its orientation. The combination of these three sensors provides reduced error in both static and dynamic environments.

Gyroscopes are typically used to determine inclination or rate of inclination of an object. Like the one in Figure 10, conventional gyroscopes exploit the of inertial properties of a spinning wheel. At high speeds the wheel's rotary axis continues to point in the same direction while the gimbal is tilted. Gyroscopes must first have an inertial frame to reference. This frame is fixed to the body for all time. As the object begins to rotate the frame will rotate with the object while the inner gimbal with the spinning wheel remains on its original rotational axis. In order to reduce measurement errors the wheel must have a high angular momentum. For gyroscopes angular momentum is defined by the distribution of mass on the wheel and its angular velocity. The angular momentum can easily be increased by placing the majority of
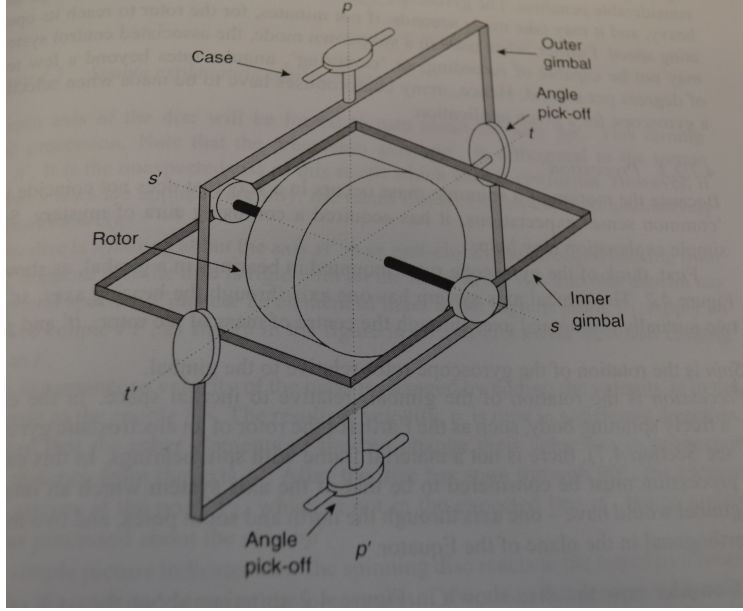
Figure 10. Example of a one degree-of-freedom gyroscope [35]

the mass near the edge of the wheel [35]. This reduces the power necessary to spin the wheel at a higher angular velocity, while maintaining the high angular momentum. Modern gyroscopes are mostly used for calculating dynamic Euler angles. At static angles the readings tend to drift. However this problem can be fixed by validating the Euler angles calculated with the gyroscope with another sensor.

A magnetometer provides a vector measurement of the Earth's magnetic field in reference to the fixed, magnetometer reference frame. Since the (inertial) reference frame for Earth's magnetic field is fixed for all time, the Euler angles are calculated by solving for the rotation matrix between the inertial and magnetometer reference frames. However, solving for the rotation matrix is an overdetermined problem and must be solved using a deterministic algorithm. In order to use a deterministic algorithm such as the *Triad* algorithm, there must be a second sensor with vector information [15]. DC accelerometers sense the change in velocity by measuring the force produced by a seismic mass. The device typically encompasses a small cantilever mass that uses capacitive changes to monitor the position of the mass [9].

The DC, or direct current, corresponds to recording slower changes in acceleration when compared to accelerometers used in vibrational testing. When the IMU is not moving, the acceleration vector is oriented in the direction of gravity. Using the combined information of magnetometer and DC accelerometers, the *Triad* algorithm solves for the rotation matrices between each sensor's inertial reference frame and the sensor-fixed reference frame [15].The IMU can be used to measure the Euler angles and triaxial accelerations which can determine the IUT's orientation and position. Furthermore, these measurements provide an opportunity to study aeroelastic effects and sting rigidity.

2.6   Statistical Control System Characterization

When a system exhibits peculiar nonlinear behavior, conventional linear modeling techniques will not suffice. One example of nonlinear behavior is exhibiting different magnitudes of signal attenuation for inputs of different amplitudes but the same frequency. The difference in attenuation does not adhere to the homogeneity (or amplification property) of a linear system shown in equation (43) [30].

$$\mathbf{T}[kx(t)] = k\mathbf{T}[x(t)] \tag{43}$$

In order to characterize the nonlinear system statistical analysis is performed using various frequencies and amplitudes. At each frequency, the signal bias (or mean), normalized magnitude, and phase shift are calculated. Since mechanical systems do not perform exactly the same every time, a number of tests (n) are conducted for the statistical calculations. The signal bias (b), for periodic signals, is calculated by dividing the sum of all the data points, in m full periods (T), by the total number data points ($N = \frac{mT}{\Delta t}$), as shown in equation (44). Each of these signal biases are averaged over the number of tests performed. For a linear system the signal bias

corresponds to the output's magnitude when the frequency is zero.

$$b = \frac{\sum_{k=1}^{n} \left(\frac{\sum_{i=1}^{N} y_i}{N} \right)}{n} \tag{44}$$

The normalized magnitude is determined by finding the peak-to-peak amplitude of each period (A_i) and averaging over the number of periods in the signal (N_p). Each normalized magnitude is averaged over the number of tests performed as shown in equation (45). The amplitude is then normalized by the peak-to-peak amplitude of the input signal. Signal attenuation is signified by $P < 1$ and signal amplification corresponds to the result $P > 1$.

$$P = \frac{\sum_{k=1}^{n} \left(\frac{\sum_{i=1}^{N} A_i}{N_p} \right)}{n} \tag{45}$$

Next the phase shift is calculated by determining phase shift angle required to linearly correlate the input u(t) and output y(t) signals, shown in equations (46) and (47). The phase angle between the input and output is calculated using the dot product rule, shown in equation (48). The dot product is rearranged and formatted for discrete data to form equation (49), solving for the phase angle.

$$u(t) = b + A \sin(2\pi f t) \tag{46}$$

$$y(t) = b + A \sin(2\pi f t - \varphi) \tag{47}$$

$$u(t) \cdot y(t) = |u(t)||y(t)| \cos \varphi \tag{48}$$

$$\varphi = \cos^{-1} \left(\frac{\sum_{k=1}^{N} u_k(t) y_k(t)}{\sqrt{\sum_{k=1}^{N} |u_k(t)|^2 \sum_{k=1}^{N} |y_k(t)|^2}} \right) \tag{49}$$

2.7 Proportional Feedback

Proportional control is one of the most widely used forms of control. Typically proportional feedback is accompanied by derivative, integral, or both derivative and integral control. For proportional feedback, the relationship between the input to the open-loop system $u(t)$ and the error $e(t) = \theta_{des}(t) - \theta_m(t)$ (where m(t)=y(t)) is:

$$u(t) = K_p e(t) \tag{50}$$

This type of control is often referred to as position feedback when the output of the system is the measured position (or angle). The error is the difference between the desired angle $(\theta_{des}(t))$ and the measured angle $(\theta_m(t))$. The proportional gain term, K_p is multiplied by the error correcting the system. Figure 11 shows an example of a control system which uses proportional control with negative feedback. This is known as the closed-loop system. The open-loop system is a control system where the output has no effect on the input to the system [24]. Using Figure 11, the open-loop system occurs between u(t) (u(t)=e(t)-0) and m(t) and does not include the feedback path. For a steady-state input signal such as a sine wave, proportional gain in negative feedback increases the magnitude of the output. This is excellent for rectifying attenuation of an input signal like a trajectory. However increasing the gain too much can cause instability to occur at lower frequencies than where it may have occurred in the open-loop. Furthermore, proportional control can increase the phase lag of the closed-loop system over the open-loop system.
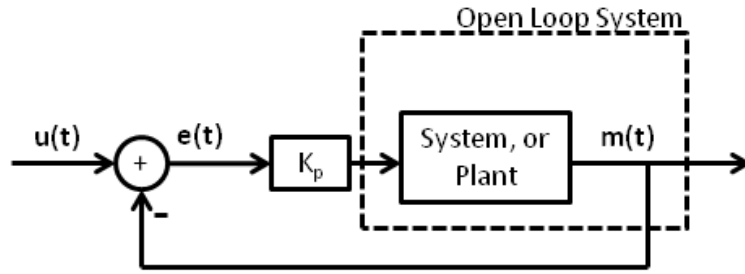
Figure 11. Control diagram of a proportional control. The closed-loop system is the entire diagram and the open-loop system is the dashed box.

2.8   Chapter Summary

Chapter II provided the necessary background required to understand and investigate the challenges of this research effort. Details were provided about the reference frames essential to dynamic wind tunnel testing and the kinematics of the MTA. Also this chapter presented previous efforts using forced-motion test rigs to study unsteady aerodynamics. Next this chapter presented commonly used techniques used for the acquisition of aerodynamic, position and orientation data. Finally *Chapter II* examined the statistics necessary to characterize a control system with inherent noise and motivated the use of proportional feedback for rectifying position errors.

III. Experimental Setup

3.1 Motion Test Apparatus Design

The MTA is a 6-DOF, forced-motion rig designed to maneuver an IUT through a set of desired trajectory points using some combination of the six joint motors. The joint motors were sized to achieve realistic MAV motions during low Reynolds number wind tunnel testing. Wires and cables that provide power and commands for the MTA were managed using flexible tracks or paths to ensure no wires were kinked or pinched. Each motor has a digital encoder able to sense the orientation of the joint. When power is not applied to the MTA from its computer, the brakes in each joint are engaged ensuring no movement can occur. On-board, each motor is controlled by an ELMO® controller using angular velocity commands. The MTA is
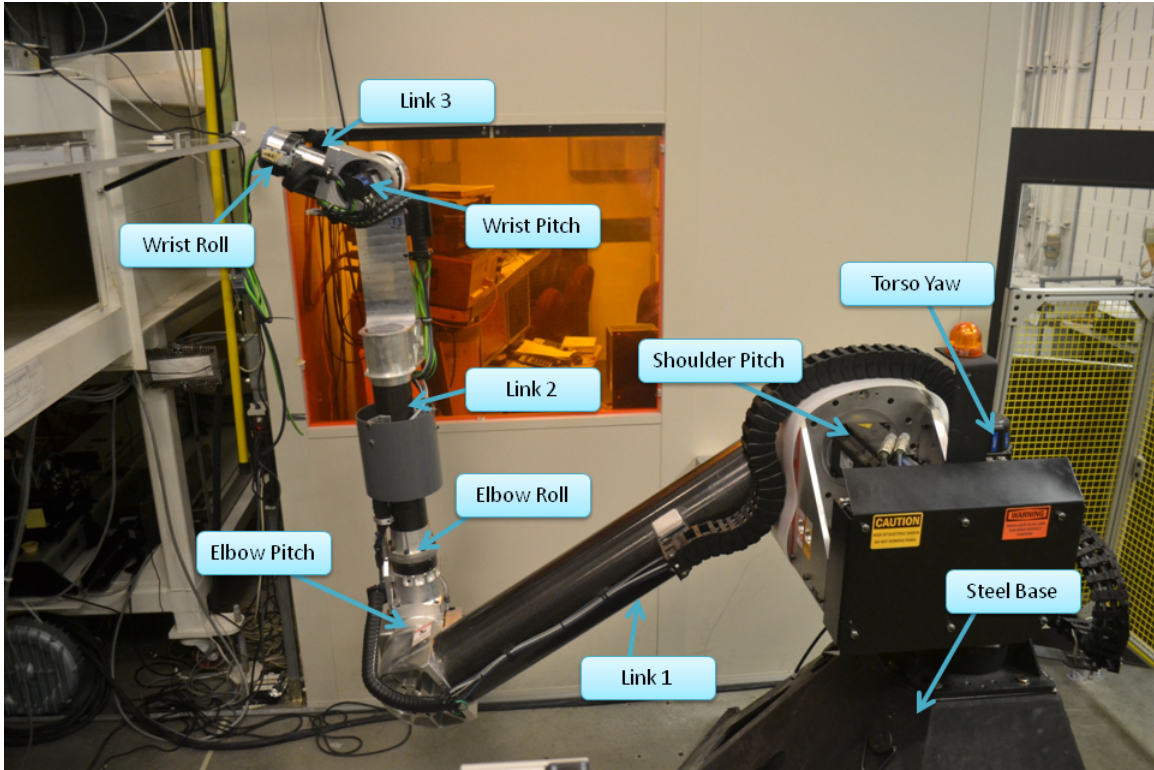
Figure 12. Motion Test Apparatus

37

surrounded on two sides by an aluminum fence to prevent personnel from getting too close during operation. Access is restricted on the other sides by the control room and wind tunnel, shown in Figure 13. The fence has a gate with an interlock, which will emergency stop the MTA motion if the gate is opened.

Figure 13. Fence (left) surrounds the MTA on two sides to prevent personnel injury. The interlock circuit (right) must be closed to operate the MTA.

Steel Base.
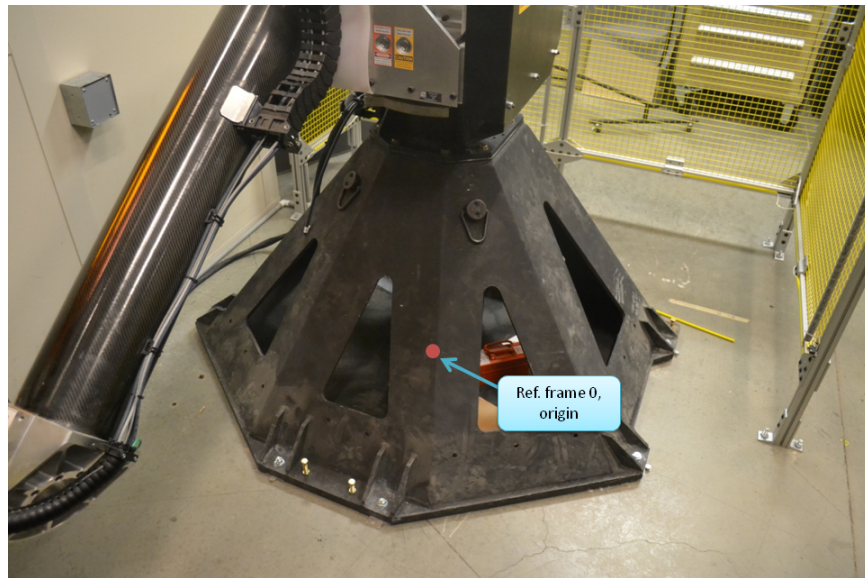
Figure 14. Steel base: built to resist deflections during motions

The MTA rests upon a massive steel base built to eliminate arm deflections during extremely quick movements. It weighs in excess of 1200 pounds and has an overall

dimensions of 46 in by 60 in by 32.25 in (depth, width, and height). Six leveling bolts were used to level the base. After the leveling, the base is secured to the floor using eight-6 in long concrete bolts with shims placed as needed. The origins is depicted in Figure 14 and proceeding figures depicted with a dot, though depth is difficult to indicate without tools such as a 3-view drawing.

Torso-Shoulder Joints.

The MTA's torso and shoulder are comprised of two motors which control the pitch and yaw of the first, and largest, link. These are the largest motors controlling the arm due to the large torques required to move the lower links. The hardware information for each of the joints can be found in Table 1. The torso yaw joint is centered on top of the steel base. The shoulder-pitch joint is offset from the center in order to accommodate both of the motor housings and allow for greater range of motion.
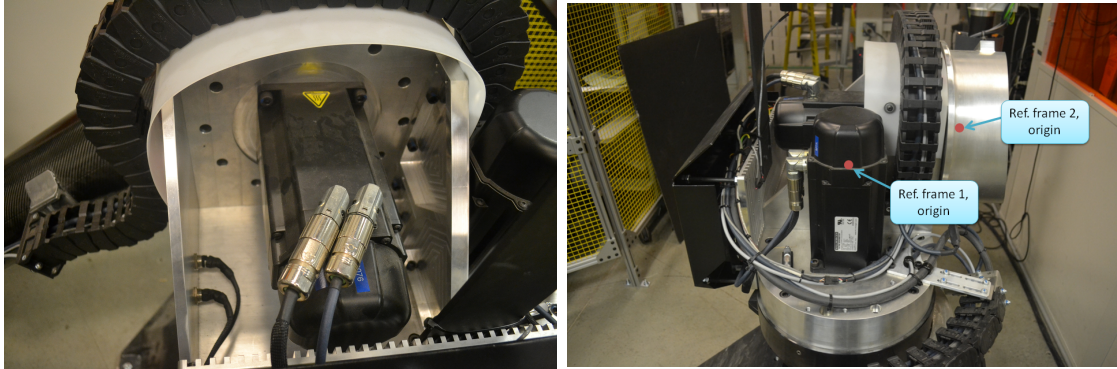
Figure 15. (Left) shoulder-pitch motor and (right) torso-yaw motor

Table 1. Description of the hardware for the torso yaw and shoulder pitch joints.

Manufacturer	Mfg Part Number	Description
Kollmorgen	AKM65N-ANC2DB-00	BLDC with EnDat Absolute Encoder
ONVIO	DM08055BE0N0000	Zero Backlash Gearbox
ELMO	G-DRU-A35/800SES	ELMO Drum HV

Originally the MTA software limited the range of motion of the torso to $-93.0° \leq \theta_{tr} \leq 96.2°$. When it was installed at AFIT the software limits were modified to $10° \leq \theta_{tr} \leq 20°$. As a secondary precaution, a large metal limiter, shown in Figure 16, serves as a "hard stop" and prohibits the torso yaw motor from exceeding the software limits as well. These new limits ensure that the MTA cannot rotate and impact either the control room or fence.
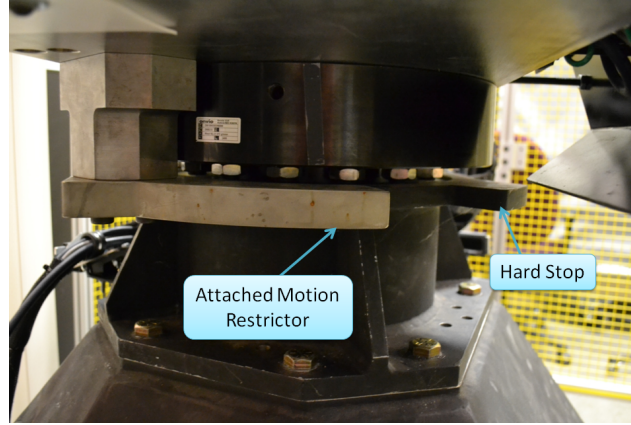
Figure 16. The motion restrictor was attached to limit the torso's rotation.

Elbow Joints.

The elbow is comprised of two motors which control the pitch and roll of the forearm and wrist. As seen in Figure 17, the elbow-roll motor is housed internally while the elbow-pitch motor is housed externally on the side of the joint. The hardware used to design the elbow joints is presented in Table 2 and Table 3.
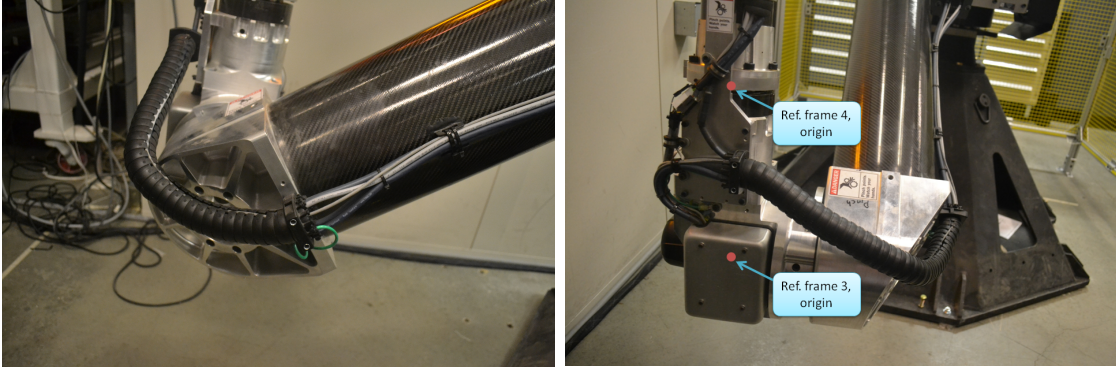
Figure 17. Elbow joints: two views of the elbow-pitch and elbow-roll joints.

Table 2. Description of the hardware for the elbow pitch joint.

Manufacturer	Mfg Part Number	Description
Kollmorgen	AKM52K-ANC2DB-00	BLDC with EnDat Absolute Encoder
ONVIO	DM05078BE0N0000	Zero Backlash Gearbox
ELMO	G-TRO12/400SES	ELMO Drum HV

Table 3. Description of the hardware for the elbow roll joint.

Manufacturer	Mfg Part Number	Description
Kollmorgen	AKM22E-ANC2DB-00	BLDC with EnDat Absolute Encoder
ONVIO	DM0355BE0N0000	Zero Backlash Gearbox
ELMO	G-TRO6.1/400SES	ELMO Trombone

Wrist Joints.

Similar to the elbow joint, the wrist is also comprised of two motors that control the pitch and roll using hardware given in Table 4 and Table 5. The wrist-roll motor is housed internally, and the wrist-pitch motor is housed externally. Cables are routed through the MTA to the face of the wrist in order to provide electrical support for data acquisition systems such as force balances. On the front face there are 8, 1/4"-20 threaded holes that can be used to mount a sting, models, or other extensions to the MTA system.
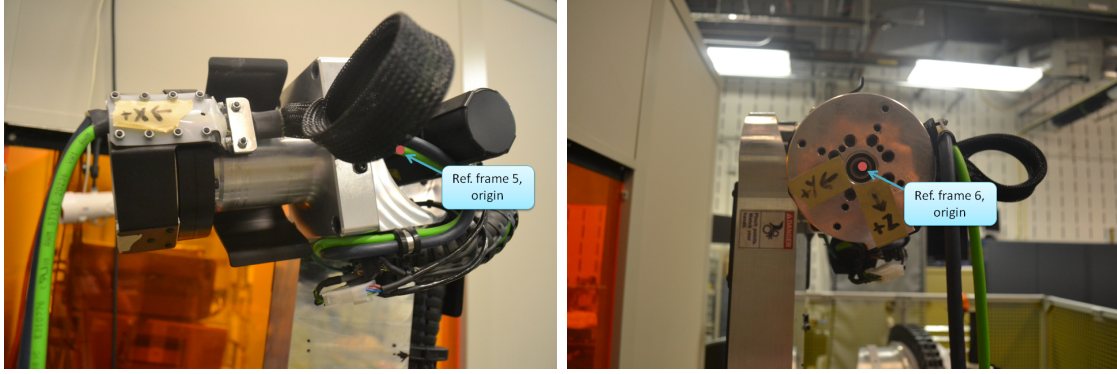
Figure 18. Wrist joints: the side view of wrist (left) displays the wrist-pitch motor housing and electrical cable protruding from the MTA; the front face (right) shows the mounting interface.

Table 4. Description of the hardware for the wrist pitch joint.

Manufacturer	Mfg Part Number	Description
Kollmorgen	AKM22E-ANC2DB-00	BLDC with EnDat Absolute Encoder
ONVIO	DM0355BE0N0000	Zero Backlash Gearbox
ELMO	G-TRO6.1/400SES	ELMO Trombone

Table 5. Description of the hardware for the wrist roll joint.

Manufacturer	Mfg Part Number	Description
Kollmorgen	AKM22E-ANC2DB-00	BLDC with EnDat Absolute Encoder
ONVIO	DM02015BE0N0000	Zero Backlash Gearbox
ELMO	G-TRO6.1/400SES	ELMO Trombone

MTA Computer.
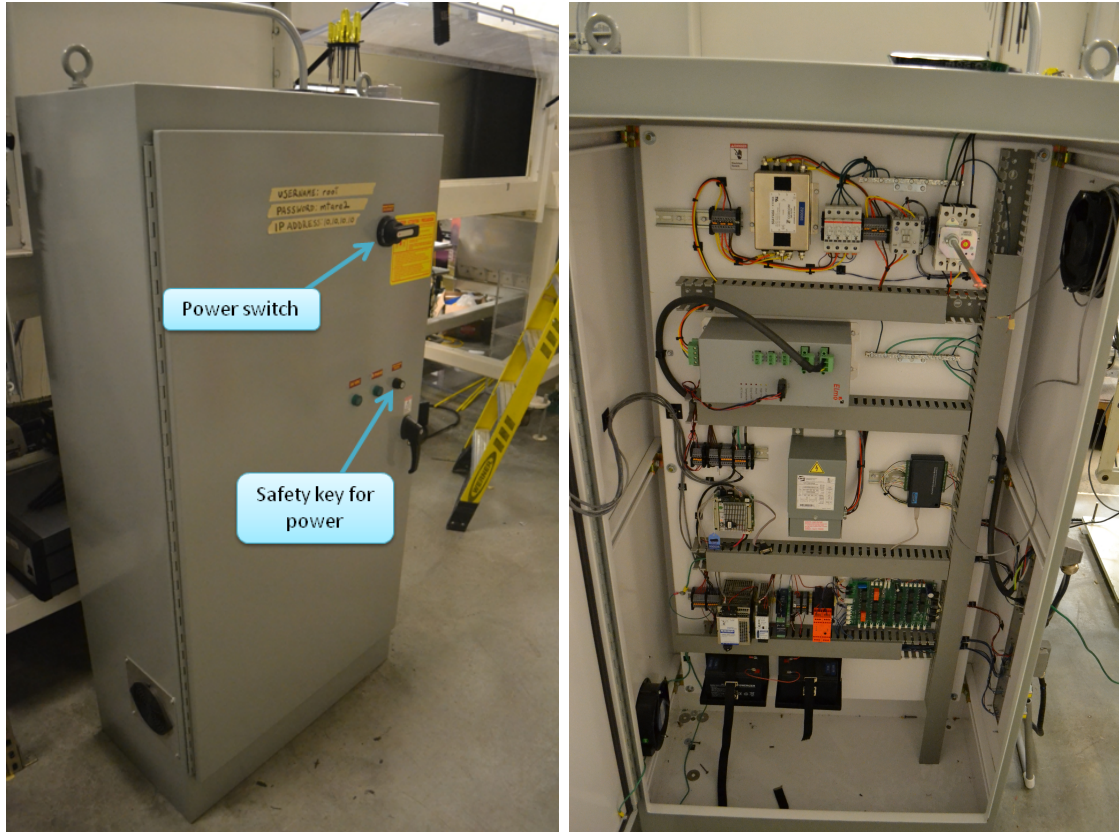
Figure 19. MTA Computer and cabinet are located on the east side of the AFIT low-speed tunnel. It provides power to the MTA and calculates kinematics necessary for trajectories and post-processing. The right picture shows the inside of the cabinet where the computer is housed.

All of the joints are simultaneously commanded by the off-board MTA computer shown in Figure 19. In the planning phase (prior to executing the trajectory), the MTA source code uses inverse kinematics to calculate the six joint angles for each of the trajectory waypoints. Since there is more than one solution, the "elbow-down" solution is chosen, when applicable, for consistency and safety. Angular velocities are calculated using the slopes between the waypoint and its nearest neighbor on each side. If the slopes are the same sign, they are averaged together. If the slopes are opposite signs, then the velocity is set to zero.
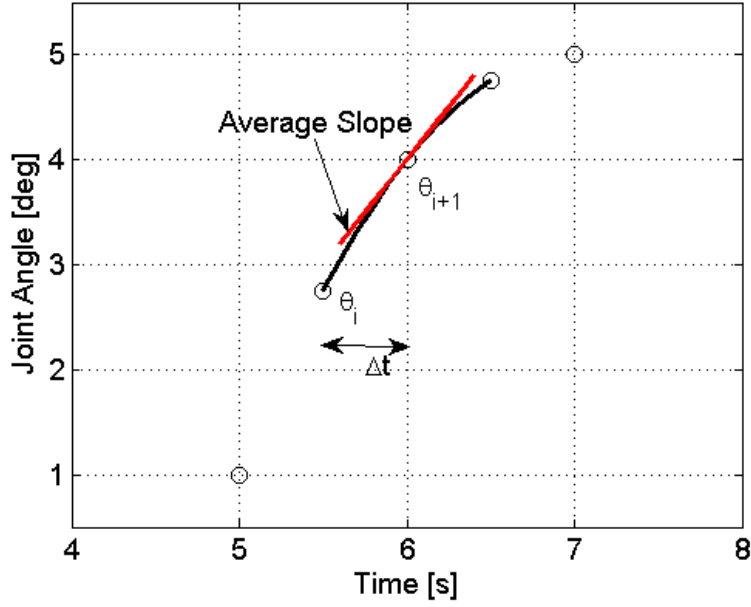
Figure 20. Example of a joint position profile

$$\theta(t) = C_1 t^3 + C_2 t^2 + C_3 t + C_4$$

$$where,$$

$$C_1 = \frac{-2}{\Delta t^3}(\theta_{i+1} - \theta_i) + \frac{1}{\Delta t^2}(\dot{\theta}_{i+1} + \dot{\theta}_i)$$

$$C_2 = \frac{3}{\Delta t^2}(\theta_{i+1} - \theta_i) - \frac{1}{\Delta t}(\dot{\theta}_{i+1} + 2\dot{\theta}_i)$$

$$(51)$$

$$C_3 = \dot{\theta}_i$$

$$C_4 = \theta_i$$

The joint angles and velocities are fitted with a cubic polynomial between each pair of neighboring waypoints using equation (51). These coefficients are stored as a lookup table during trajectory executions. The derivative of equation (51), shown in equation (52), is used for determining the angular velocities commands for each of the joints.

$$\dot{\theta}(t) = 3C_1 t^2 + 2C_2 t + C_3 \tag{52}$$

During execution, the computer is queried for the joint angular velocity commands. The computer first determines which two waypoints the desired time lies between. Using the stored polynomial coefficients corresponding to the desired time's neighboring waypoints, the relative time, t, is determined by the difference between the desired time and earlier neighboring waypoint. Angular velocity commands are sent from MTA Computer to each of the joint's ELMO® Motion Controllers where the command is converted to voltage and transmitted to the joint's motor. Readings from the digital encoders are relayed back to the MTA Computer for post-processing. The timestamp of each set of recorded joint angles is approximately the time that the processor reads the data. The processing delay between the measured and record times is negligible, because it is on the order of 10^{-4}s. After the trajectory is executed, the MTA Computer uses forward kinematics to transform the recorded joint angles into the model's position and orientation at each discrete time with respect to the MTA-inertial reference frame [**?**].

Table 6. These four commands are essential to operating the MTA.

Command	Description
mtaHome	Moves the model to the first position in the commanded trajectory file
mta	Executes the trajectory
mtaAngles	Determines the current joint angles and Cartesian position
mtaMoveTo	Moves individual joints to new commanded angles

There are four important commands, shown in Table 6, for operating the MTA. Using the host computer these commands are given to the MTA Computer to operate the MTA. These commands are the basic commands necessary for operation. More details on syntax for each of these commands can be found in the MTA User Manual [**?**].

3.2 The MTA Control System

Trajectory files are converted to sets of cubic-polynomial coefficients with respect to joint positions prior to executing the trajectory in the program: `mta`. During execution, the MTA Computer is queried for angular velocity commands and sends commands to the joint control systems. Each joint control system is comprised of a single input and multi-output feedback system, shown in Figure 21. The ELMO® Motion Controllers use measured angles from the motors encoder for position and velocity feedback. The "measured" discrete angular velocity is determined by dividing the difference between the current and previous position by the time difference between measurements.
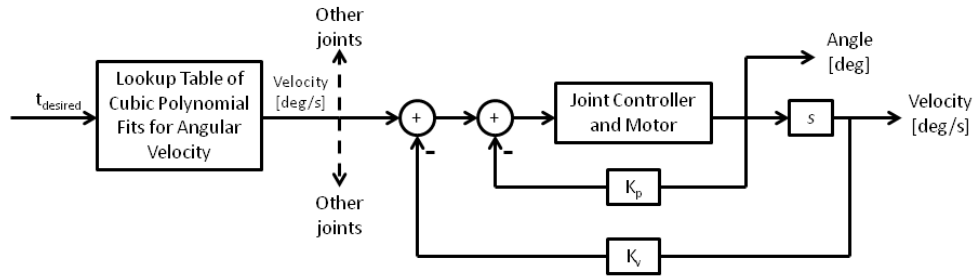
Figure 21. Block diagram of a joint motor and controller. Demonstrates how the controller receives its commands

Each controller was tuned independently for greatest bandwidth by the manufacturer, Re2 Inc [33]. During the tuning process each ELMO® Motion Controller determined a linear model for each of the joint motors as assembled but with no test apparatus attached. Because the MTA Computer individually sends each of the six joint angular velocities to the respective joint's control system, each joint is acting independent of the other five joints. Therefore, there is no global position feedback working to correct errors in the model's Cartesian position. As the motion becomes

more complex, more joints are actuated, each with their individual phase lag, thus compounding position errors. For example, with careful planning the model could be placed such that the pitch oscillation about the quarter-chord only requires the wrist roll motor. However, placing the quarter-chord out of line with the axis of rotation of the wrist face would require additional joints to be actuated to perform the pitch oscillation. The incorporation of more actuators would induce error independently by each joint. During the course of this research, it was found that the model of each joint behaves in a slightly nonlinear manner. Unfortunately repeating the same input trajectory with the same experimental setup does not produce precisely the same output each time. Each execution of a pitch oscillation with a fixed frequency and amplitude led to mildly varying signal bias, amplitudes, and phase shift.

3.3   Operating the MTA

The MTA Computer is powered on by turning the key to on and turning the power switch to on. Without the MTA Computer on, no power is being supplied to the robotic manipulator. Using a host computer, shown in Figure 22, a trajectory file is created in which a model's position and orientation are specified for time increments of 0.008 s, such as Figure 23. This section will go into more detail on trajectory design

Figure 22. Laptop used to communicate with the MTA Computer using ssh protocol.

47

later. Once the trajectory file is created the host computer is connected to the MTA computer using Secure Shell (ssh) protocol. Then the trajectory file is copied from the host computer to the `re2mta` folder on the MTA computer.

Time	X	Y	Z	Phi	Theta	Psi
0	-0.064	-2.151	-1.806	0	0	-1.64061
0.008	-0.064	-2.151	-1.806	0.021923	0	-1.64061
0.016	-0.064	-2.151	-1.806	0.043791	0	-1.64061
0.024	-0.064	-2.151	-1.806	0.065548	0	-1.64061
0.032	-0.064	-2.151	-1.806	0.08714	0	-1.64061
0.04	-0.064	-2.151	-1.806	0.108511	0	-1.64061
0.048	-0.064	-2.151	-1.806	0.129609	0	-1.64061
0.056	-0.064	-2.151	-1.806	0.150379	0	-1.64061
0.064	-0.064	-2.151	-1.806	0.170769	0	-1.64061
0.072	-0.064	-2.151	-1.806	0.190728	0	-1.64061
0.08	-0.064	-2.151	-1.806	0.210205	0	-1.64061
0.088	-0.064	-2.151	-1.806	0.229151	0	-1.64061
0.096	-0.064	-2.151	-1.806	0.247518	0	-1.64061
0.104	-0.064	-2.151	-1.806	0.26526	0	-1.64061
0.112	-0.064	-2.151	-1.806	0.282331	0	-1.64061
0.12	-0.064	-2.151	-1.806	0.29869	0	-1.64061
0.128	-0.064	-2.151	-1.806	0.314294	0	-1.64061
0.136	-0.064	-2.151	-1.806	0.329104	0	-1.64061
0.144	-0.064	-2.151	-1.806	0.343083	0	-1.64061
0.152	-0.064	-2.151	-1.806	0.356195	0	-1.64061
0.16	-0.064	-2.151	-1.806	0.368408	0	-1.64061
0.168	-0.064	-2.151	-1.806	0.379689	0	-1.64061
0.176	-0.064	-2.151	-1.806	0.390012	0	-1.64061
0.184	-0.064	-2.151	-1.806	0.399349	0	-1.64061
0.192	-0.064	-2.151	-1.806	0.407678	0	-1.64061
0.2	-0.064	-2.151	-1.806	0.414977	0	-1.64061
0.208	-0.064	-2.151	-1.806	0.421227	0	-1.64061

Figure 23. Sample formatting for trajectory files. Headers are included as reference only and should be removed for execution

For safety, all personnel and unnecessary items are outside the fence that encloses the MTA. Before executing the trajectory, ensure that the model is positioned at the first point in the trajectory file using the `mtaHome` command. This will ensure the best results for tracking the trajectory and also provides the error between current position and desired position. The current position of the model can found using `mtaAngles` command. The motion is executed when the operator presses the green flashing button on the control panel shown in Figure 24.

Figure 24. The red light flashes when an emergency stop is engaged. The green light flashes when the MTA is ready to execute the trajectory.

During all movements, the operator should be prepared to emergency stop the motion if there is unexpected motion which might damage equipment. After the MTA has positioned the model at the first point of the trajectory, the trajectory is ready to be executed using the `mta` command. Once the operator ensures the area is cleared, the motion is executed by pressing the green flashing button. While the trajectory is executed, the MTA Computer is recording data such as the joint angles and joint angular velocity commands at each timestamp. Once the trajectory motion is completed, the MTA Computer disables power to the motors, engages the brakes, and computes the forward kinematics for the model's Cartesian position throughout the motion. Raw data files corresponding to the model's time-accurate position and other pertinent information should be copied from the MTA Computer to the host computer since these files are overwritten on the MTA Computer after every execution. For more details the operator should refer to the MTA User Manual created by Re2 Inc [31].

Model Offset.
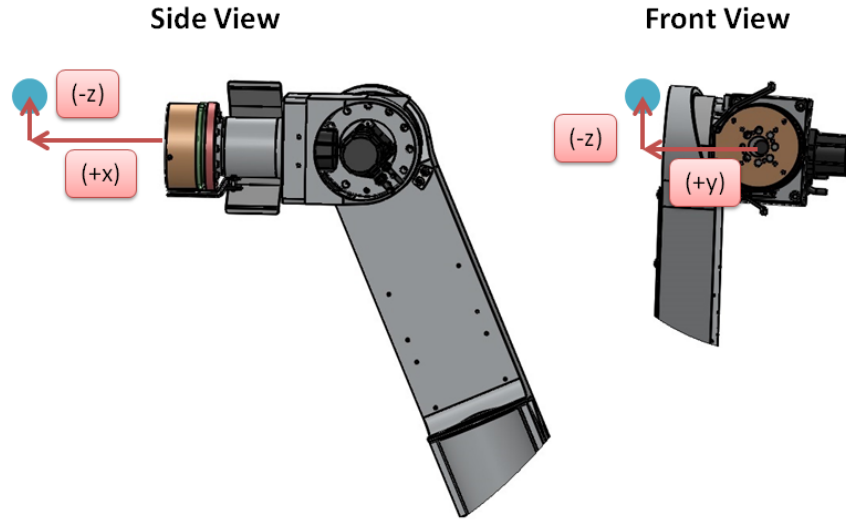
Figure 25. The red sphere symbolizes the selected model's control point at which the trajectories occur.

Within the software written for the MTA, the operator can specify an offset location for the model. The model's position, or offset, is given with respect to the center of the wrist face. In the `re2mta` folder there is a file named `MtaParameter.txt`. Along with other parameters this file contains the specified offset for the model. The sixth, seventh, and eighth parameters in the file specify the x, y ,and z offset respectively. This location is included in the kinematics, thus ensuring that the trajectory occurs about the model's position. For the purposes of wind tunnel testing, the model's offset was prescribed at the quarter-chord of the chord line on the half span of the model.

Designing a Trajectory.

The first column of the model's trajectory file is the timestamp specified with a time interval $0.008\,\mathrm{s}$, as shown in Figure 23. The next three columns specify the location of the model's body-fixed reference frame, x_b, y_b, and z_b, with respect to the

MTA-inertial reference frame at each discrete time. The subsequent three columns specify the roll, pitch, and yaw angle of the model's body-fixed reference frame with respect to the MTA-inertial reference system at each discrete time. In order to simplify the determination of a trajectory, a Matlab® program was created for this thesis; the code for this program can be found in Appendix B. In most dynamic wind tunnel tests, the important relation would be the location of the body-fixed reference frame with respect to a fixed, wind reference frame. Assuming the wind reference frame is centered in the wind tunnel and oriented with x_w pointing in the direction of the freestream velocity, the user can design a trajectory for the flight path of the body-fixed reference frame using software of choice (Excel®, Matlab®, Notepad®, etc.). Once this file is created the user will load the file in the *Trajectory Coordinate Transformation* Matlab® program to convert the coordinates to MTA-inertial reference frames. Using the same program, the Cartesian position output file can also be converted back to body-fixed reference frame for post-processing.

Figure 26. The user can specify the location of the MTA-model reference frame and maximum moving distances on the Operating Conditions Tab of the *Trajectory Coordinate Transformation* program.

For the program to position the model in the correct initial location, the user

must specify the location and orientation of the MTA-model reference frame origin with respect to the MTA-inertial reference frame in the "Operating Conditions" tab. The MTA-model reference frame's origin, coincident with the body-fixed reference frame's origin, is the location where the trajectories are to begin. On the same tab, the user must specify the maximum directional-constraints. These are not necessarily hardware or MTA software limits. Therefore, a concern exists that it is possible to design a trajectory and transform it using this software that will result in an impact with the tunnel, wall, or floor. Currently in the AFIT Low Speed Wind Tunnel, the arm's movement is constrained radially in the x_i-z_i plane to $0.1143\,\mathrm{m}$ and $\pm 0\,\mathrm{m}$ in the y_i-direction. These constraints are shown with respect to the wind tunnel environment in Figure 27.
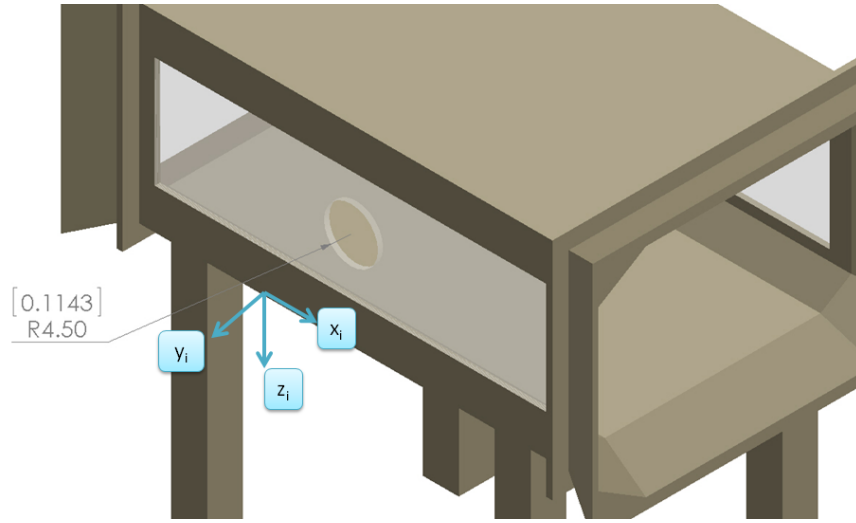
Figure 27. CAD a model of the wind tunnel used to demonstrate the constraints imposed by the wind tunnel's window. The units of the window's hole are [meters] and inches.

Currently the *Trajectory Coordinate Transformation* program does not place limitations on maximum rotations. Once the operating conditions are specified, the user will navigate to the "Coordinate Transformation" tab to import the initial trajectory file. Because the program is capable of performing transformation in both

directions, the operator will select either "Model to MTA" or "MTA to Model" in the drop down. The initial trajectory file for a "Model to MTA" transformation can be written in a variety of units. However, when transforming from body-fixed (or model) to MTA-inertial reference frame, the incoming file's units must be specified. The output units default to meters and radians for the MTA Computer to accept the trajectory. The output file of the MTA Computer, upon completion of a trajectory, has units of meters and degrees still referenced to the MTA-inertial reference frame. When transforming from MTA-inertial to body-fixed reference frame the "MTA to Model" transformation's output units may be uniquely specified by the user. Finally the output filename must be specified with extension "*.txt". The file is written to the same directory as the input file.

Figure 28. On the Coordinate Transformation Tab the user can specify which transformation needs to occur, the incoming/outgoing units (respective to transformation), and input and output filenames.

To begin the transformation, the user must push the "Convert" button. For "Model to MTA" the first operation is converting the specified units of the input file to meters and radians. Next the program ensures that the trajectory file was created with a sampling frequency of $125\,\mathrm{Hz}$ ($\Delta t = 0.008\,\mathrm{s}$). If the sampling frequency

is incorrect, the *Trajectory Coordinate Transformation* program will perform a cubic spline interpolation of the input file. The program outputs plots of the original trajectory overlaid with the new interpolated trajectory for user verification. Next the program transforms each Cartesian location from the body-fixed reference frame to the MTA-inertial reference frame. Finally, all Cartesian locations are offset to the specified location of the MTA-model reference frame's origin from "Operating Conditions" tab.

For the "MTA to Model" function, the first operation is to remove the offset between the MTA-model reference frame and MTA-inertial reference frame. The program assumes that input file's units are consistent with the output units of MTA Computer (meters and degrees). Next the Cartesian coordinates are transformed from MTA-model reference frame to body-fixed reference frame. Finally, the units of the input file are converted to the desired units for the output file.

3.4 Model and Sting Design

The wind tunnel models were designed as a rectangular wing using a symmetric NACA 0012 airfoil section. The planform dimensions are 4 in chord by 8 in wing span. In Figure 29, the left model's fuselage was designed to accept the Nano25 force balance. The face of a Nano25 is positioned at the quarter-chord of the wing, which is the desired reference location for force and moment data. In Figure 29, the right model was designed to mount directly to the sting without the Nano25. On the starboard wing of this model, four shallow cavities were built into the model to place four pressure transducers tangent to their respective surfaces. On the top surface the cavities are placed at 25 and 75 percent of the chord length; the bottom surface mirrors the top surface.
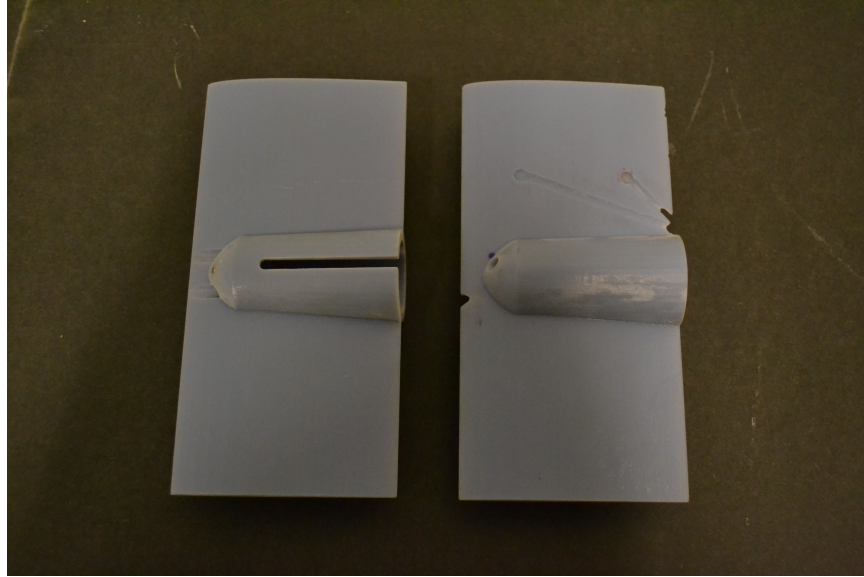
Figure 29. The wind tunnel model (left) was designed for integration with the force balance. The second wind tunnel model (right) was designed to mount without the force balance and also has four cavities for pressure transducers.

In order to attach a wind tunnel model to the MTA, a sting had to be designed to attach to the MTA wrist and support the model in the tunnel. In many dynamic wind tunnel experiments force and moment data is desired relative to motions about the aerodynamic center or quarter-chord of a wing. The sting, shown in Figure 30 was designed with the intent of performing pitch oscillations and pitch-plunge oscillations. In order to significantly reduce the complexity of the maneuvers, the sting was designed to place the quarter-chord of the model coincident to the wrist roll axis of rotation, enabling pitch oscillations using only the wrist roll motor and controller. Provided the wings of the model were mounted perpendicular to the wrist face, the sting design was not critically impacted by the plunging motion. However, due to the diameter of the hole cut in the window of the tunnel, it was important to keep the MTA links a safe distance from the tunnel. Lengthening the sting provided slightly more maneuverability in the wind tunnel's translational directions up/down and forward/backward by keeping the MTA links outside the tunnel.
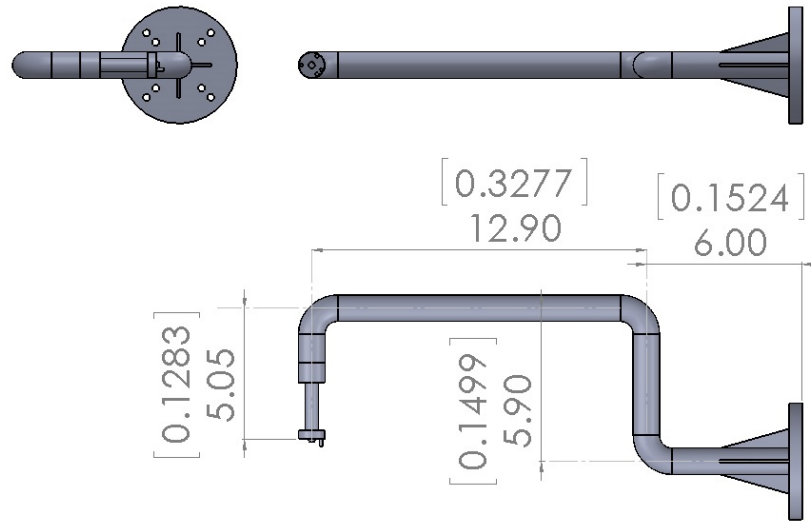
Figure 30. The sting was designed to attach the model to the MTA such that the quarter-chord of the model was in-line with the center of the wrist face.The units displayed in the figure are [meters] and inches.

Three bends, presented in Figure 30, were desired for the sting in order to support the model from the leeward side. The sting members are 1 in diameter, stock aluminum. The 1/2 in thick base was welded to the clocked members to 1/1000 in precision. The sting weighs 1.355 kg. The most leeward member of the sting was placed a reasonable distance from the trailing edge of the wing in order to not greatly influence the flow. Material was removed from the end closest to the model to allow access to tapped holes corresponding to the force balance. Two dowel pins, shown in Figure 31 were placed on the face of the model-end to align the force balance during assembly. The opposite end the sting is secured to the MTA using eight 1/4 in machine screws.
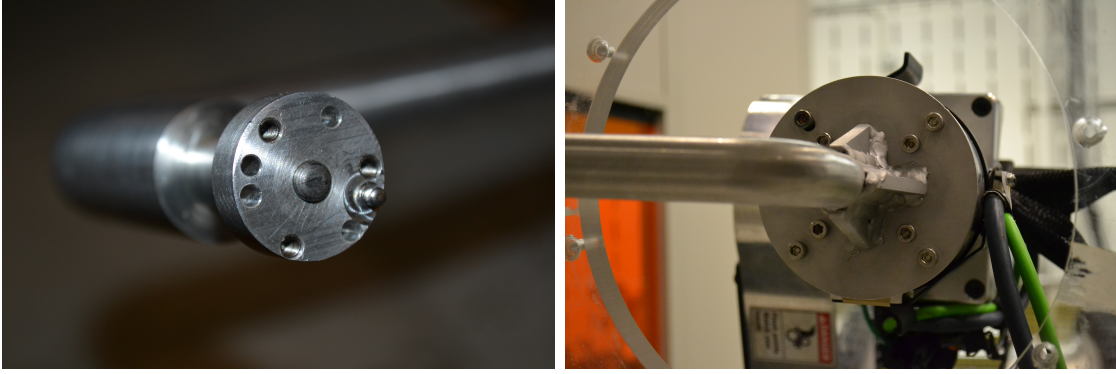
Figure 31. The dowel pins (left) on the model end of the sting ease properly mounting the model or force balance to the sting. At the other end of the sting (right), the sting is attached to the MTA using eight $1/4\,$in machine screws.

3.5 Integration with the Wind Tunnel

The MTA was originally designed for UF-REEF low Reynolds number Aerodynamic Characterization Facility (ACF) [2], which is larger than the AFIT Low Speed Wind Tunnel. The MTA was designed to operate within the UF-REEF's open test section wind tunnel. Since the test section at AFIT is smaller and closed, the MTA arm was extended into the tunnel through a circular hole in the Plexiglas window on the side of the test section, shown in Figure 32. While this does limit some of the larger motions originally intended for the MTA, valuable research is still expected from the MTA system, used in combination with the AFIT Low Speed Wind Tunnel.
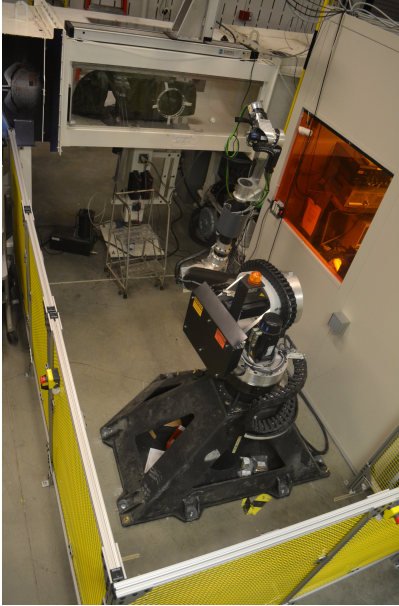
Figure 32. The MTA in its current location relative to the AFIT wind tunnel.

Positioning the MTA.

Originally, the MTA was positioned with its base approximately 3.143 m from the window of the wind tunnel's test section. In series of tests performed during the summer of 2014, this position proved to be problematic possibly due to the large moment arm acting on the shoulder pitch joint. In order to execute the trajectories with the model in the tunnel, the MTA arm was nearly extended to its maximum length. Performing small, precise joint movements, similar to those involved in a small amplitude (± 5 cm) plunge oscillation, proved difficult due to the shoulder and elbow pitch joint motors' unsatisfactory compensation for the inertial forces like gravity. In October 2014, the base was moved approximately 0.592 m closer to the test section. This allowed for larger rotations and increased angular velocities to accomplish the trajectories. However, these increased angular velocities were far from the limits of the actuators, leaving room for increased plunging amplitude and/or frequency. For example, during a simple plunge oscillation with an amplitude of 5 cm, in its original

position, the shoulder pitch joint rotated less than one degree from its initial angle. In its new position it rotated $\pm 2°$ from its initial angle. This small difference significantly improved the response of the shoulder pitch joint.

After the MTA was installed in its new location, two motion profiles were initially developed by Dr. Patrick Rowe, from Re2 Inc. With the wind tunnel window open, the following profiles, with increasing complexity, were executed: pitch-plunge oscillation and store separation. Encoder feedback showed that each of these oscillations were qualitatively appropriate but presented unacceptable quantified position and orientation accuracy during their execution. During the 1 Hz pitch-plunge oscillation with amplitudes $\pm 25°$ and ± 5 cm respectively, the mean plunge height was approximately 9 cm greater than the specified height. Some of the position error was attributed to varying phase lag between each of the joints necessary for the plunge motion. The mean pitch angle was approximately 5.5° greater than the desired mean pitch angle. To emulate a store separation, a MTA trajectory file was created to perform a curved motion in a horizontal plane. The prescribed motion was a 90° rotation along a 4 in arc, as shown in Figure 33 (left). While the path was qualitatively reasonable, position error increased as the MTA attempted to move the IUT along the desired path. By the final location, the IUT had traveled approximately 5 cm out of plane, as shown in Figure 33 (right). These findings indicated that enhancements were necessary to improve the position accuracy before conducting wind tunnel experiments. In order to improve the position accuracy during a pitch oscillation, experiments were conducted to characterize the wrist roll motor and controller.
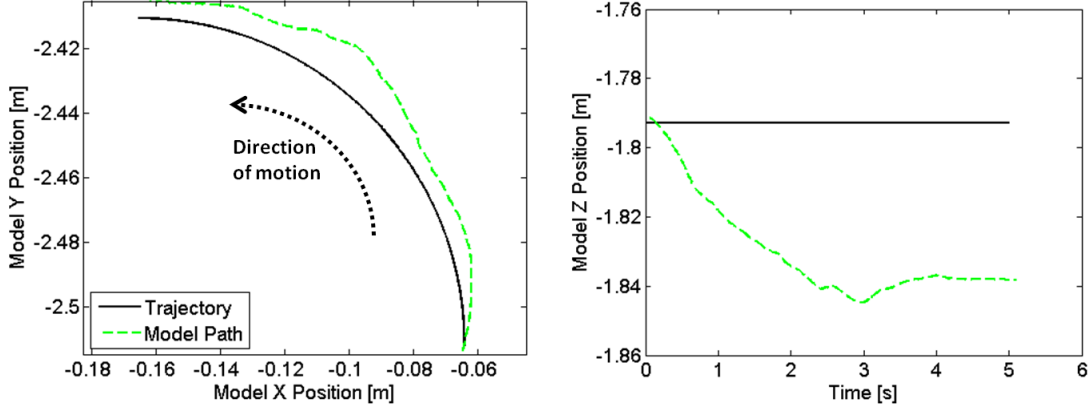
Figure 33. In the new location, the MTA continued to demonstrate unacceptable position and orientation error.

Operational Adjustments.

During operation in the Spring of 2014 an issue occurred where the wrist's pitch motor/controller would not function properly. During a pitch oscillation, which only used the wrist roll joint, the wrist pitch joint dropped under the combined load of the wrist, sting, and model. When the joint is not necessary for the motion, voltage applied to the motor is only enough to maintain the current angle. The controller was found to be defective and the issue was resolved by replacing the ELMO® controller for the wrist pitch motor. This problem did raise concerns about installing delicate sensors, such as a 6-DOF load cell, which can be easily damaged if dropped or overloaded.

When attempting to execute long duration tests, such as a pitch oscillation at 0.1 Hz for 15 cycles, the computer issued a segmentation fault after approximately 75 s. In the source code for the MTA, there are two memory buffers that store joint angle data during execution. However one buffer was only set to record 6000 points, approximately 75 s of data. Therefore the segmentation fault occurred when the computer attempted to write past the end of the memory buffer. The code has since been fixed by Re2 Inc.

60

The final issue discovered during the operation of the MTA was a repeated times-tamp in random outputs. Occasionally an output file would randomly have two Cartesian positions at the same timestamp. It was concluded that this anomaly was a result of two tasks competing for the processor. The Contoller Area Network (CAN) bus which is receiving the encoder measurements loses priority of the processor because of a random process. According to the manufacturer, Re2 Inc., when the CAN bus regains the processor, it reads the first measurement and tags it with a timestamp, and then immediately reads the next measurement and tags the second measurement with the same timestamp. Since there is no way to predict when the CAN bus will lose priority of the processor, there is not a correction for the source code. Therefore, this issue was addressed in post-processing using a Matlab® routine to find the repeated timestamps and remove the first duplicate timestamp and corresponding Cartesian position.

3.6 Defining the Stationary Process

For time-invariant systems, which is a desired attribute of the MTA, a system's output should be repeatable with the same input. This is especially crucial for determining the effect of a modification on an experiment. However, when measurement noise is inherent in the output signal, a number of outputs must be averaged in order to statistically characterize the noise. In order to determine when a noisy signal is stationary, additional output signals must be averaged either temporarily or over the ensemble until the statistics of the signal are not changing significantly. Ensemble averaging is the process of averaging, at each timestamp, the value in each signal across a number of tests. If a signal is periodic, then temporal averaging can be applied. By viewing each signal as a period of a function, the signals can be appended temporally. A stationary process is defined as a stochastic process in which the statistics do not

change with time or with the ensemble. Furthermore, the statistics of the signal such as the mean, standard deviation, and correlation of the combined signals have no significant changes. While the reality of mechanical systems is that the output will not be exactly repeatable every time, the MTA sometimes demonstrated significant deviations from run-to-run with an identical input file.
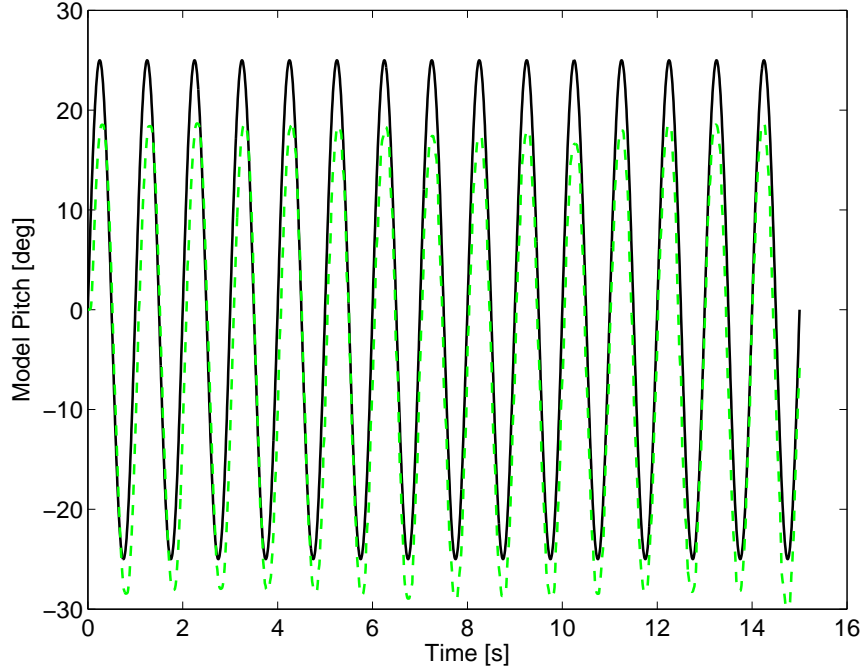
Figure 34. 25°, 1 Hz **trajectory (solid, black line) used in the stationary process experiments with output from the wrist roll encoder (dashed, green line).**

A 1 Hz pitch oscillation with a 25° amplitude about 0° pitch was repeated; each trajectory was 15 s. The necessity of this study can be seen in Figure 34, where the prescribed motion is presented as the solid black line, while the actual position output from the wrist roll motor encoder is shown with a dashed, green line. In principle, the two plots should be coincident or nearly so. However intermittently, an angle offset occurs and occasionally the amplitude is also inaccurate. Before each test was conducted, the model was homed to $\theta_b = 0° \pm 0.05°$. Homing is defined as positioning the IUT at the position and orientation corresponding to the first timestamp in the

trajectory. Since the output should begin and end at the same angle, the signals were temporally averaged. Starting with two outputs, the second experiment was appended to the first experiment and the statistics were calculated for the combined signal. Then the third output signal was appended to the combined signal and its statistics were calculated. The statistics of the previous combined signal (outputs 1 and 2) and the new combined signal (outputs 1, 2, and 3) were compared for significant changes. If there are no significant changes, the process is said to be stationary after two signals are averaged. If there are significant changes, the next output is appended onto the combined signal and its statistics are calculated. The comparison of the previous combined signal statistics (mean and variance) and the new combined signal statistics is analyzed for significant changes. These operations were repeated until there were no significant changes in the statistics of the combined signals. A total of 20 tests were conducted. Any atypical results, as presented in Figure 35, were noted but excluded from the analysis and that test was repeated. The removal of atypical results did not hinder the characterization of the MTA wrist motor/controller system, since experiments where atypical responses occur would not show significant aerodynamic data for analysis. Atypical response were rare and only occurred, on average, 1 out of every 35 tests conducted. The cause of an typical response is still unknown at this time.
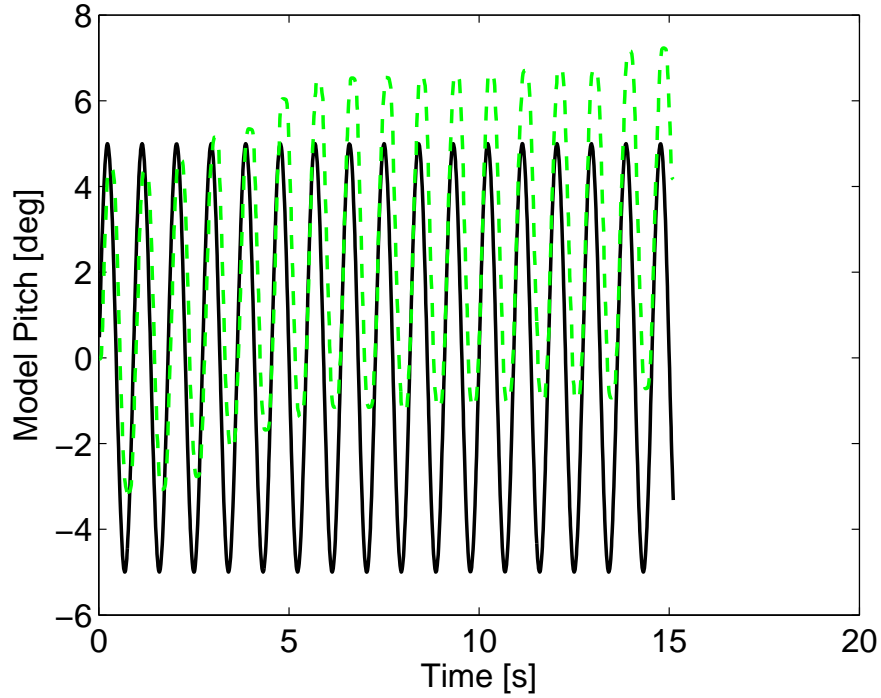
Figure 35. Example of an atypical result (dashed, green line) for given a trajectory (solid, black line)

3.7 Modeling the Wrist Roll Motor and Controller

After determining the number of tests required for a stationary process, the MTA's wrist roll motor and controller (the wrist roll system) was characterized. A linear model was initially used to characterize the wrist roll motor/controller. However the linear model was unsuccessful since it did not capture some of the nonlinear behavior exemplified by the system. The second attempt used a test envelope of varying sine wave frequencies and amplitudes shown in Table 7. Using only the wrist roll system, sine wave pitch oscillations were conducted about the model's quarter-chord. Ten tests were conducted at each test point in the envelope. Each trajectory lasted for the longer of two time lengths: 15 s or 15 periods.

Since the results of this experiment are likely to be dependent on the forces and moments acting on the MTA, it is important to have the sting and model attached to

Table 7. The 21 frequency-amplitude pairs tested using, pitch oscillations to characterize the performance of the wrist roll motor and controller.

Amplitude [deg]	Frequency [Hz]						
5	0.3	0.5	0.7	0.9	1.1	1.3	1.5
15	0.3	0.5	0.7	0.9	1.1	1.3	1.5
25	0.3	0.5	0.7	0.9	1.1	1.3	1.5

the MTA. As stated in Section 3.6, atypical results were removed from the analysis. Those tests were repeated to ensure there were ten unique results for each frequency-amplitude pair. Each test was executed after the wrist was homed to $\theta_b = 0°\pm0.05°$. Using the procedure established in Section 2.6, each test point's ten results were ensemble averaged to determine the signal bias, or mean pitch angle. Then, values for the extrema were acquired. For each complete period the absolute values of the two extrema were added. This Peak-to-Peak (P2P) value was then averaged over the number of periods. For frequencies greater than $1\,\mathrm{Hz}$, there were more than 15 peak-to-peak amplitudes included in the average. Next the phase lag of the output to the input signal was calculated. The phase lag was calculated using the dot product of the two signals, as shown in equation (49).

3.8   Proportional Control for Improved Performance

Once the statistics of the wrist roll system were determined, it was deemed prudent to improve its performance using feedback control. For the remainder of this section the initial wrist roll system (the motor and controller) is described as the open-loop system. In order to improve the performance of an open-loop system, negative feedback sends the current joint angle back to the MTA Computer where it determines the error between the current joint angle and the desired joint angle. The computed error is multiplied by a programmable gain value. As the gain increases, the error is reduced quicker. However the proportional gain must be tuned to avoid instabilities

especially at higher frequencies.

Two test points in the previous test matrix for the open-loop system were found to be the poorest performing based on the statistics of the open-loop system. At 5° amplitude and 0.3 Hz, the mean pitch angle was close to 0° but the output signal experienced approximately 26% amplitude attenuation. At 25° amplitude and 1.5 Hz,the mean pitch angle had a 23% error while the normalized amplitude was approximately 93%. Closing the loop with negative feedback improved both of these issues. Three proportional gain values were tested at each of the test points described above. Ten tests were conducted with each of the proportional gains, and one atypical test was removed and repeated. Statistics were calculated using the same techniques developed in Section 2.6. The gain that provided the best overall improvement at the test points was chosen for evaluating the closed-loop system's performance in the test matrix from Section 3.7.

3.9 Evaluation of the Closed-Loop System

After the proportional gain was finalized, the performance of the closed-loop system was evaluated. The test matrix from Table 7 was repeated using the closed-loop system. Using the same methodology described in Section 2.6, the statistics were calculated to quantify the improvements. Nine atypical results were removed from the evaluation and the model's pitch angle was homed to 0°±0.05° before each test. As with the previous testing, the sting with the model was attached to the MTA during evaluation.

3.10   Secondary Position and Orientation Sensor

Figure 36. The Inertial Measurement Unit (IMU) determines the Euler angles using triaxial gyros, triaxial DC accelerometers, and triaxial magnetometers.

In order to ascertain sting rigidity and aeroelastic affects, an IMU, shown in Figure 36 was attached to the sting just behind the model as shown in Figure 38. Furthermore the IMU was used to corroborate the Euler angles calculated by the MTA Computer. The Microstrain® 3DM-GX1 IMU uses triaxial gyros, triaxial DC accelerometers, and triaxial magnetometers to track its orientation. Its embedded microprocessor contains a programmable filter algorithm, which blends these static and dynamic responses in real time. The IMU uses the combined information of the triaxial magnetometer and triaxial DC accelerometer to calculate its static orientation. During motion the IMU relies mostly on the triaxial gyroscopes to calculate the dynamic orientation. Using proprietary algorithms, the three sensor signals are combined to provide smooth, accurate data collection according to the manufacturer. The IMU was connected to a laptop computer dedicated to its operation during the experiments. A serial-to-USB cable connected the IMU to the laptop. Commands were sent to the IMU using a Matlab® GUI program developed specifically for the IMU by Cobb making use of the existing routines provided by the IMU manufacturer [4] [1]. These Matlab® were further modified by the author to meet the specific needs for use with the MTA. The IMU is specified to be capable of digitally reporting the Euler an-

67

gles at 100 Hz. However this is only theoretically possible if the sampling mode is set to "continuous." Continuous mode does not allow Matlab® to send commands while sampling. Instead using the "polled command" mode, the maximum sampling rate achievable is approximately 22 Hz. This sampling frequency was achieved while operating the Matlab® program in "Silent Mode," which suspended the screen updates until the test was finished.
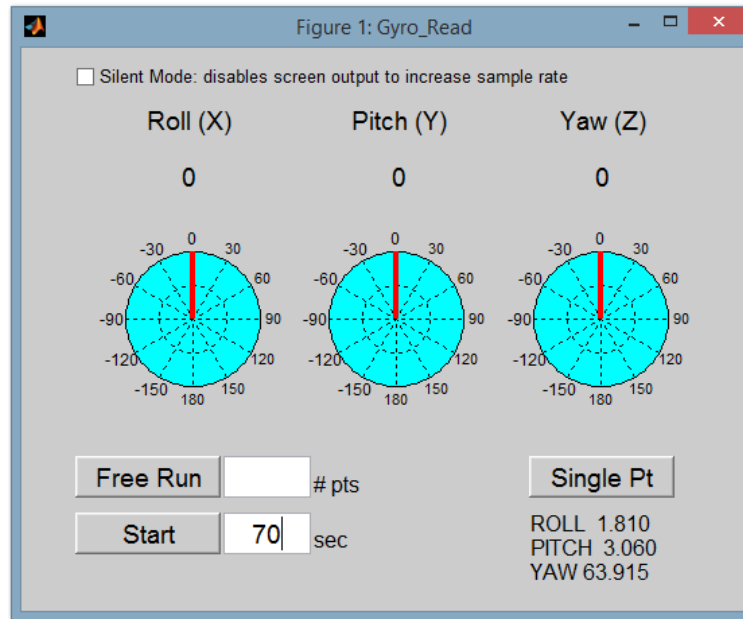
Figure 37. This Matlab® program reads and displays the Euler angles measured by the IMU.

The graphic interface for the developed Matlab® program is shown in Figure 37. The Euler angles are displayed in near real-time. At the end of each execution, the program plots the Euler angles and allows the operator to save the recorded data for post-processing. This program, *IMU Front Panel.m*, is capable of running for a set amount of time, individually sampling, and free running. At this current time, it is manually triggered by the operator from the dedicated laptop computer, so the IMU Program is not synchronized with the MTA Computer. Typically the program was initiated about 5 s before the trajectory executed and collected data for the duration

of the trajectory and 5 s of dead time after the trajectory. The IMU data was generally time-shifted during post-processing in order to match the MTA Computer output as a first approximation.

3.11   Validating MTA Output

As stated in Section 3.1, after the trajectory is executed, the MTA Computer uses the recorded joint angles from each timestamp to calculate the Cartesian position of the model. In order to confirm reliability of the forward kinematics, an IMU was attached to the sting, as shown in Figure 38, during dynamic testing. As mounted, the IMU axis system is rotated from the body-fixed and MTA-model axis systems. When comparing MTA and IMU data, it is necessary to associate the correct Euler angle from the IMU or MTA with the respective Euler angle in the body-fixed system.
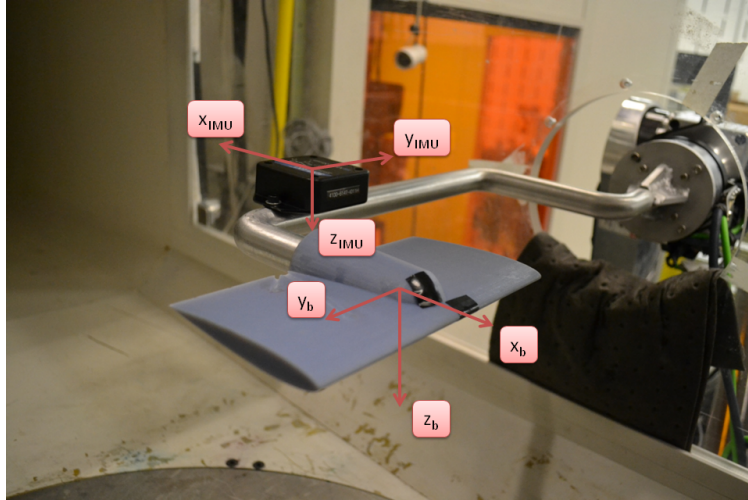
Figure 38. The IMU is attached to the leeward side of the sting in order to not interfere with the wind over the wing.

Possible discrepancies could be associated with inaccurately calculated Cartesian positions or due to the sting flexing during oscillations. Initially, the model's straight-and-level position was estimated assuming that the wind reference frame and MTA-inertial reference frame had coplanar x-y planes ($\theta_w = \phi_i$ and $\phi_w = \theta_i$). Static tests

69

were first conducted to determine the drift and noise of the sensor over time. The Matlab® program *IMU Front Panel* was set to calculate the Euler angles while the IMU was completely still. Each test lasted approximately 120 seconds. The IMU was set on the sting during this phase of testing because that would be the location of the IMU when most of the data will be recorded for other testing.

Next, static tests were conducted to establish the MTA-inertial angles necessary for straight-and-level flight relative to the wind tunnel, and the model was leveled with respect to the wind tunnel. The IMU was centered on the floor of the wind tunnel, and the markings on the wind tunnel were used to align the IMU with the wind direction. The wind tunnel floor was assumed to be level ($\phi_w \approx \theta_w \approx 0$). These Euler angles were recorded for later use when taring the sting for straight-and-level relative to the wind tunnel. After the IMU is calibrated for straight-and-level, dynamic tests were conducted to validate the calculated Cartesian positions.

Dynamic oscillatory pitch tests were conducted with frequencies of $0.3\,\mathrm{Hz}$, $1.1\,\mathrm{Hz}$, and $1.5\,\mathrm{Hz}$ and amplitudes respectively $\pm 5°$, $\pm 15°$, and $\pm 25°$. The wind tunnel was not operating during these tests. These trajectories only require the MTA to activate the wrist roll motor. Therefore the only angle that should be changing with time is ϕ_i. If the sting is tilted or askew from straight or the sting is flexing during the motion, then the IMU records oscillations occurring in more than one axis. However, assuming that the sting is rigid, the IMU remains at a fixed distance from the axis of rotation. These results were analyzed to determine if the sting remained rigid and to validate the calculated Cartesian positions.

3.12   Data Acquisition System and Aerodynamic Sensors

All aerodynamic load signals were acquired using the NI® Data Acquisition (DAQ) system. This system is housed in the PXIe-1078 chassis. The DAQ system is designed

to run as a remote system for later applications with a MAV flight test feedback system designed by Calspan®. The controller communicating to the Windows® computer is the PXIe-8133 using Ethernet protocol. Attached to slot 6 of the chassis, shown in Figure 39, is the DAQ Card: PXI-6123. This card allows for the simultaneous sampling of up to 8 analog signals, such as voltage, at speeds up to 500 kilo-samples per second.
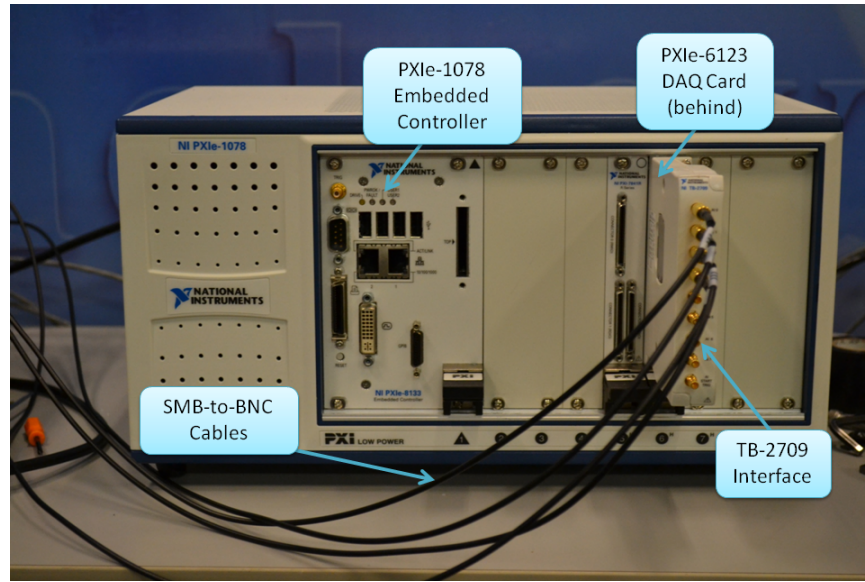
Figure 39. The NI® data acquisition (DAQ) system is used to acquire the voltage signals from the force balance or pressure transducers.

Attached to the PXI-6123 card is an interface, TB-2709, between the DAQ card and the analog signals. The interface's protocol requires SMB plugs to read in the analog signals. The Labview® Virtual Instrument (VI) file is created on the Windows® computer, shown in Figure 40, and passed to the PXIe-8133 Controller to carry out the operation. The number of samples and sampling frequency are set using the VI-file.
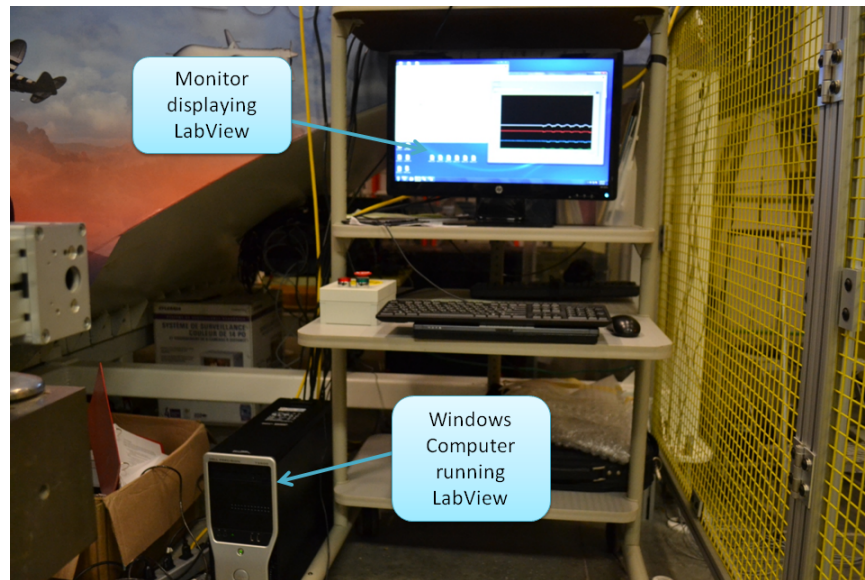
Figure 40. This runs LabView® and communicates to the remote DAQ controller using Ethernet protocol.

Two types of aerodynamic sensors were acquired for measurements of aerodynamic data. The ATI® Nano25 Six-Axis Force/Torque Transducer, presented in Figure 41, is a monolithic structure which uses three stainless steel sensing beams to sense the applied force and torques. Semiconductor strain gages are attached to each beam. These strain-sensitive resistors, connected through a Wheatstone bridge, determine the strain in the beam based on the change in resistance.
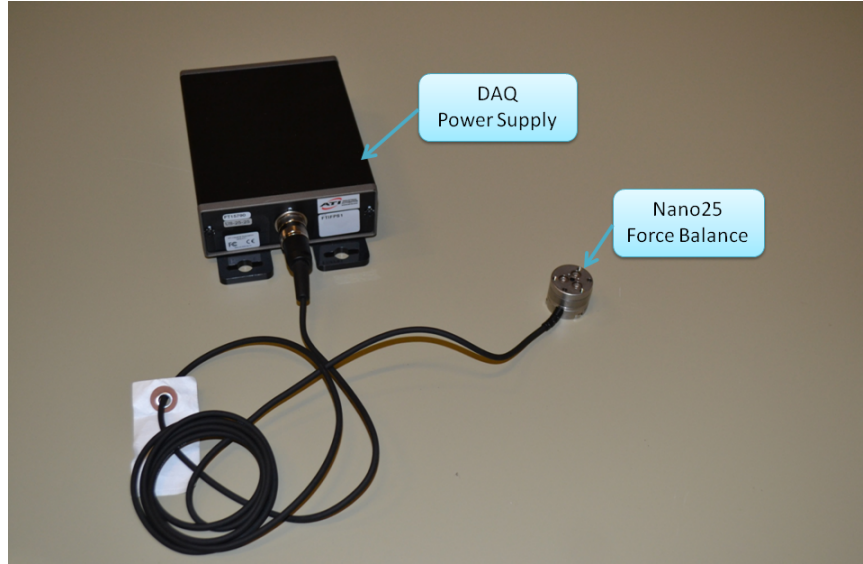
Figure 41. The Nano25 force balance and off-board power supply.

The transducer measures 25 mm in diameter and 21.6 mm thick. Table 8 shows the sensing range and measurement resolution corresponding to the axis system in Figure 42. Both the mounting side and tool side are capable of being clocked and attached to a sting and model, respectively. The power is supplied to the transducer by an off-board power supply which reduces the required size of the actual force balance.
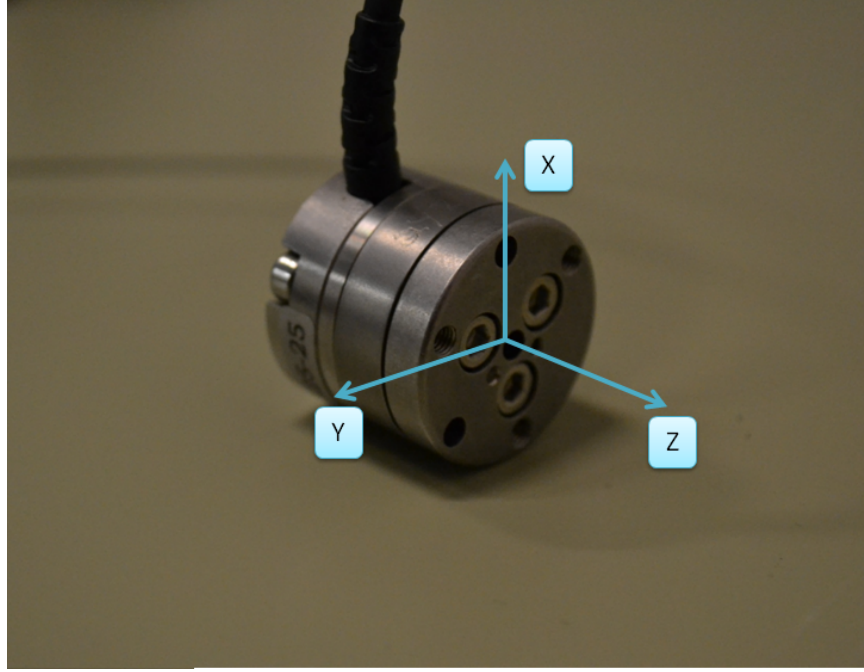
Figure 42. Nano25 axis system.

Table 8. The sensing ranges ($\pm$) and resolution are in accordance with Calibration US-25–25.

	F_x,F_y	F_z	T_x,T_y	T_z
Sensing Ranges [lb_f, lb_f-in]	25	100	25	25
Resolution [lb_f]	1/112	3/112	1/80	1/160

ATI$^®$ transducers have been used for numerous applications including use as a sensor for control feedback in a robotic arm. By attaching the transducer in-between the robotic manipulator and the tool, the robot can sense how much pressure it is applying for welding. The robot controller can adjust the amount of pressure applied in order to perform a consistent weld [41].

Figure 43. The Endevco®, Model 8515C-15, pressure transducer (left) is mounted on the wing using bee's wax and electrical tape to secure the wires. The pressure transducers are connected to the Endevco® DC Differential Voltage Amplifier, Model 136 (right).

The second type of aerodynamic sensor acquired were four Endevco®, Model 8515C-15, piezoresistive pressure transducers. These were used to record absolute pressure readings at four locations on the wing of the model. Each sensor, shown in Figure 43, measures 6.30 mm in diameter and is 0.76 mm thick. The pressure transducers provide approximately 0.010-0.015 Volts per 1 Volt of excitation and are rated up to 180 kHz. The absolute pressure range is 0 to 15 psia. Their small size makes them ideal for flush-mounting on a curved surface such as a wing. Each pair of pressure transducers are connected to an Endevco® Model 136, DC Differential Voltage Amplifier. The two Model 136 units provide each transducer with 10V excitation. The output of the transducer is passed through a 10 kHz low-pass filter and is amplified to produce an output of 200mV/psi. The output of the amplifiers is connected to the PXI-6123 card for signal acquisition.

3.13 Incorporation of Dynamic Pressure Measurements

With the secondary position sensor properly configured and the MTA wrist roll closed-loop system finalized, pressure transducers were attached to the NACA 0012 wing at the mid-span. Two sensors were flush-mounted on each surface of the wing
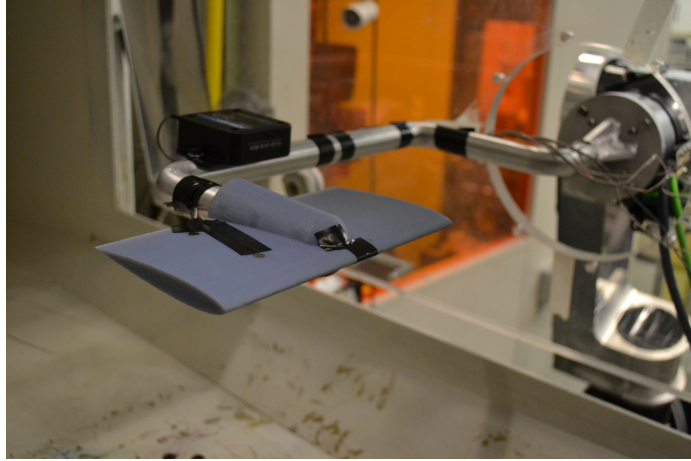
Figure 44. The pressure transducers are attached to wing and the IMU is screwed into place on the sting.

(top and bottom) at the quarter-chord and three-quarter-chord of the mid-span. These cavities were precisely cut such that the surface of the transducer was tangent (flush) to the surface just in front of the cavity. The wires of each transducer followed a groove path towards the center of the wing's trailing edge and were covered with electrical tape to ensure they did not move during testing.
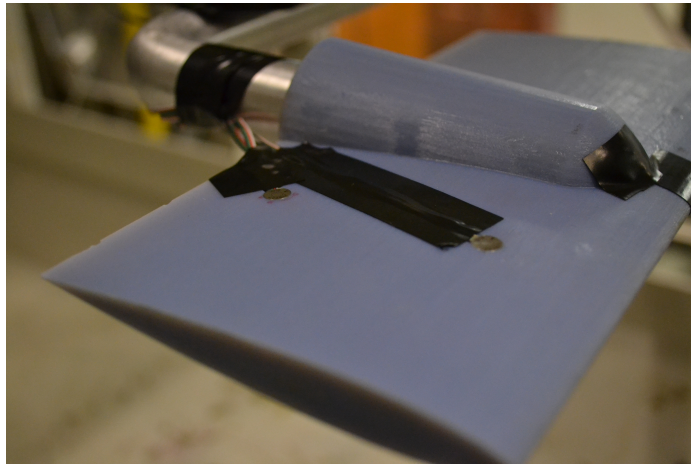
Figure 45. The pressure transducers are held in place with bee's wax and the wires taped below the surface in a groove. The wires then trace the sting out of the window tunnel.

The wires follow the sting out of the wind tunnel window and attached to the amplifier cables outside tunnel, as shown in Figure 46. Having the connections inside

76

the tunnel caused interference in the signals. The cables were taped to the window's handle and given slack. This ensured that the cables were not under tension while the pitch oscillation occurred. This same procedure was followed for the IMU cable.
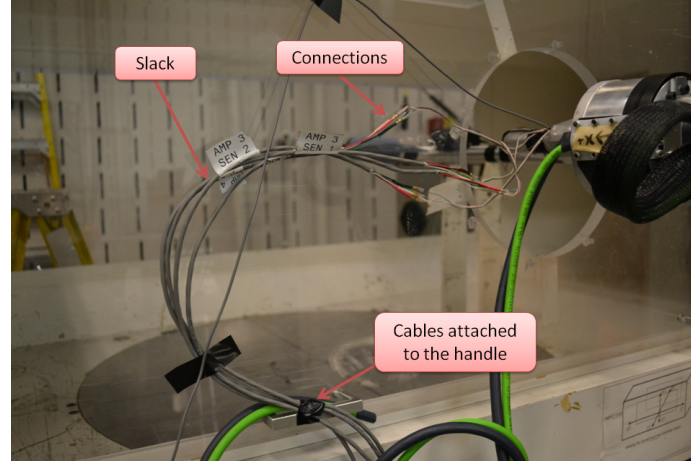
Figure 46. The cables are attached to the handles to ensure there is no connections. Slack was given between the handle and the sting to allow for movement.

LabView® was set to record the pressure transducer signals at a 1 kHz sampling rate. The DAQ was manually triggered slightly before the trajectory began. The pitch oscillation was performed with one frequency, 1.0 Hz, at three amplitudes, $\pm20°$, $\pm30°$, and $\pm50°$. The specifications and locations of the pressure transducers is listed in Table 9. The sensitivities are used by the amplifier to determine the pressure from the transducer's voltage signal.

Table 9. This table provides the specifications and locations of the pressure transducer for these experiments.

S/N	Surface	% chord	Amplifier	DAQ Signal	Sensitivity [mV/psi]
K19222	Top	25	3, Sensor 1	V0	13.35
K19227	Top	75	3, Sensor 2	V1	10.73
K19228	Bottom	25	4, Sensor 1	V2	11.20
K19079	Bottom	75	4, Sensor 2	V3	10.52

The intent of the extreme pitch angles was to find evidence of dynamic stall. These tests were the first performed with the closed-loop system and a non-zero

freestream velocity. Preliminary studies were performed to evaluate the closed-loop system performance in the presence of dynamic loading.

3.14   Chapter Summary

Chapter III presented an overview of the design and operation of the MTA. This chapter also discussed the design of the wind tunnel models and sting. After installing the MTA at the AFIT Low Speed Wind Tunnel, preliminary evaluations were conducted using two complex trajectories: pitch-plunge oscillation and store separation. The encoder data from these motions revealed position and orientation inaccuracies which needed to be corrected prior to conducting wind tunnel experiments. In order to correct the pitch orientation inaccuracy, it was necessary to characterize and enhance the MTA wrist roll motor controller. Position feedback was applied to correct signal bias and amplitude attenuation present in the open-loop system. Next, it was important to validate the orientation of the model calculated by the MTA Computer using a secondary, independent position and orientation sensor. Finally, dynamic wind tunnel experiments were conducted to collect limited unsteady aerodynamic data during pitch oscillations.

IV. Results

This chapter discusses and analyzes the findings of the research conducted. Initially, the performance of the MTA was evaluated using three precomputed paths: pitch oscillation, pitch-plunge oscillation, and simulated store separation. These preliminary investigations revealed position inaccuracy which needed to be corrected before conducting wind tunnel experiments. In the sections below, improvements to the wrist roll motor and controller system were made to increase position accuracy. The IMU was evaluated as a secondary position sensor to validate the MTA's Euler angles. Next the MTA's wrist roll motor and controller were modeled using a time-domain technique. This data showed that the system needed a properly tuned feedback controller. After tuning the proportional gain the new closed-loop system was evaluated using the same test matrix. Comparing the results explicitly showed the improvements from the position feedback. The secondary sensor and pressure transducers were incorporated into the experiment to conduct dynamic wind tunnel testing. The data from these experiments were analyzed and conclusions were drawn about the unsteady aerodynamics observed during testing. Necessary intermediate steps and results are described in the sections below.

4.1 Determining the Stationary Process

When noise is inherent in the output of a control system, it is crucial to average a number of output responses together in order to statistically characterize the response of a system. This is done using either an ensemble average or temporal average technique. For the MTA wrist roll motor and controller, henceforth known as the open-loop system, there were large discrepancies between output signals from the same input. Due to these discrepancies, a system's response to an input with a specific

79

frequency and amplitude cannot be characterized with a single test. A stationary process is called an ergodic process if the response of n tests is statistically the same as the response of the next n tests [23]. In order for n tests to be considered a stationary process, the statistics of n outputs must also show negligible difference from the statistics of $n+1$ outputs. While conducting thousands of tests would ensure convergence of the statistics, it was prudent to determine the minimum number tests necessary for good (statistical) results in order to minimize workload. The open-loop system was tested with the same input 20 times. The input consisted of a pitch oscillation at 1 Hz and 25° amplitude. Figure 47 shows the normalized signal bias, or normalized mean pitch angle, as the number of tests averaged is increased. Each bias was normalized by the input amplitude, 25°.
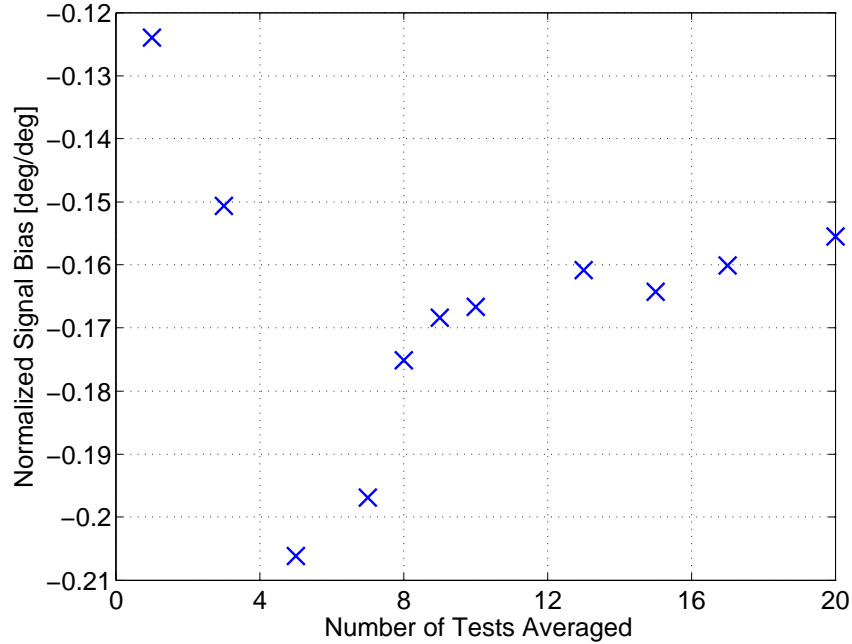
Figure 47. The signal bias, or mean pitch angle, was normalized by the input amplitude and was averaged over n tests.

The tests were ensemble averaged by averaging the data at each timestamp over the number of tests. Since the timestamps of each test were slightly different, the data was interpolated, using the cubic spline technique, from a sampling frequency

of approximately 80 Hz to 125 Hz. This was the same frequency as the trajectory. Matching sampling frequencies ensures that the phase lag can be calculated from the digital signals. The interpolated data was averaged to calculate the signal bias for n tests. If the open-loop system tracked the input, the signal bias would be zero for all tests. This was the first sign that the open-loop system is unable to track a pitch oscillation with the wrist roll motor and controller. As the number of tests was increased, the normalized signal bias converges at approximately -0.16. At least 9 tests are necessary in order to reach the asymptotic limit.

Using the output from the same 20 tests, the normalized amplitude (Figure 48) and phase lag (Figure 49) were calculated to note their statistical variation. Because the output data was not always smooth near the extrema of the sine wave, a specialized peak finding function was created in Matlab® in order to find the extrema of the oscillation. The function computed the first derivative of test signal and searched for where the derivative was changing signs. Based on frequency the function determined the tolerances for "near zero." At lower frequency ($f \leq 0.7$) the tolerance was on the order of 10^{-3}. However, at higher frequencies, the tolerance was on the order of 10^{-2} or 10^{-1}. The peak-to-peak amplitude was normalized by the peak-to-peak amplitude of the input oscillation. Considering Figure 48, the normalized amplitude, converges after approximately 9 tests as well. Meanwhile, the phase angle did not appear to converge, but an ergodic process only requires that the correlation (or phase angle) be finite. While fixing the phase lag is not an objective of this research, it is necessary to fully describe the input-to-output relationship.

Figures 47–49 demonstrate that after 9 tests the open-loop system can be approximated by a stationary process. However for the remainder of the experiments 10 tests were performed at each test point. This hypothesis was extrapolated to amplitudes and frequencies around 1 Hz and 25° sine waves, so that the open-loop system's re-
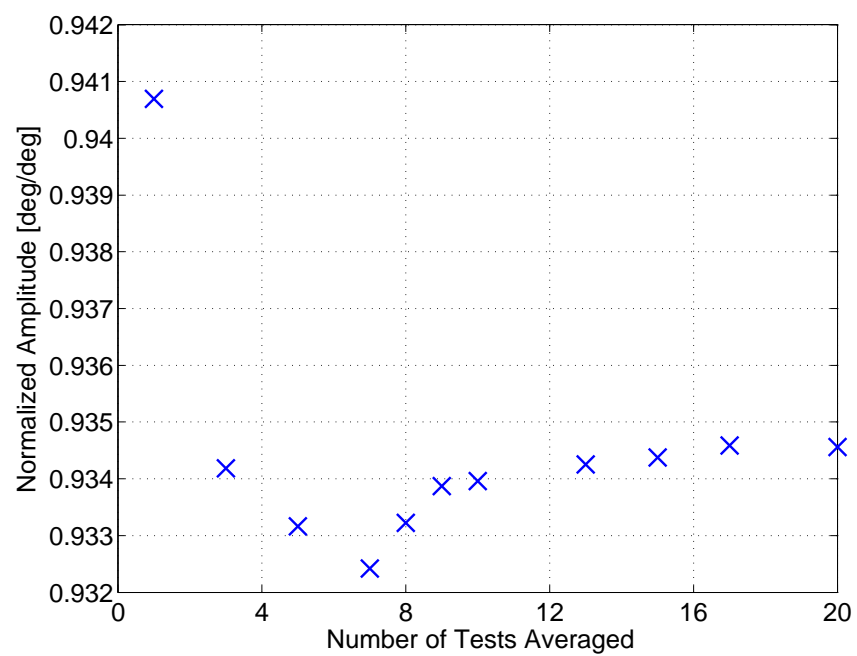
Figure 48. The normalized signal amplitude was averaged over n tests.
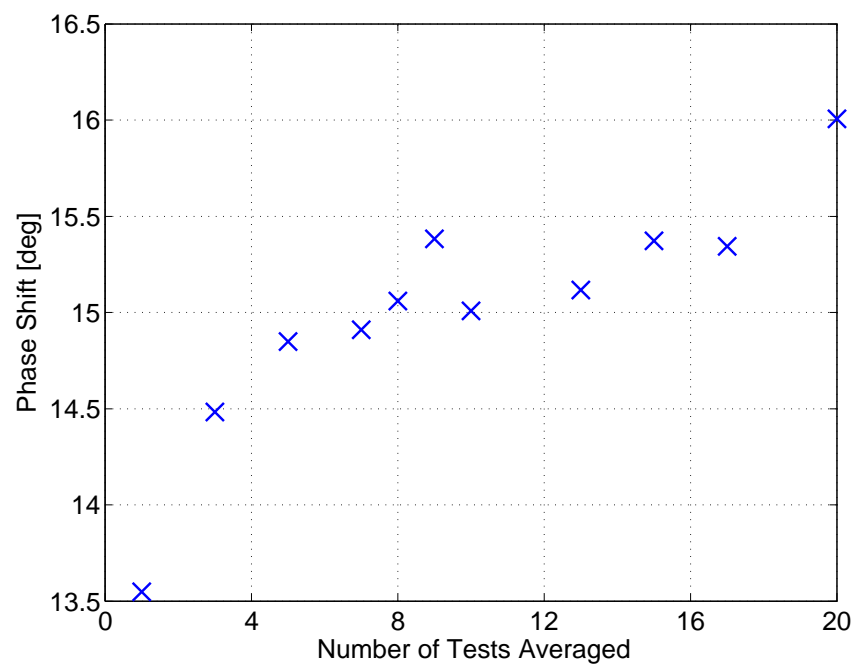
Figure 49. The phase shift was averaged over n tests.

sponse to an input can be characterized by conducting 10 tests at an input frequency and amplitude.

4.2 Wrist Roll System Model

Since the open-loop system violated the homogeneity property of a linear system, it could not be fully characterized using classical linear techniques in either the time-domain or frequency-domain. The MTA wrist roll motor and controller were characterized in the time-domain using sine waves of varying frequency and amplitude. The frequency range was from $0.3\,\text{Hz}$ to $1.5\,\text{Hz}$ at increments of $0.2\,\text{Hz}$. At each frequency the amplitude was varied among $\pm 5°$, $\pm 15°$ and $\pm 25°$. This provided a reasonable test matrix for the characterization of the MTA wrist roll motor and controller. Figure 50 is an example of three of the ten tests that were conducted at each frequency-amplitude pair. The solid black line is the trajectory (or input), and the dashed green line is the model's pitch angle (or output). Graphs of the other test points are located in Appendix A.

Table 10 shows the raw results before normalizing with respect to the input amplitude. In most cases, the phase angle increased as frequency increased. Figure 51 shows the normalized mean pitch angle, or signal bias, as a function of frequency and amplitude. At 10° peak-to-peak amplitude the mean pitch angle is nearly constant. However, at fixed amplitudes greater than 10°, the normalized mean pitch angle moves further away from 0°. Also the sign of the angle becomes negative as the frequency and amplitude increase. The increase in signal bias is possibly a consequence of the transient response of the motor. As the frequency and amplitude increased, the controller increased the command velocity to compensate for zero instantaneous velocity at the start. The increased compensation caused an overshoot as the trajectory began the second half of the cycle.
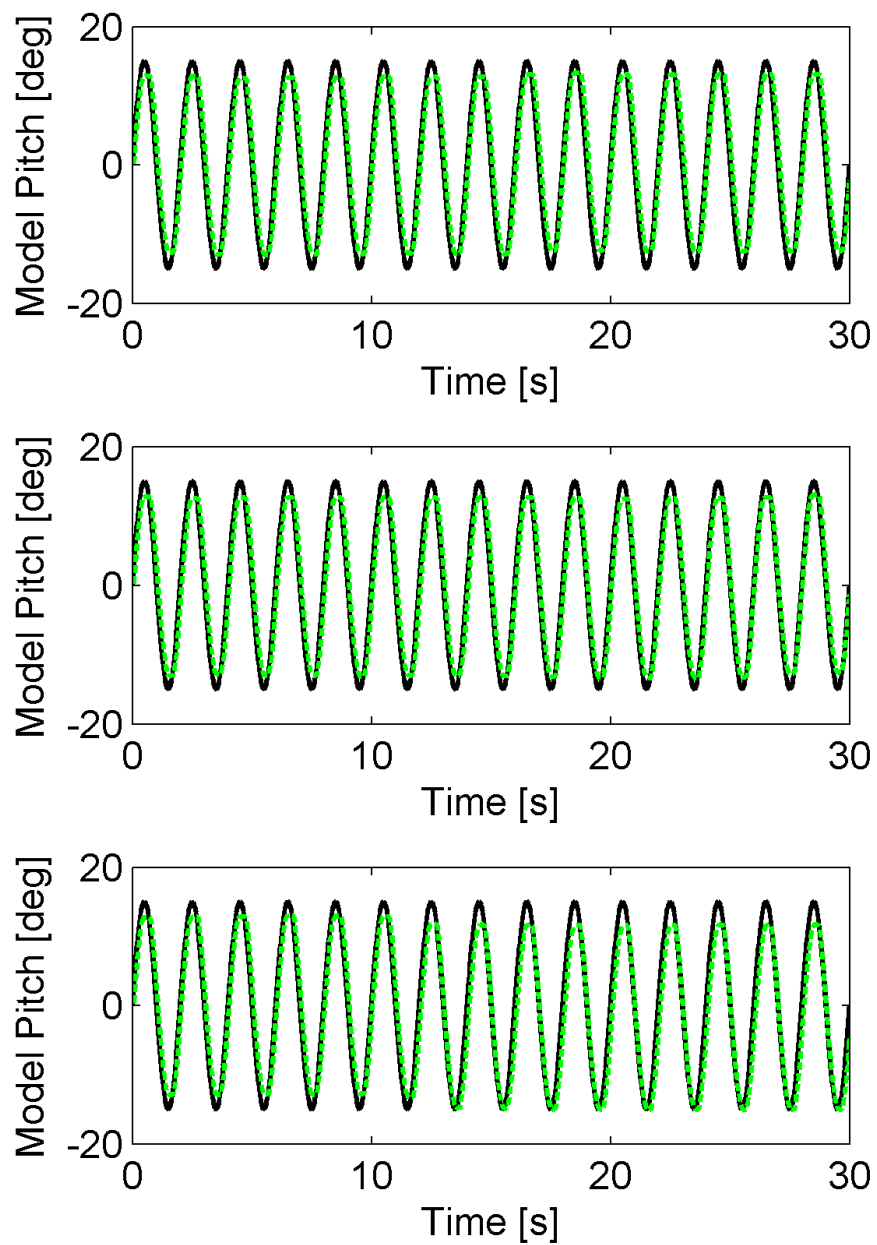
Figure 50. The input-to-output (solid, black line and dashed, green line respectively) relationship for the 3 of 10 tests conducted at $0.5\,\mathrm{Hz}$ and $15°$.
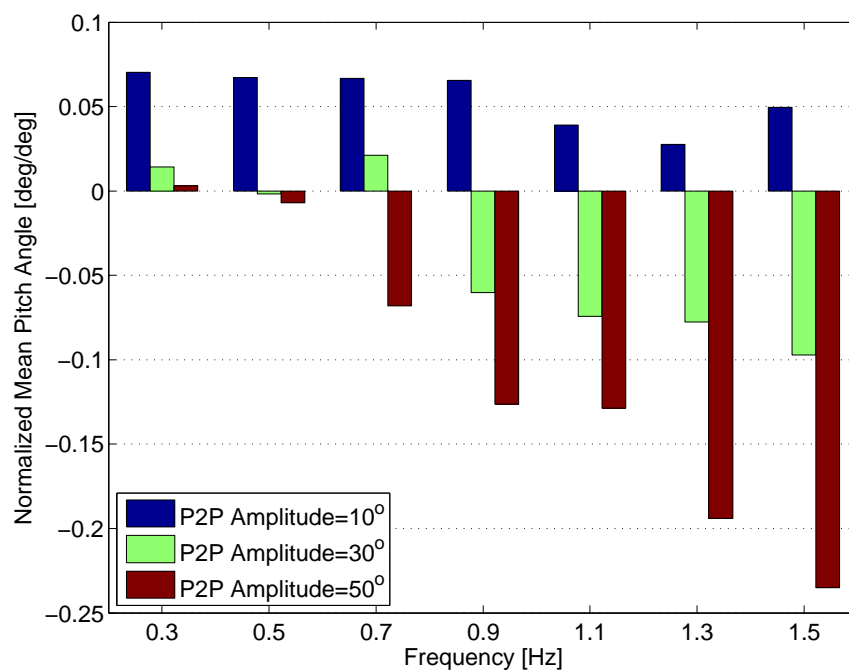
Figure 51. Normalized signal bias was compared by frequency and amplitude.
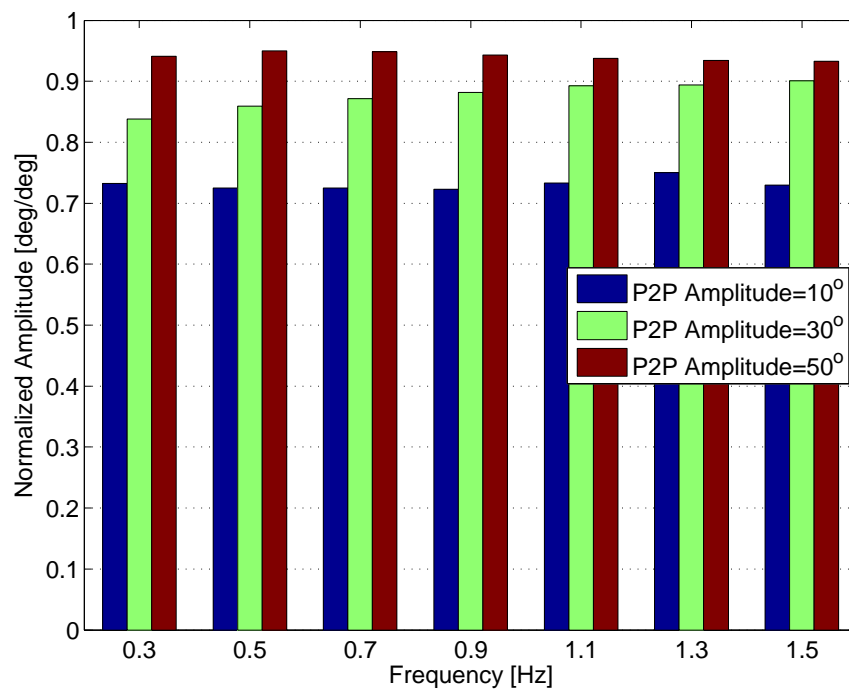
Figure 52. Normalized amplitude for each of the frequency-amplitude pair is compared.

85

Table 10. The raw test results for the open-loop system were averaged over 10 tests at each frequency-amplitude pair before normalizing.

Amplitude [deg]	Frequency [Hz]	Mean [deg]	Peak-to-Peak Amplitude [deg]	Phase Angle [deg]
5	0.3	0.3517	7.3225	14.1510
5	0.5	0.3361	7.2505	18.2337
5	0.7	0.3340	7.2506	21.1847
5	0.9	0.3272	7.2275	25.0474
5	1.1	0.1948	7.3309	23.8850
5	1.3	0.1374	7.5006	17.3587
5	1.5	0.2478	7.2967	30.5601
15	0.3	0.2134	25.1524	9.2667
15	0.5	-0.0251	25.7747	12.0833
15	0.7	0.3163	26.1354	12.7095
15	0.9	-0.9023	26.4602	12.7095
15	1.1	-1.1141	26.7883	16.4615
15	1.3	-1.1633	26.8216	19.8897
15	1.5	-1.4566	27.0230	23.2056
25	0.3	0.0753	47.0555	24.7646
25	0.5	-0.1727	47.4910	5.7329
25	0.7	-1.6993	47.4355	13.5001
25	0.9	-3.1548	47.1699	16.6784
25	1.1	-3.21945	46.8980	23.2600
25	1.3	-4.8505	46.7060	19.7753
25	1.5	-5.8754	46.6383	24.1052

Figure 52 shows the normalized peak-to-peak amplitude as a function of frequency and amplitude. The output peak-to-peak amplitude is normalized by the input peak-to-peak amplitude. In Figure 52, optimum performance is reflected by this ratio being equal to unity. For a fixed input amplitude, the amplitude attenuation was nearly equal. As the input amplitude increased, the amplitude attenuation decreased. The increased performance was likely a result of the increased commanded angular velocity of the motor. With lower input amplitudes, the angle is changing much more slowly near the extrema of trajectory and therefore the commanded velocity is relatively low. It is possible that the commanded velocity does not provide sufficient voltage for the motor to overcome stiction.

Figures 53 and 54 show the same results as Figures 51 and 52 but with error bars representing the limiting cases of the 10 tests. In Figure 53, as frequency was increased, all amplitudes exhibit a wider range of responses. Meanwhile in Figure 54, the open-loop system responded consistently for all frequencies and amplitudes. The open-loop system is characterized by amplitude attenuation at lower amplitude pitch oscillations and greater signal bias at higher frequency, higher amplitude pitch oscillations. The open-loop system also exhibits increased phase angle as the frequency is increased. A feedback loop was added to the `mta` code under the `re2mtaexp` folder to reduce the position error. Reducing the position error will correct the signal bias and amplitude attenuation, but will not correct the phase lag. However, for the pitch oscillation conducted by one joint, phase lag between the input and output will not affect the aerodynamic data. The phase lag is a result of the I/O delay of the MTA Computer and the magnitude of the angular velocity at the first timestamp.
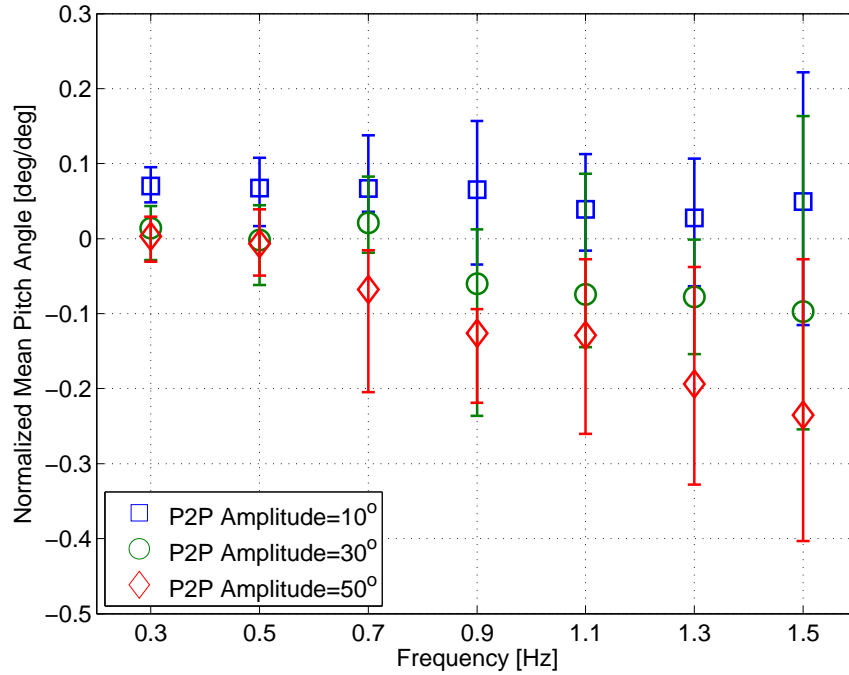
Figure 53. The normalized, mean pitch angle has error bars representing the limiting cases of the 10 tests conducted at each frequency-amplitude pair.

Figure 54. The normalized amplitude has error bars representing the limiting cases of the 10 tests conducted at each frequency-amplitude pair.

4.3   Determining the Proportional Gain

When applying position feedback to an open-loop system, the feedback term must be tuned to provide the appropriate response. The proportional gain is tuned for the best results either to accomplish design requirements or to correct the worst or most important test point. Two locations in the open-loop response were chosen based on their poor performance. With a sine wave input at 0.3 Hz and 5° amplitude, the open-loop system experienced the largest amplitude attenuation (approximately 26%). Meanwhile with a sine wave input at 1.5 Hz and 25°, the open-loop system presented the largest mean pitch angle error of approximately 23%. Three proportional gains were compared to the open-loop response to determine their effectiveness.

Figures 55 and 56 show the results of testing conducted with proportional gain (K_p) values of 0.5, 1, and 1.5. The data was normalized using the same techniques discussed in Section 4.2. The proportional feedback considerably improved the open-

loop system as expected. The magnitude of the signal bias, shown in Figure 55, was greatly decreased by the position feedback. The best results for 1.5 Hz, 25° occurred when the proportional gain equaled one. As the gain increased to 1.5, the magnitude of the signal bias began to increase. The proportional gain had very similar effects on the signal bias for 0.3 Hz, 5°. Similarly the position feedback continued to correct the attenuation as the gain was increased. However as the proportional gain was increased to 1.5, the output corresponding to the 1.5 Hz, 25° input was amplified.
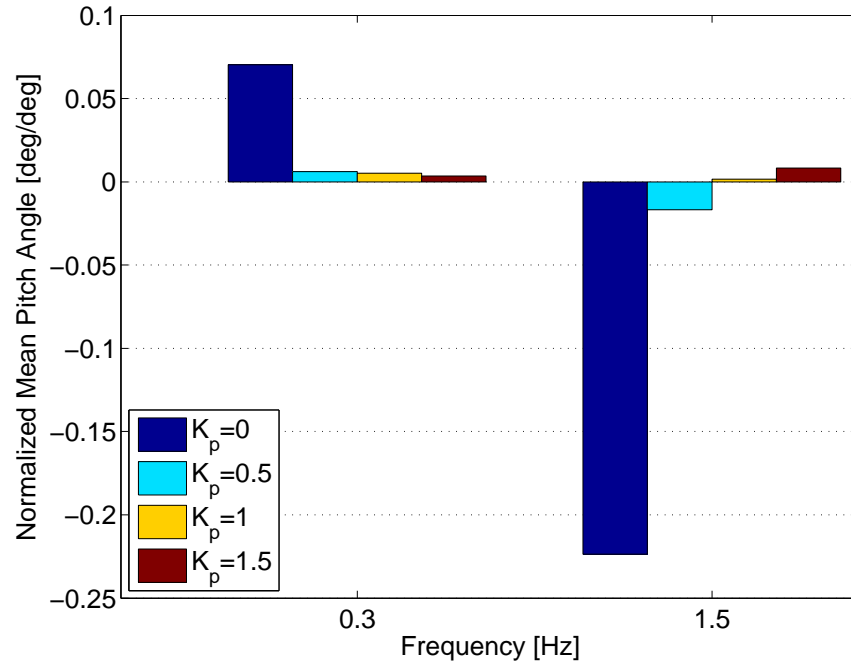
Figure 55. The normalized signal bias is computed for the two test points with three values of proportional gain and compared to the open-loop system.

Once again Figures 57 and 58 show the same data as Figures 55 and 56 but with error bars representing the limiting cases observed. Incorporating the feedback loop compresses the limiting cases for all gain values. Not only were the signal bias and attenuation improved, but the MTA wrist roll motor and controller responded more consistently, albeit with one exception.

The proportional gain value, 1.5, provided the best improvement to 0.3 Hz, 5° input attenuation. However, the value caused greater signal bias and some amplitude
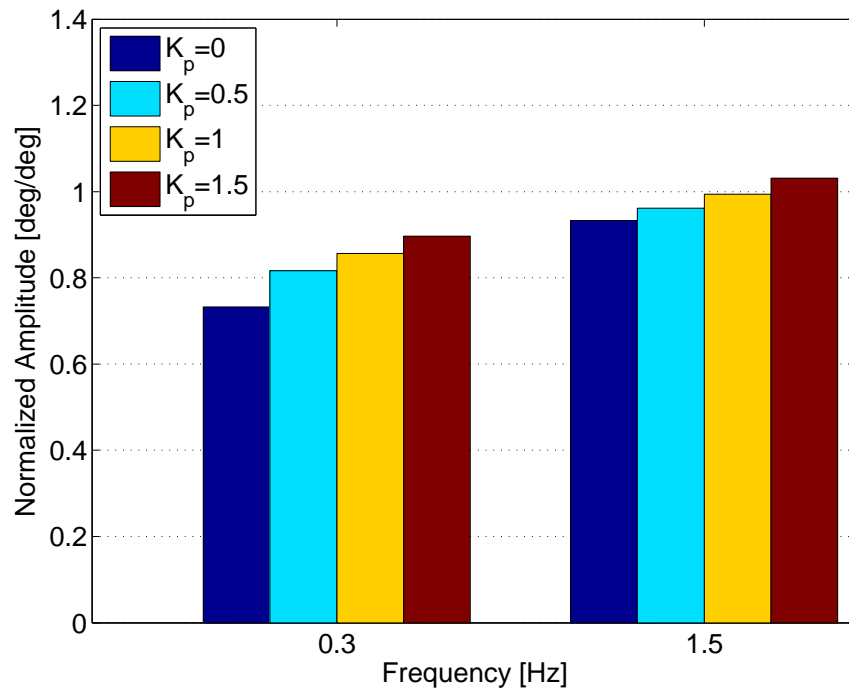
Figure 56. **The normalized amplitude is computed for the two test points with three values of proportional gain and compared to the open-loop system.**
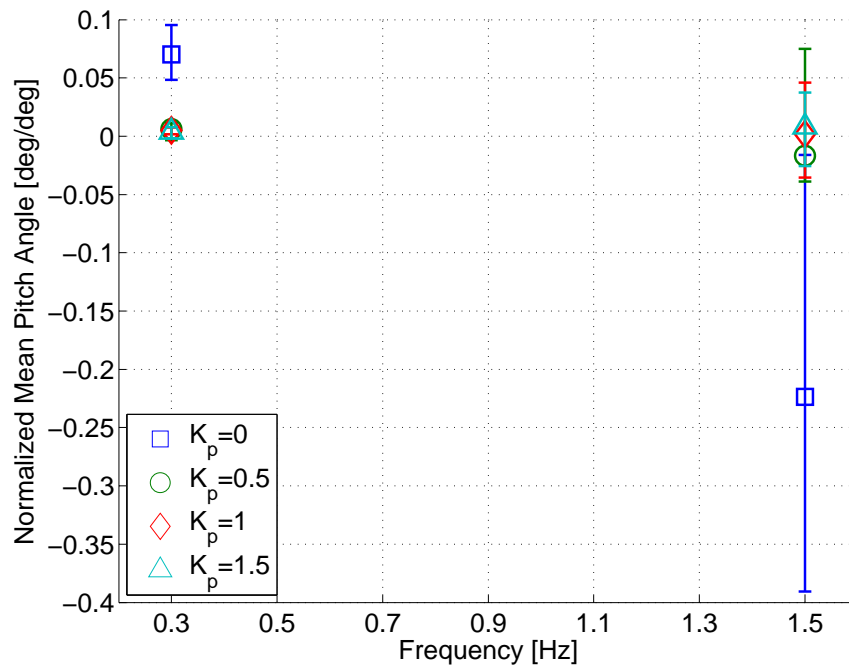
Figure 57. **The compression of the limiting cases of normalized signal bias with position feedback are compared to the open-loop system.**
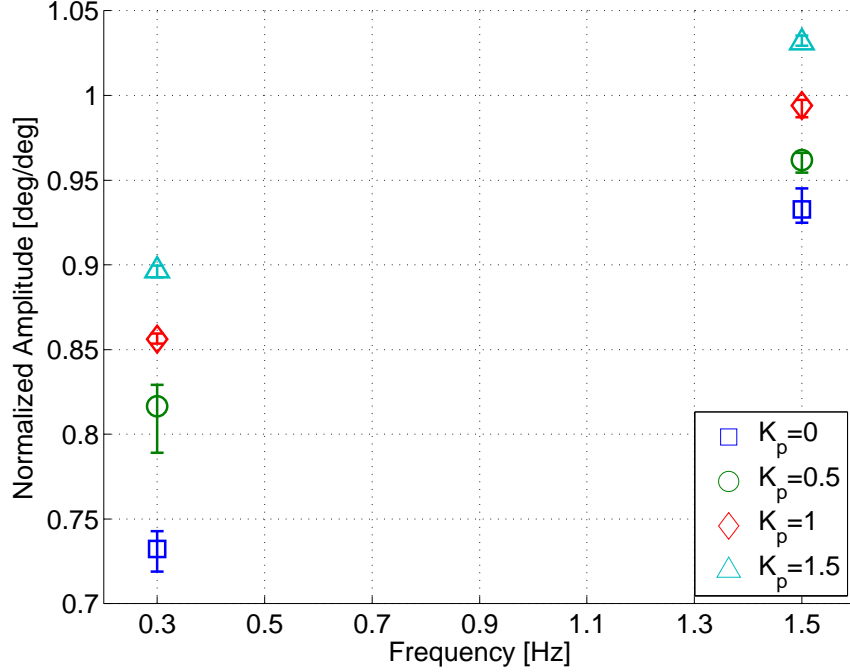
Figure 58. The compression of the limiting cases of normalized amplitude with position feedback are compared to the open-loop system

amplification to the 1.5 Hz, 25° output. The proportional gain value, 0.5, did not provide enough improvement in signal bias or amplitude attenuation. Therefore, the proportional gain was tuned to 1. This value removed the attenuation from the 1.5 Hz, 25° output and provided less signal bias in both cases.

4.4   Evaluation of the Closed-Loop System

Using the proportional gain finalized in the previous set of experiments, $K_p = 1$, the closed-loop system's performance was evaluated using the same test matrix used in Section 4.2. Figure 59 shows three of ten tests conducted on the closed-loop system for the same test point shown in Figure 50. While the improvement may not be clear with visual comparison, Table 11 provides the evaluated results before normalizing with respect to the input amplitude.

As expected, the phase angle increased slightly in most cases. However when
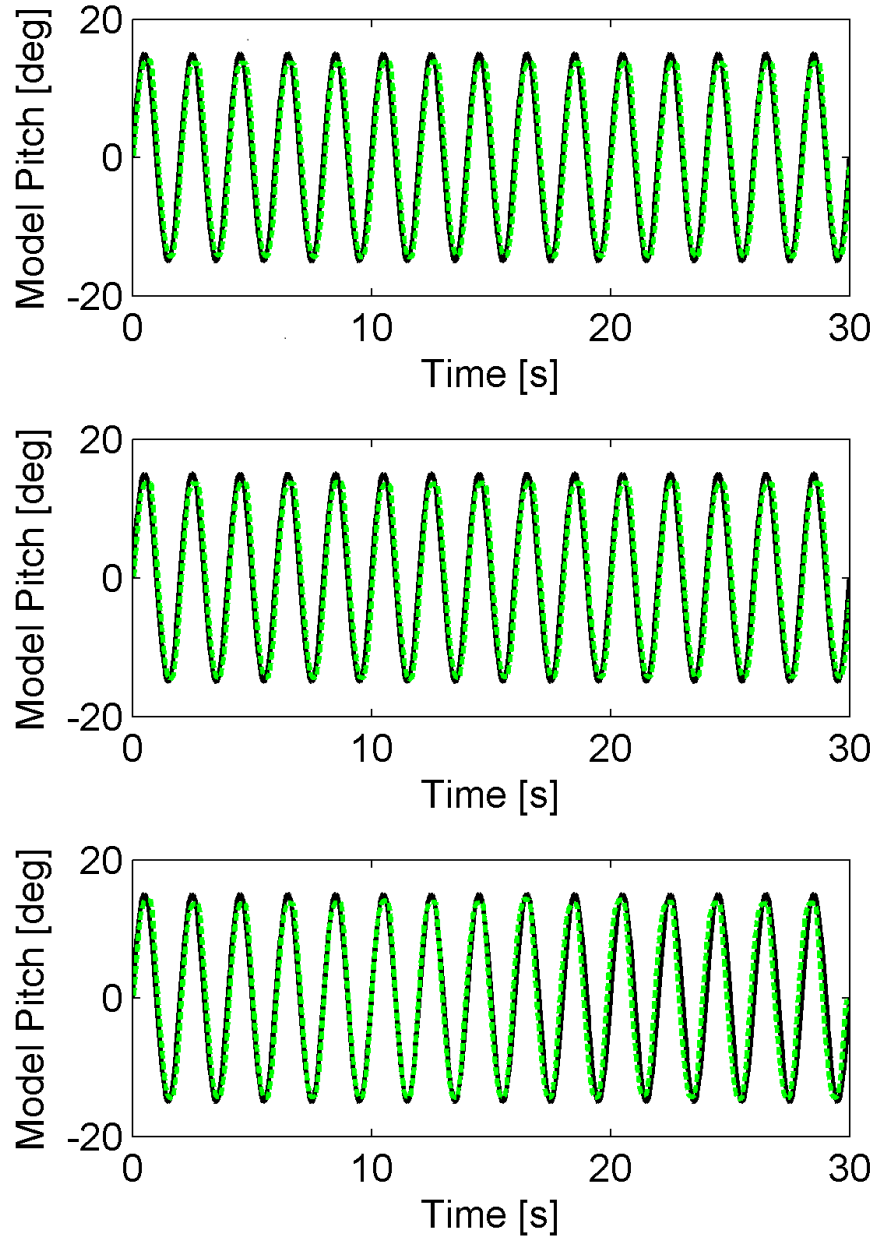
Figure 59. The input-to-output relationship for **3 of the 10 tests conducted at** $0.5\,\mathrm{Hz}$ **and** $15°$ **for** $K_p = 1$.

Table 11. The raw test results for the closed-loop system were averaged over 10 tests at each frequency-amplitude pair before normalizing.

Amplitude [deg]	Frequency [Hz]	Mean [deg]	Peak-to-Peak Amplitude [deg]	Phase Angle [deg]
5	0.3	0.0207	8.5809	15.3560
5	0.5	0.0237	8.1467	20.1263
5	0.7	0.0521	7.9069	22.2498
5	0.9	0.0252	7.7918	23.0258
5	1.1	-0.0114	7.9304	23.5978
5	1.3	0.0284	7.7480	28.8995
5	1.5	0.0100	7.7407	30.5303
15	0.3	0.0082	28.9431	6.7308
15	0.5	3.58E-05	28.0564	10.2726
15	0.7	-0.0023	28.1621	16.1971
15	0.9	0.0368	28.4698	15.9254
15	1.1	-0.0275	28.6890	15.9207
15	1.3	-0.0846	28.6560	23.5320
15	1.5	-0.0742	28.5832	21.6380
25	0.3	0.0195	50.9187	7.9436
25	0.5	0.0502	50.5855	9.7501
25	0.7	-0.0081	50.4545	10.2880
25	0.9	-0.0742	50.3710	13.7205
25	1.1	-0.1612	50.2491	18.1125
25	1.3	-0.4269	50.1299	19.8270
25	1.5	0.2096	49.7915	17.1902

comparing the results from Table 10 to Table 11 there is at least an order of magnitude improvement in the signal bias, but there was less improvement for amplitude attenuation. As it was shown in the previous section, increasing the gain would have improved the attenuation at lower amplitudes but would have over amplified the input at the higher input amplitudes.

Figures 60 and 61 convey the results normalized by the input amplitude. The signal bias for all cases were at least three orders of magnitude smaller than their respective input amplitude. In all cases the normalized amplitude was attenuated less then 25%. All 25° amplitude cases were nearly perfect. In Figure 62, there was a noticeable difference between the limiting cases of the 1.5 Hz, 25° test point

and the limiting cases of the other test points. By incorporating position feedback, the gain margin has decreased, causing instability to creep into lower frequencies. While the test points at $1.5\,\text{Hz}$ demonstrated consistency, there were more atypical experiments that were excluded from these results than experienced by the open-loop system. After conducting the testing on the closed-loop system the improvements were quantified through comparison with the open-loop system.
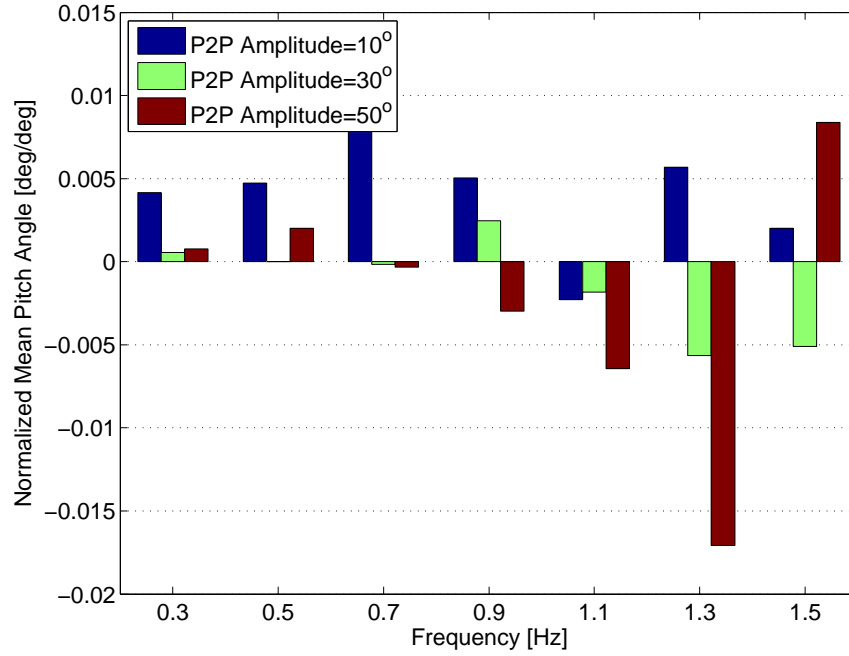
Figure 60. The signal bias, or mean angle was nearly 0 for all cases
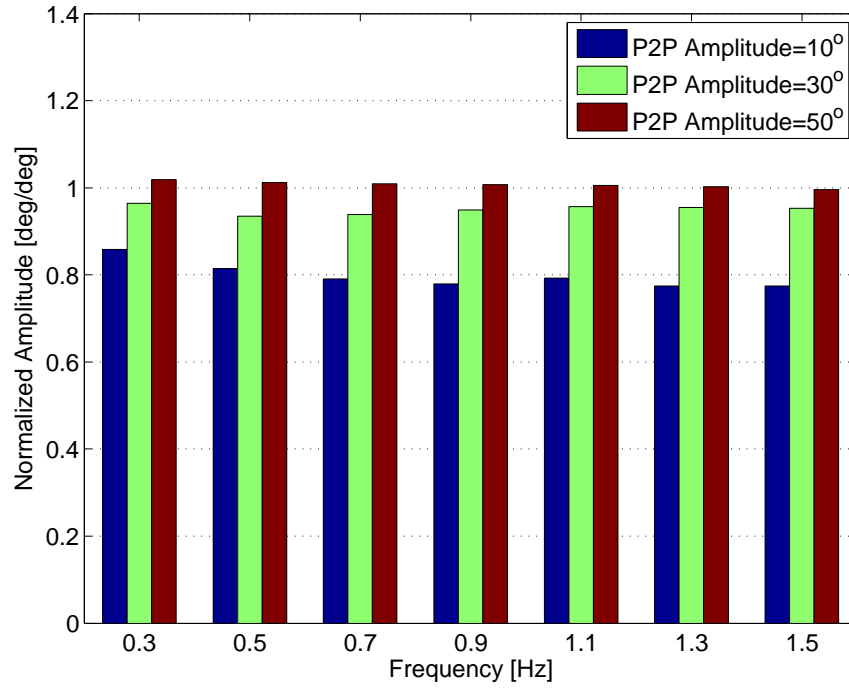
Figure 61. The amplitude attenuation was removed from the higher amplitude outputs.
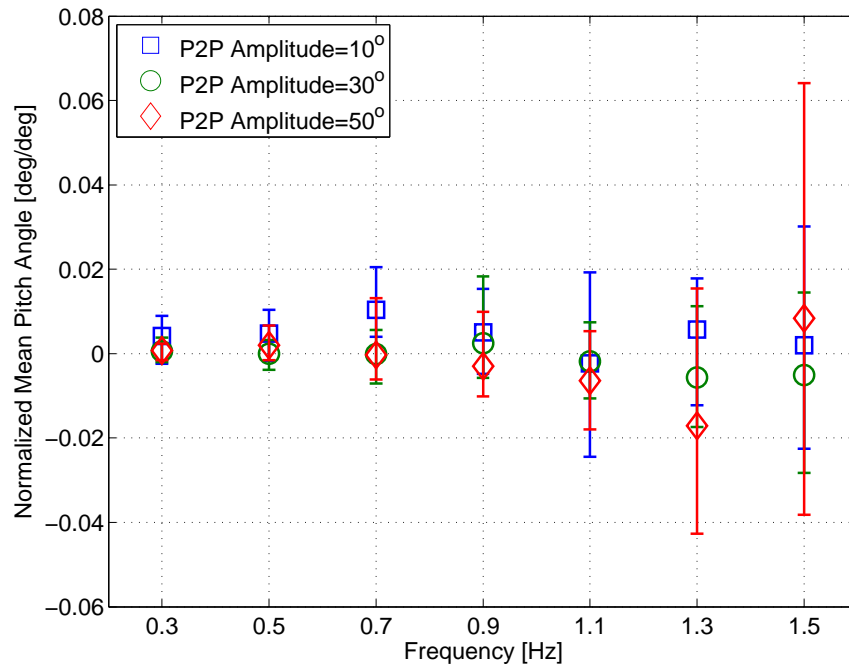
Figure 62. The normalized, mean pitch angle has error bars representing the limiting cases of the 10 tests conducted at each frequency-amplitude pair.
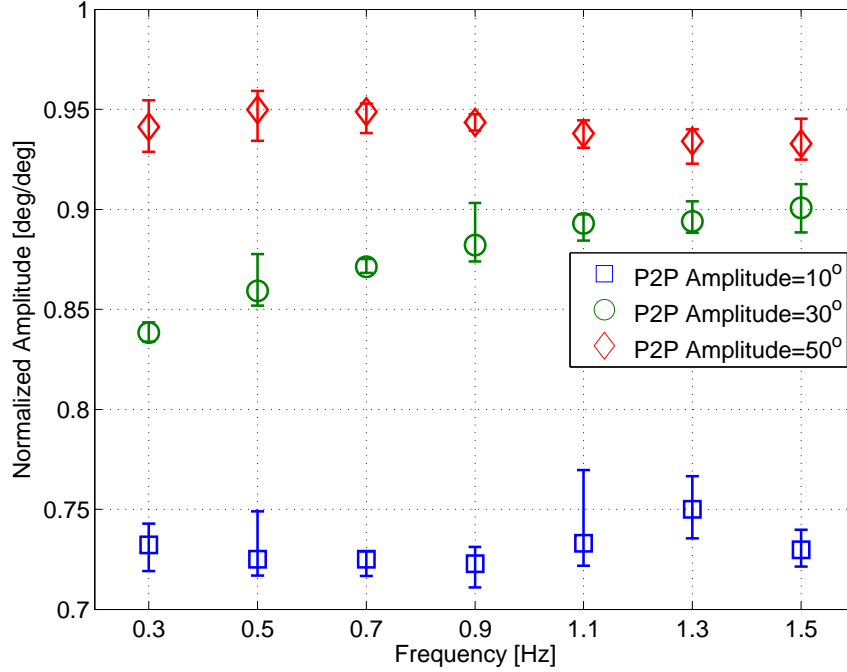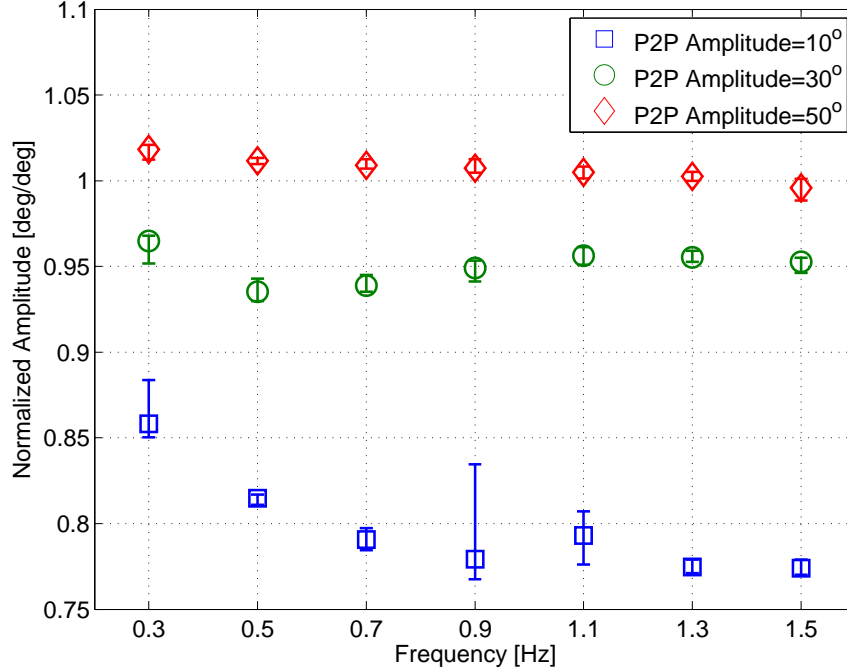
Figure 63. The normalized amplitude has error bars representing the limiting cases of the 10 tests conducted at each frequency-amplitude pair.

4.5   Comparison of the Open and Closed-Loop Results

Figure 64 shows the comparison of the normalized mean pitch angles for each amplitude. Applying closed-loop control led to considerable improvements for all frequencies and amplitudes; all mean pitch angles were accurate to within ±0.43° with position feedback. Figure 65 indicated that all amplitudes were increased as well. At the extrema of the lower amplitude oscillations, the commanded velocity of the closed-loop system was greater than the commanded velocity of the open-loop. As stiction began to adversely effect the motor, the position error increased and equivalently increased the commanded velocity resulting in less amplitude attenuation. Further improvement cannot be made to lower amplitude attenuation without increasing the proportional gain, which will cause amplification at the higher amplitudes. If a later research goal is to perform lower amplitude pitch oscillation, then the recommendation is to precondition the trajectory with a higher amplitude in order to achieve the

96
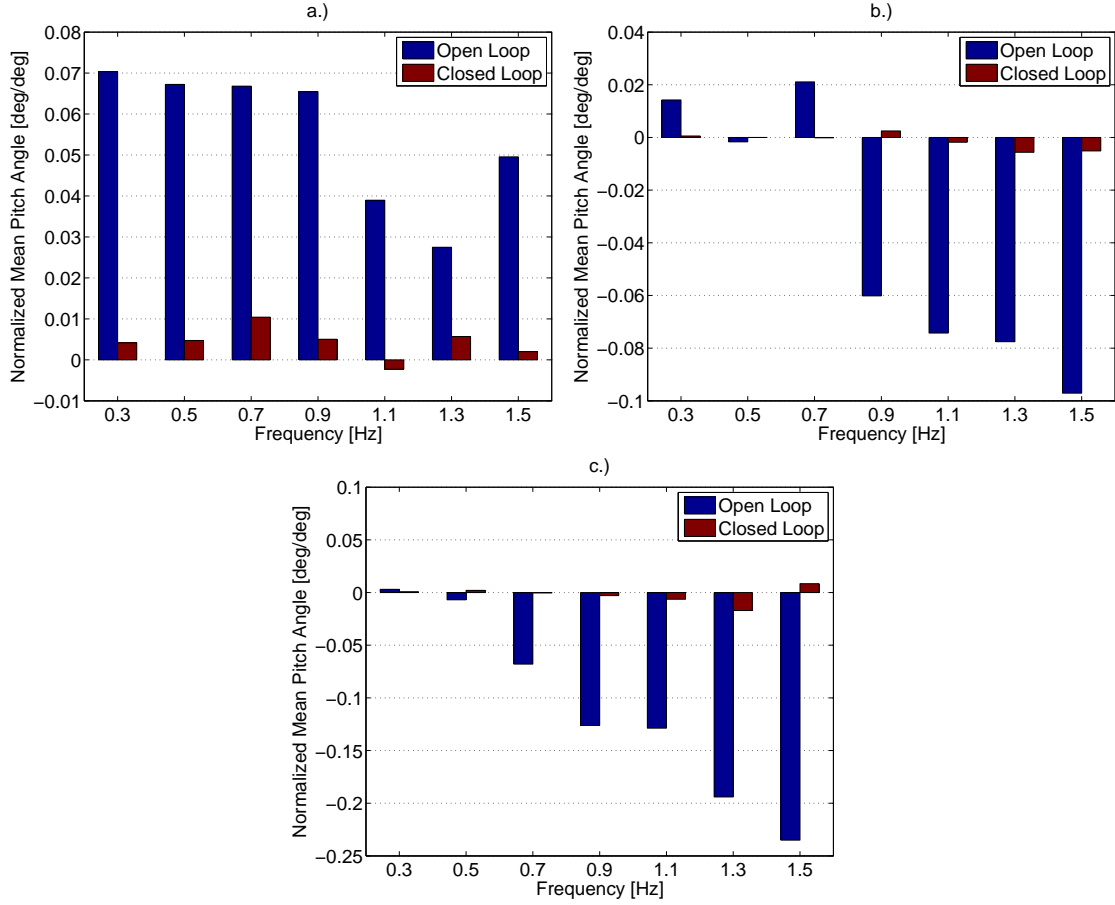
Figure 64. The comparison between the open-loop system's and closed-loop system's normalized mean pitch angle shows improvement for each amplitude: a.)5°, b.)15°, and c.)25°.

desired outcome. Figure 66 demonstrates that, for each case, the closed-loop system was more consistent.

Figure 67 also demonstrates the improvement brought about by position feedback for the limiting cases. In most cases, the amplitude response of the closed-loop system was at least on par or more consistent than the amplitude response of the open-loop system for the closed-loop response. Therefore the position feedback has enhanced the performance of the MTA wrist roll motor and controller. If phase lag needs to be corrected, a lag compensator would need to be incorporated as well. With the MTA wrist roll motor and controller properly evaluated, dynamic wind tunnel experiments
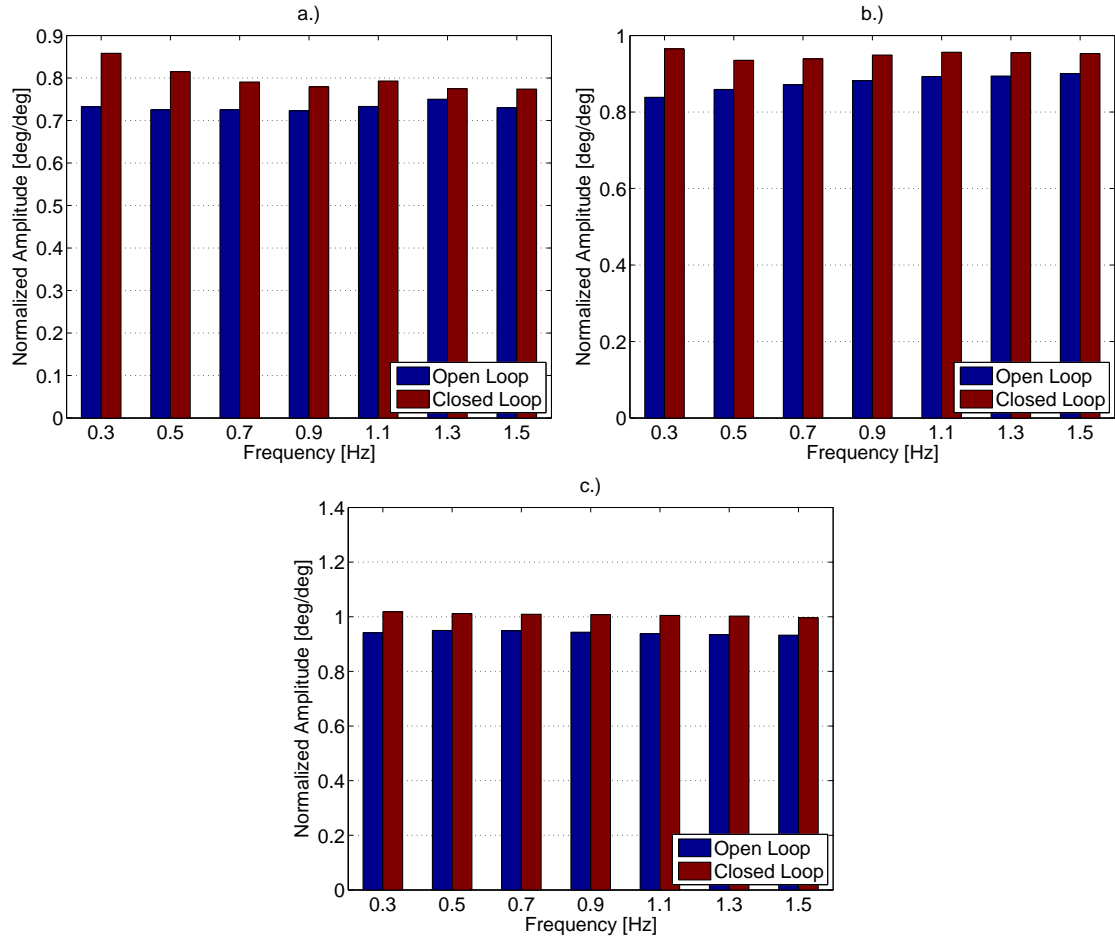
Figure 65. The comparison between the open-loop system's and closed-loop system's normalized amplitude shows improvement for each amplitude: a.)5°, b.)15°, and c.)25°.

were ready to be conducted.
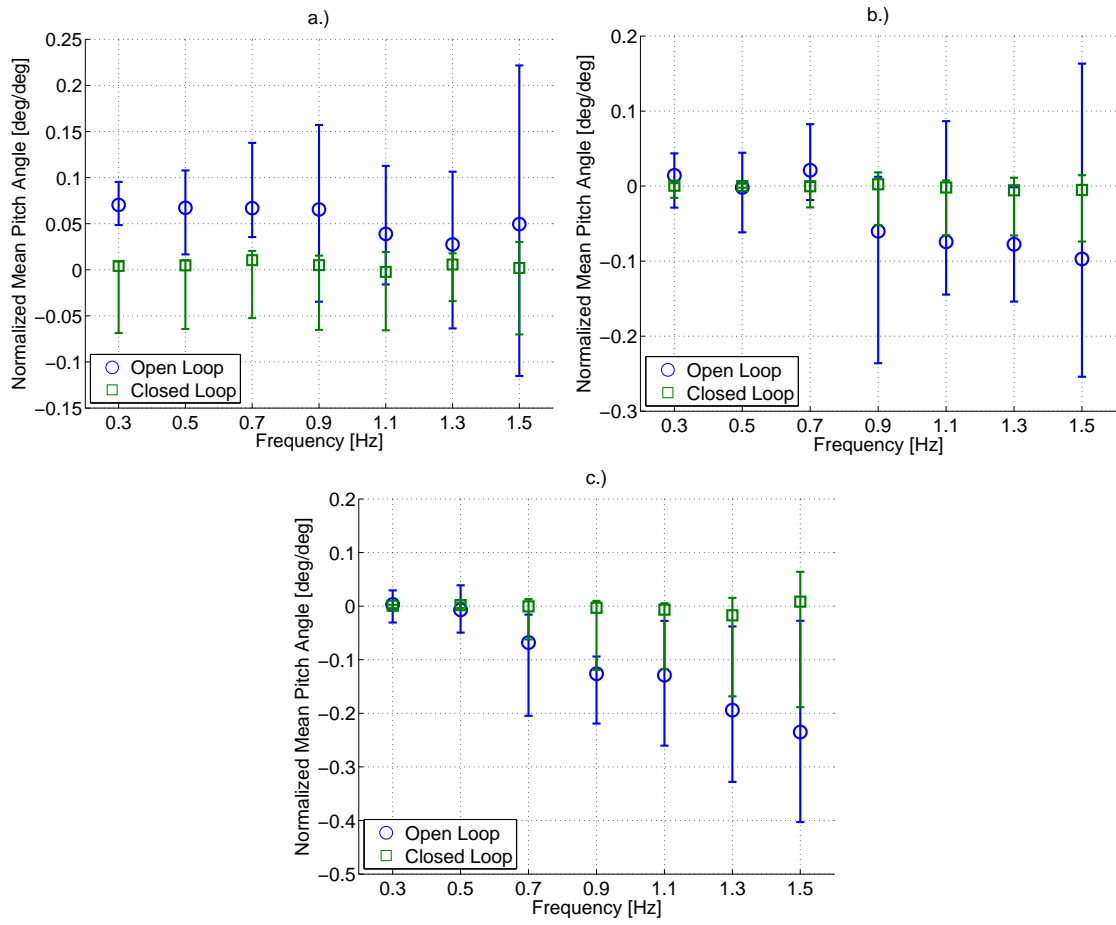
Figure 66. The comparison between the open-loop system's and closed-loop system's normalized mean pitch angle shows improvement for each amplitude: a.)5°, b.)15°, and c.)25°.
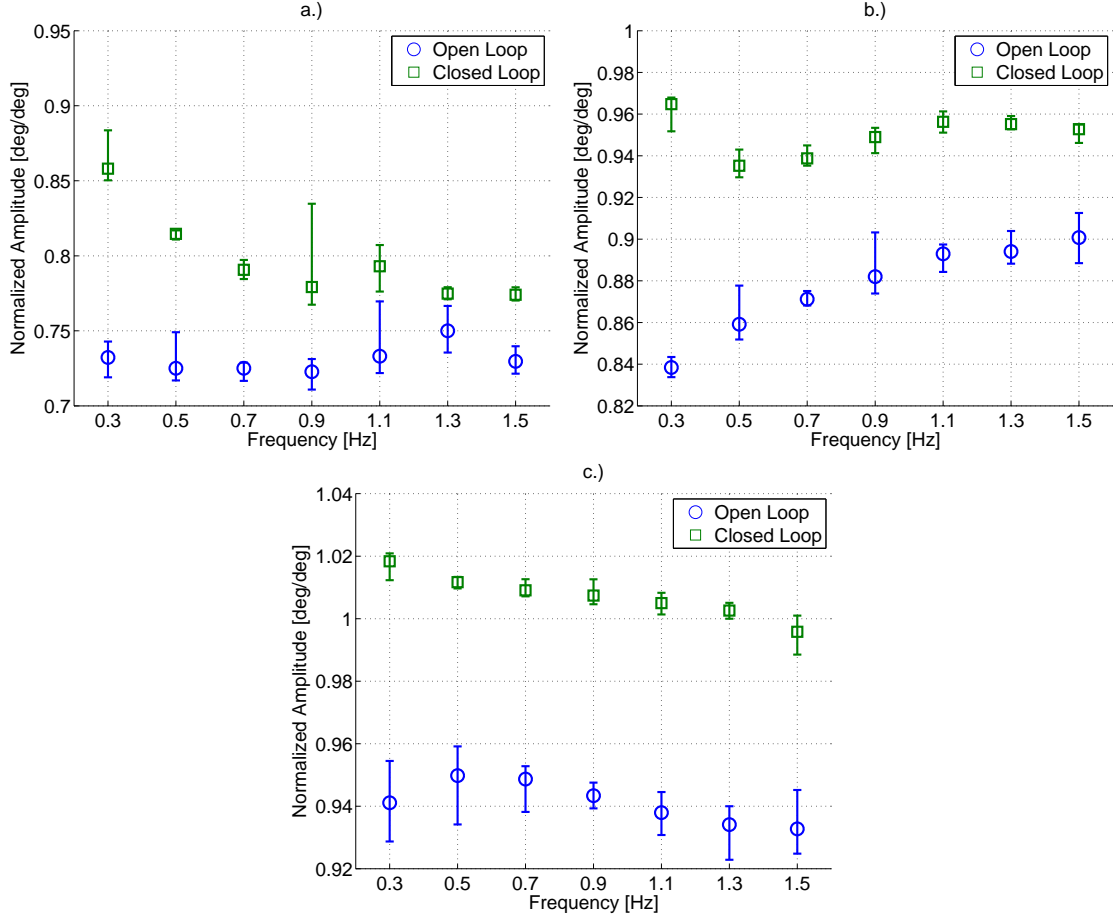
Figure 67. The comparison between the open-loop system's and closed-loop system's normalized mean pitch angle shows improvement for each amplitude: a.)5°, b.)5°, and c.)25°.

4.6 IMU Validation of Sting Rigidity and MTA Output

Before using the IMU as a secondary position and orientation sensor, the noise and drift of the IMU were observed to determine its accuracy. The IMU was attached to the sting at a static, arbitrary angle; using the Matlab® program, *IMU Front Panel* the IMU recorded data for approximately 120 s. This data, displayed in Figure 68, shows no evidence of drift. The IMU noise was quantified as follows: $\phi \pm 0.026\,58°$, $\theta \pm 0.2992°$, and $\psi \pm 0.2794°(3\sigma)$.

Directions corresponding to the straight-and-level were determined relative to the
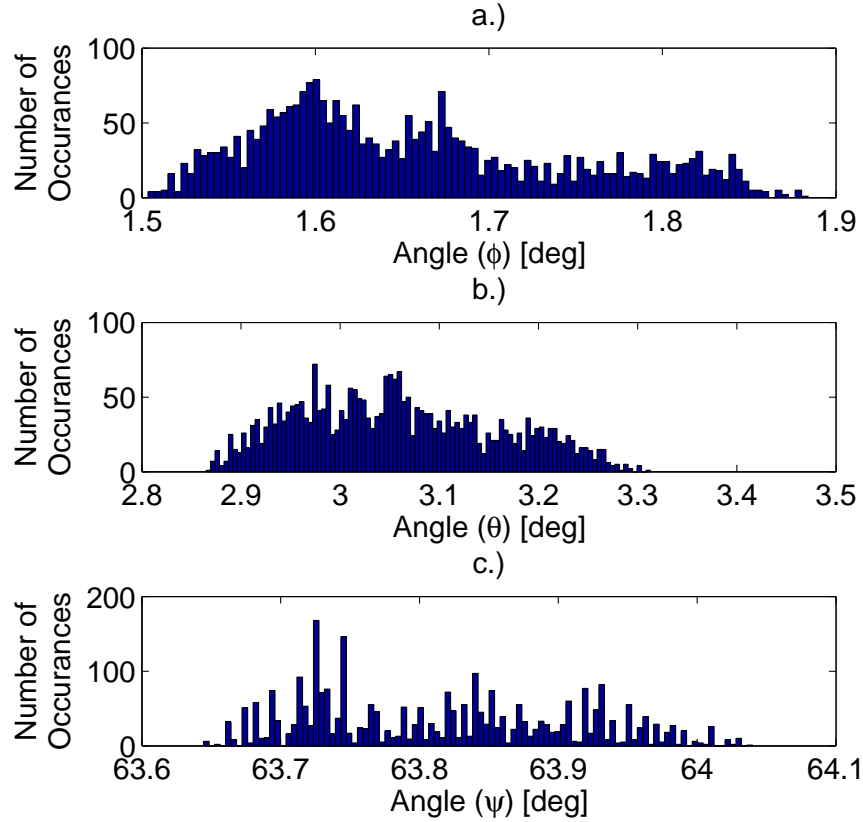
Figure 68. The histograms display no drift but some noise for each of the IMU Euler angles a.)ϕ, b.)θ, c.)ψ.

wind tunnel. The floor of the wind tunnel test section and the tunnel's centerline were assumed to be good approximations of the freestream direction in the middle of the tunnel. These IMU angles corresponding to the approximation of straight-and-level were $\phi = -3.039°$, $\theta = 1.4748°$, and $\psi = 92.353°$. These angles will be used to adjust the IMU Euler angles for comparison during dynamic testing. The straight-and-level approximation was also used to determine if the MTA-inertial x-y plane is coplanar with the wind coordinate system's x-y plane. With the IMU attached to the sting, the Euler angles of the model were computed using both the IMU and the MTA's `mtaAngles` command. The differences between the straight-and-level approximation and the IMU Euler angles on the sting were calculated. Those differences were then subtracted to the MTA angles to determine straight-and-level for the MTA. The

results showed that the MTA-inertial x-y plane and the wind x-y plane were not perfectly coplanar. The adjusted MTA angles for straight-and-level were calculated to be $\phi_i = 0.039°$, $\theta_i = -0.402°$, and $\psi_i = -67.17°$. The IMU determined that the model was at a yaw angle of approximately $-30°$ from straight. This is likely due to interference in the magnetic field due to ferrous materials and the MTA motors. However, these findings showed than an acceptable level of accuracy was achieved when by assuming the x-y planes were coplanar.

Dynamic tests were conducted using three pitch oscillations at different frequency-amplitude pairs with no freestream velocity. Since the IMU Matlab® program cannot be simultaneously triggered with the start of the trajectory, the IMU Euler angles must be time-shifted to compare with the MTA Cartesian positions. Unfortunately this could remove evidence of sting flexibility, which might appear in the IMU data as a phase lag between the IMU data and the MTA data. However, the time-shifted IMU Euler angles closely matched the frequency and amplitude for the pitch oscillation. Figure 69 demonstrates the agreement between the IMU's the MTA's θ_b. The IMU had an approximate sampling frequency of 11 Hz since it was not run in "Silent Mode." There was a small rotation about the x-axis ($\Delta\phi < 0.1°$) between the IMU coordinate system and the MTA coordinate system. Because the rotation was minimal, only a slight oscillation was recorded for the IMU's ψ. However, the IMU coordinate system is rotated $-30°$ about the z-axis from the MTA coordinate system. This causes the single-DOF rotation about the body-fixed y_b-axis to appear as a rotation about an axis not collinear with the IMU's y-axis. This results in a second oscillation that appears in roll (ϕ). As the frequency and amplitude of the pitch oscillation are increased (Figure 70), the amplitude of the roll oscillation increases. The remaining figures from this series of tests can be found in Appendix A.
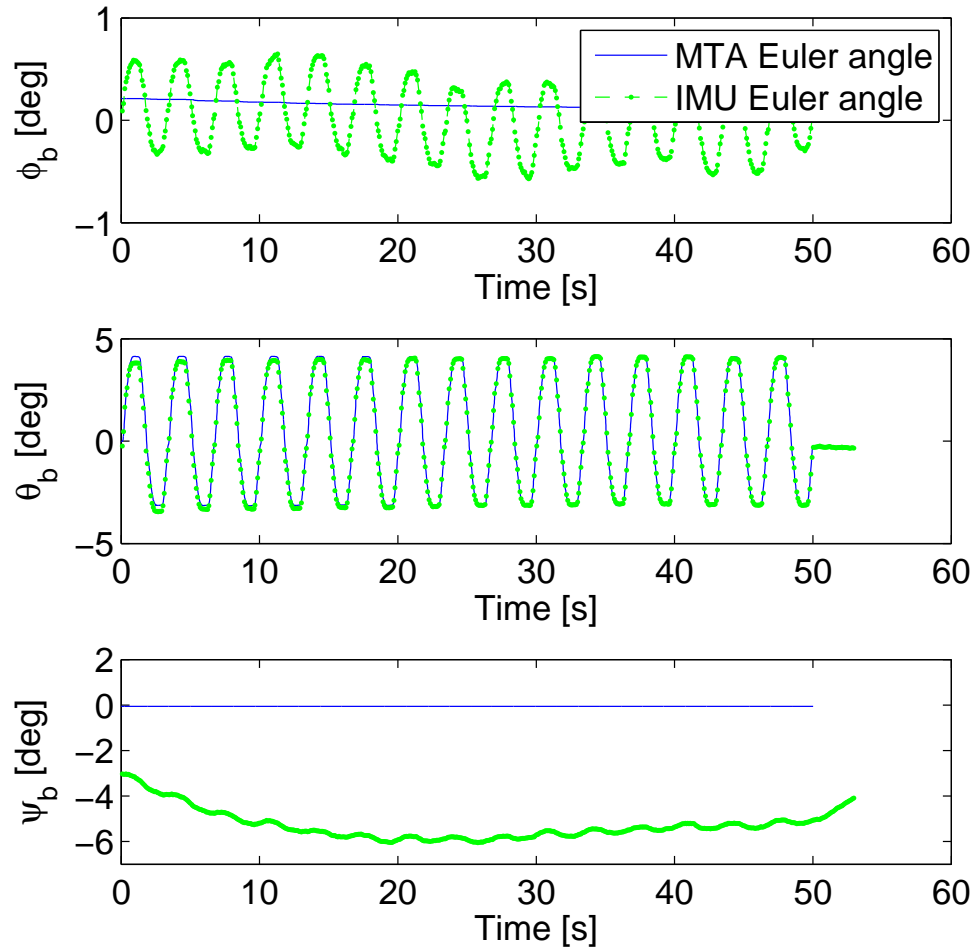
Figure 69. The time-shifted IMU Euler angle, θ_b demonstrated good agreement with the MTA Cartesian positions. However the IMU detects a small oscillations for ϕ_b and ψ_b.
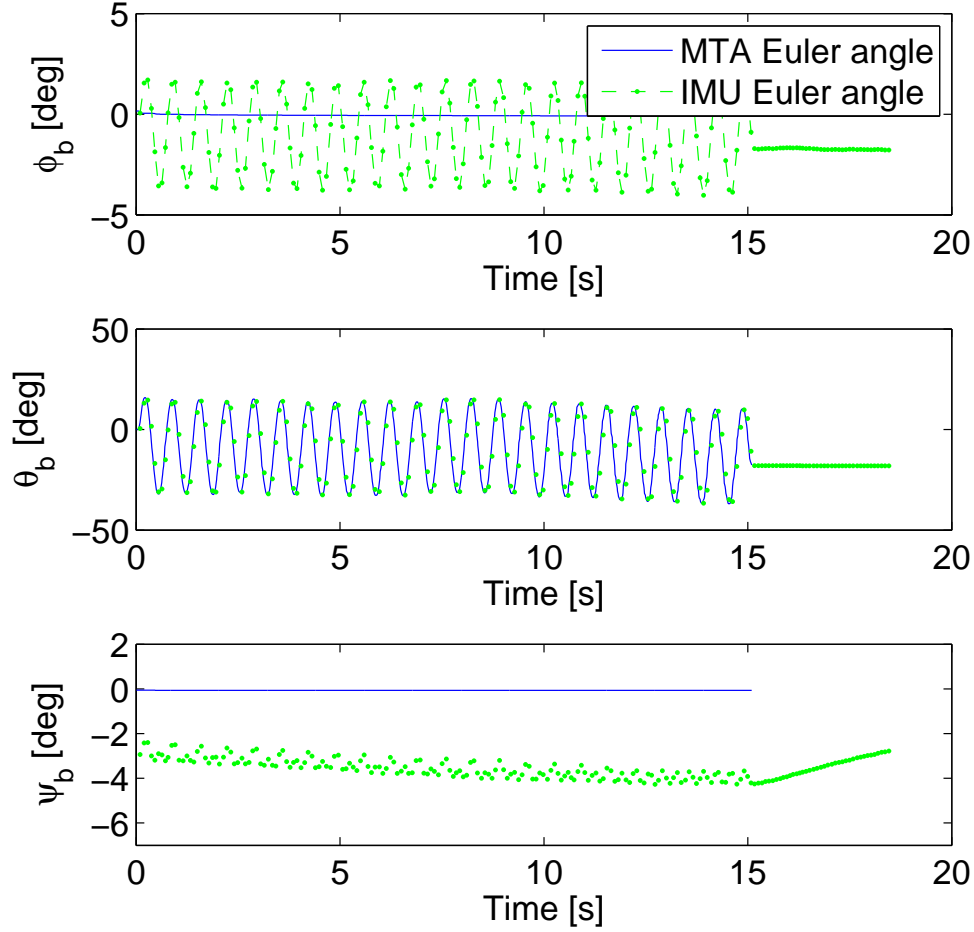
Figure 70. The amplitude of the roll oscillation increases as pitch oscillation amplitude increases.

4.7 Incorporation of Dynamic Pressure Measurements

Using the closed-loop system for the MTA's wrist roll system, dynamic wind tunnel testing was conducted. The wrist roll system oscillated the model about its quarter-chord at 1 Hz with amplitudes of 20°, 30°, and 50°. The wind tunnel was operated at nominal speeds of 60 mph for each amplitude and additionally at 120 mph for 30° amplitude. The atmospheric conditions were assumed to be 14.4 psi and 72°F. All pressure signals were only sampled for 10 s at 1 kHz to maintain simplicity in these experiments. Euler angles were simultaneously sampled at approximately

22 Hz using the IMU. The MTA also recorded the Cartesian position of the model at approximately 80 Hz.

Dynamic Pressure Analysis.

Using the DAQ, pressure data was sampled for atmospheric conditions in the wind tunnel. These voltages, which were a result of both the amplifiers and the atmospheric pressure, were used to tare the pressure data. Since the amplifier accounted for the individual sensitivity of each transducer, the voltages were converted to psi using the amplifier's output scaling: 200mV/psi. Using the same techniques applied in Section 4.6, the IMU data was time-shifted in order to match the MTA's calculated pitch angles (θ_b). It was very encouraging to see the IMU matched the model's pitch angle throughout the tests. Figure 71 compares the acquired pressure signals to the kinematic motion of 1 Hz with 20° amplitude at 60 mph. As expected when the pitch angle initially increased, the pressure sensed on the upper surface decreased, and the pressure on the lower surface increased. An interesting phenomenon that occurred at the quarter-chord on the leeward surface was a sharp decrease in pressure. This downward spike was more adverse for the upper surface as the pitch angle began to decrease. The sudden loss of pressure is possibly due to the separation on the leeward surface as the model begins to oscillate in the other direction. Even though the airfoil is symmetric, there was an unexpected amplitude difference between the pressure at the quarter-chord on the lower surface and upper surface. The amplitude of the upper surface was slightly higher than the amplitude on the lower surface. This could be due to flaws in the model's fabrication or the fabrication of the cavities for the pressure transducers, but other causes are also possible.

At the three-quarter-chord location, the pressure remained constant until the respective surface was pitched away from freestream velocity. At approximately 16°
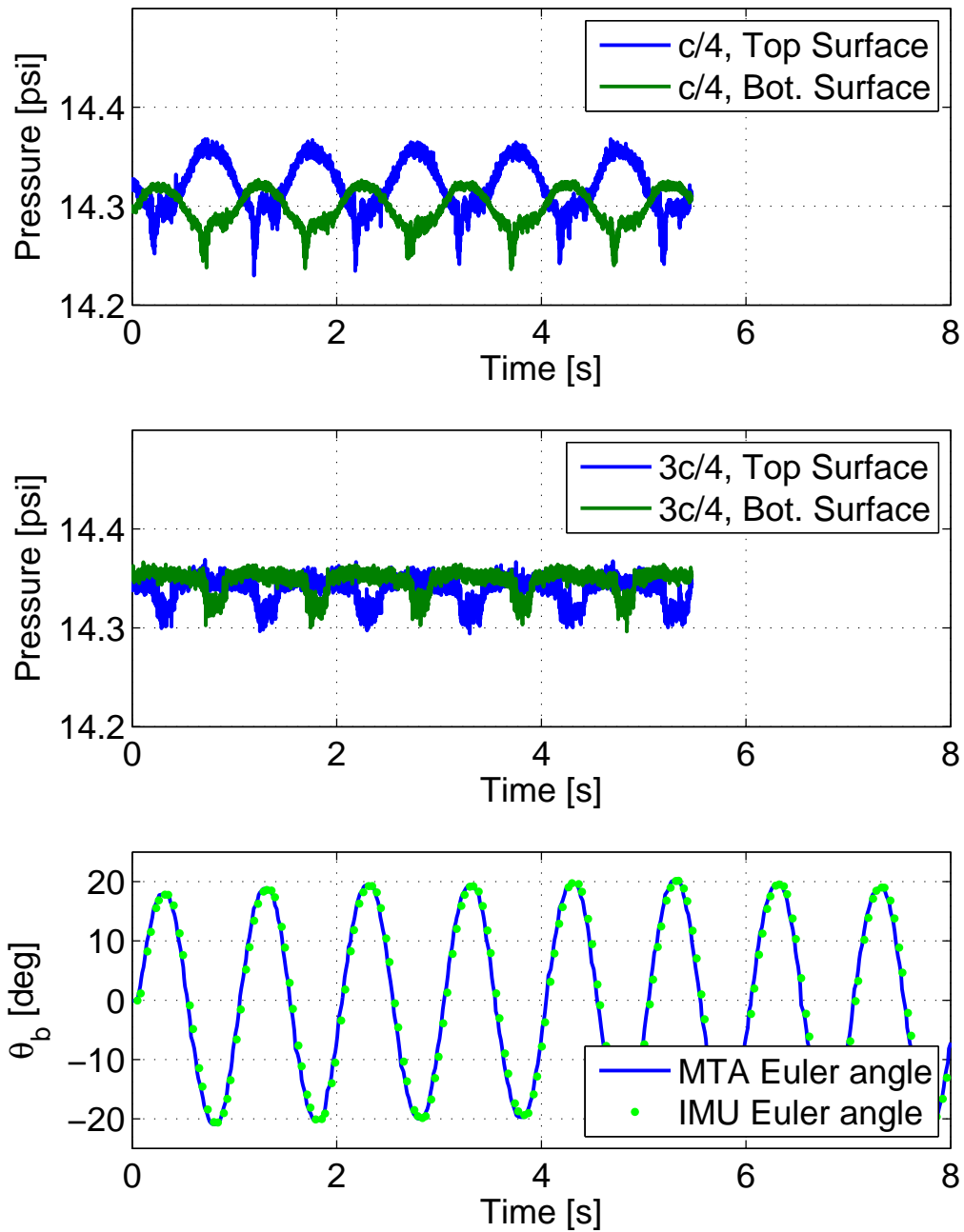
Figure 71. Pressure signals are compared to the pitch oscillation at 1 Hz and 20° amplitude to determine effects on pressure when the fan speed was 60 mph.
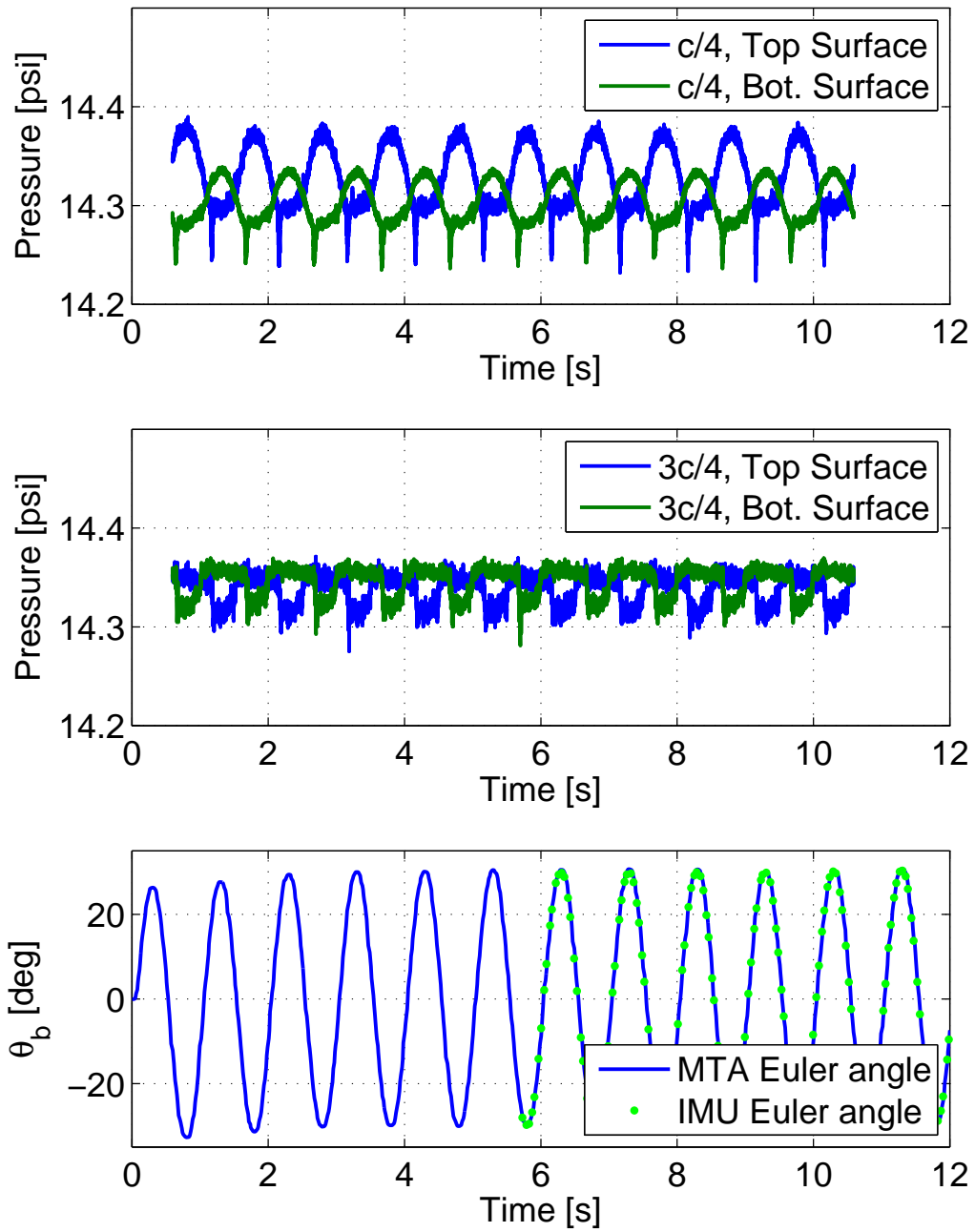
Figure 72. Pressure signals are compared to the pitch oscillation at $1\,\text{Hz}$ and $30°$ amplitude to determine the effects on pressure when the fan speed was 60 mph.

pitch, the upper surface experiences a sudden decrease in pressure. As the pitch amplitude is increased, the sudden loss of pressure is more pronounced. In Figure 72 the pressure signals were manually time-shifted to match the trend of the other tests due to a late manual DAQ trigger. However, it is apparent that as the amplitude of the pitch oscillation is increased to 50°, as shown in Figure 73, the amplitude of the pressure oscillations at the quarter-chord increase. As the amplitude is increased to 50°, clearer oscillations in the pressure signal appeared at the three-quarter-chord location. One test was conducted at a higher fan speed, 120 mph, and the results are given in Figure 74. The pitch oscillation occurred with a frequency of 1 Hz and amplitude of 30°. As expected with the increase in velocity, the mean pressure decreased.
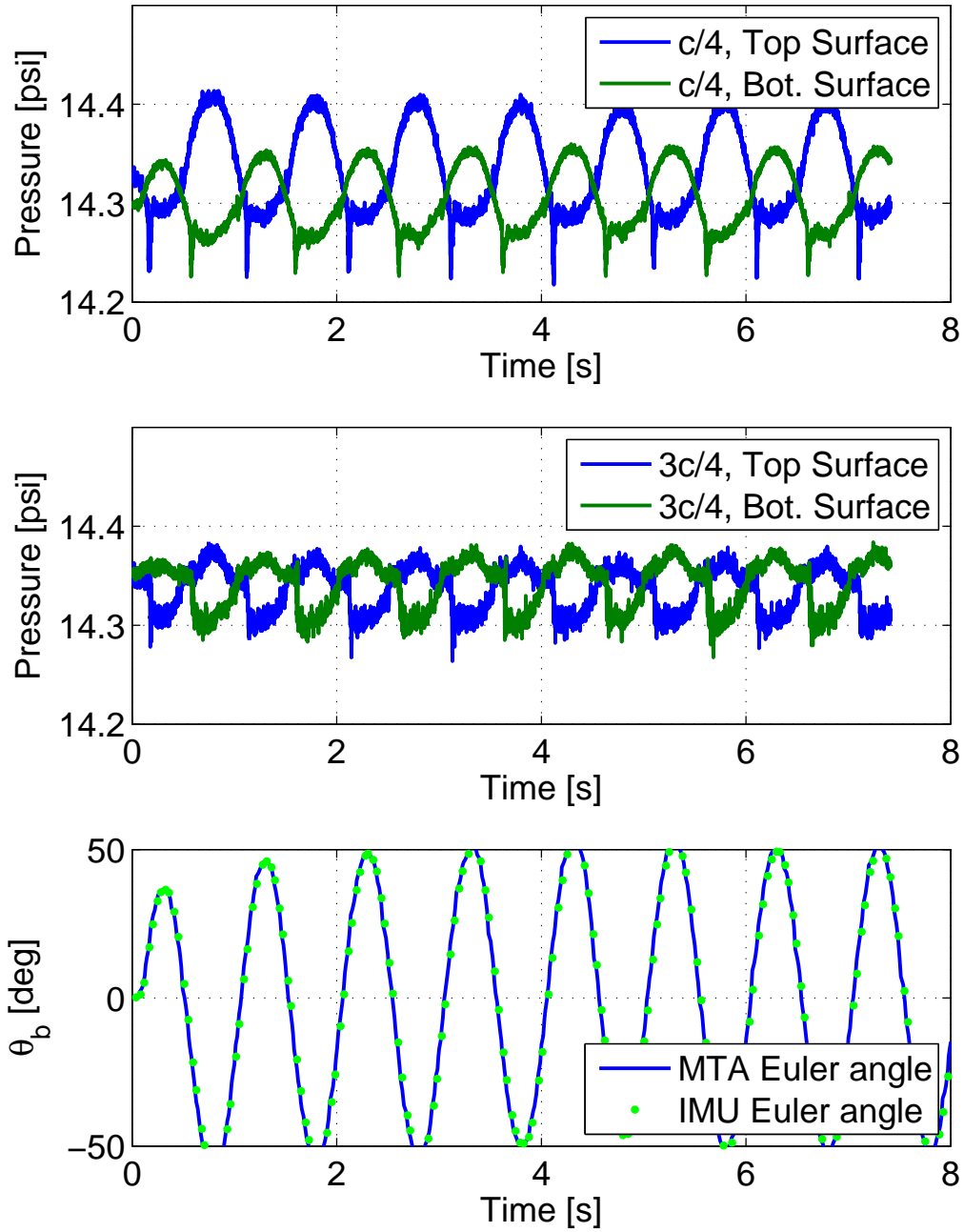
Figure 73. Pressure signals are compared to the pitch oscillation at $1\,\mathrm{Hz}$ and $50°$ amplitude to determine the effects on pressure when the fan speed was 60 mph.
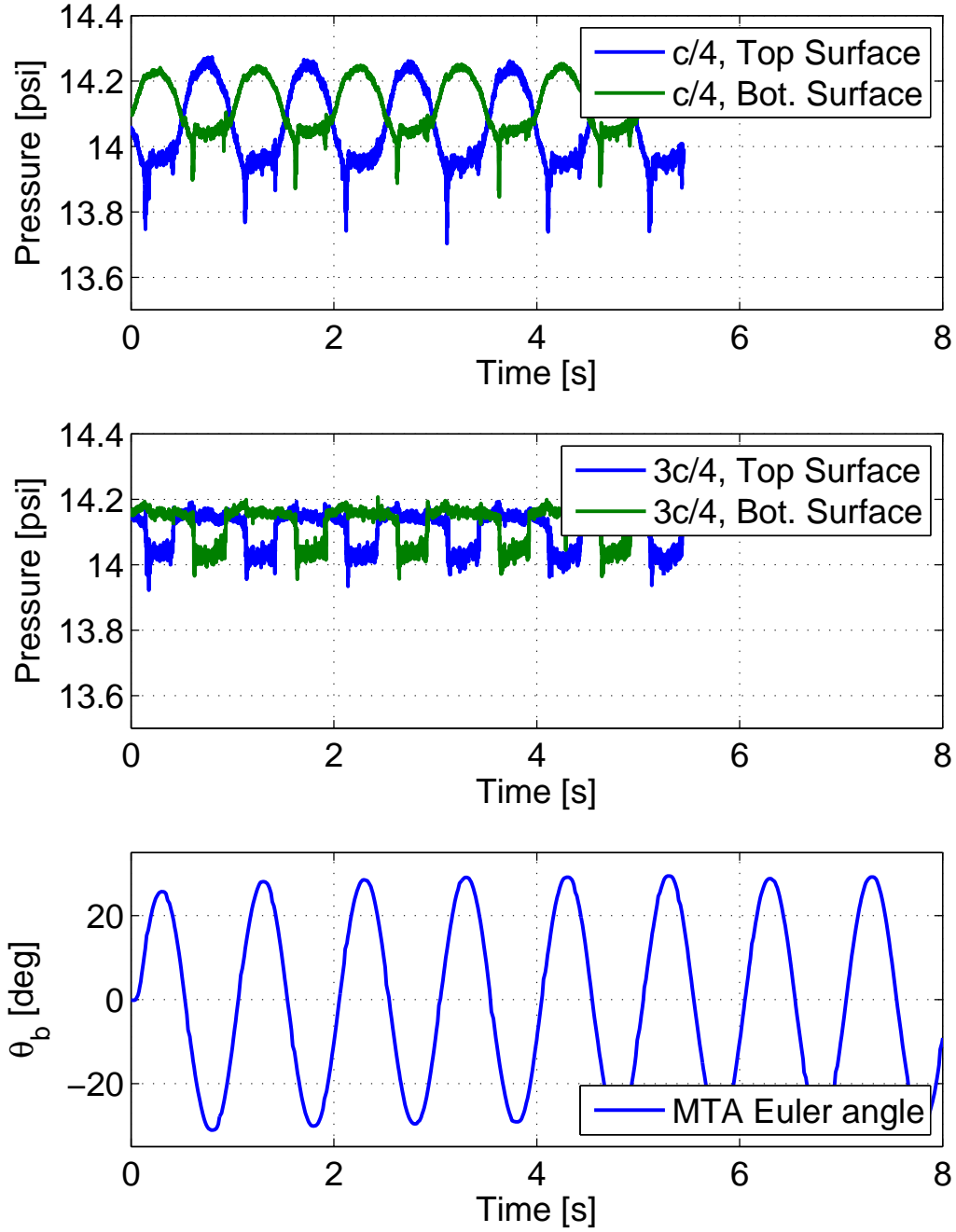
Figure 74. Pressure signals are compared to the pitch oscillation at $1\,\mathrm{Hz}$ **and** $30°$ **ampli-tude to determine the effects on pressure. The fan speed was increased to 120 mph for this test.**

In order to compare the pressure signals from each experiment, a pressure coefficient was calculated from the measured pressure signals using equation (53). Figure 75 demonstrates that as the pitch oscillation amplitude is increased, the quarter-

chord pressure signals increase. As previously mentioned, there is a noticeable arc in the three-quarter-chord pressure signals at 50° amplitude. As the fan speed is increased, Figure 76, there is little difference between the pressure coefficients of the two cases.

$$C_p = \frac{p - p_{atm}}{\frac{1}{2}\rho V^2} \tag{53}$$
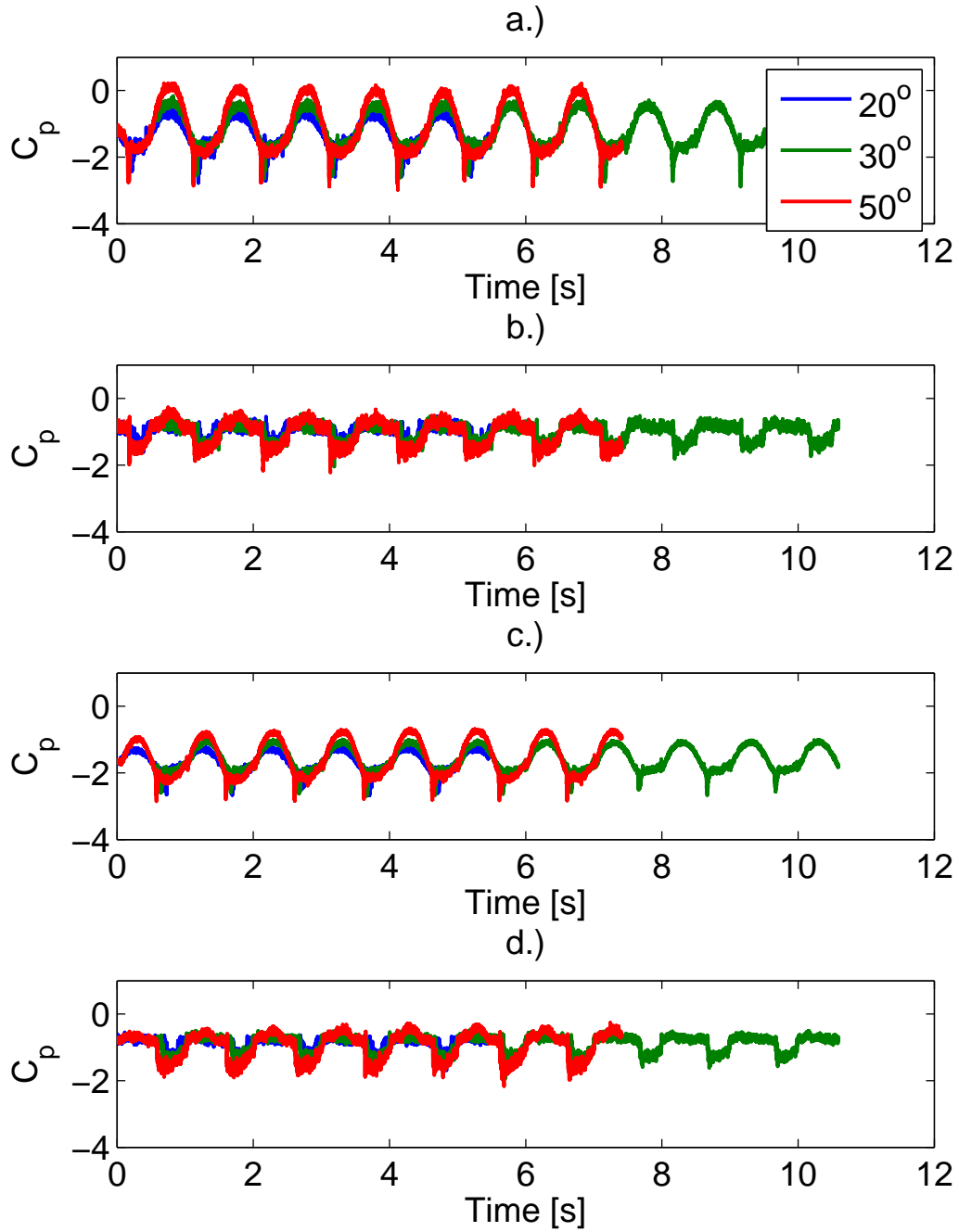
Figure 75. A pitch oscillation with frequency $1\,\mathrm{Hz}$ and amplitudes $20°$, $30°$, and $50°$ at a fan speed of 60 mph. Their pressure coefficients are compared on the a.)$c/4$ upper surface; b.)$3c/4$ upper surface;a.)$c/4$ lower surface; and b.)$3c/4$ lower surface.
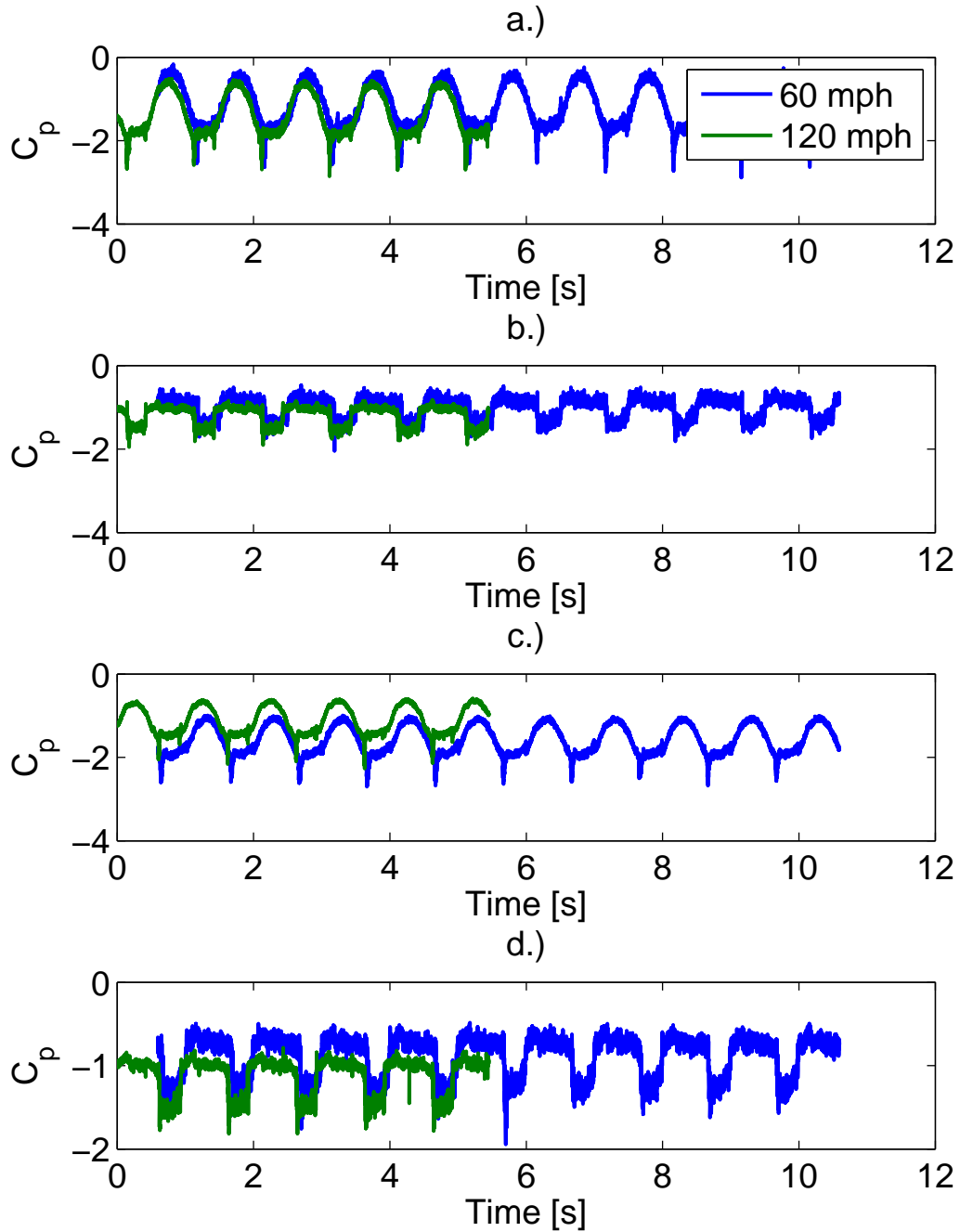
Figure 76. A pitch oscillation with frequency $1\,\mathrm{Hz}$ and amplitude $30°$ was conducted with two fan speeds (60 mph and 120 mph) in the wind tunnel. Their pressure coefficients are compared on the a.)c/4 upper surface; b.)3c/4 upper surface;a.)c/4 lower surface; and b.)3c/4 lower surface.

113

Performance of IMU and MTA closed-loop System.

The IMU recorded the Euler angles at approximately $22\,\mathrm{Hz}$, using the "Silent Mode" option on the front panel. The IMU angles were compared to the MTA Cartesian positions to verify the IMU as a secondary position and orientation sensor when the freestream velocity was non-zero. Figure 77 demonstrates the level of agreement between the IMU and the MTA output. As explained in Section 4.6, because of the large rotation about the z-axis and small rotation about the x-axis, there are fictitious oscillations in ϕ_b and ψ_b respectively. The IMU data, once again, was time-shifted such that the pitch oscillation correlated. As the amplitude increases to 30°, and then 50°, given in Figure 78, the IMU consistently matches the pitch oscillation's θ_b. When the fan speed was increased to 120 mph, the IMU failed to record the Euler angles due to a loose wire. Therefore, it can only be concluded that the IMU is validated as a secondary position and orientation sensor for nominal speeds up to 60 mph.
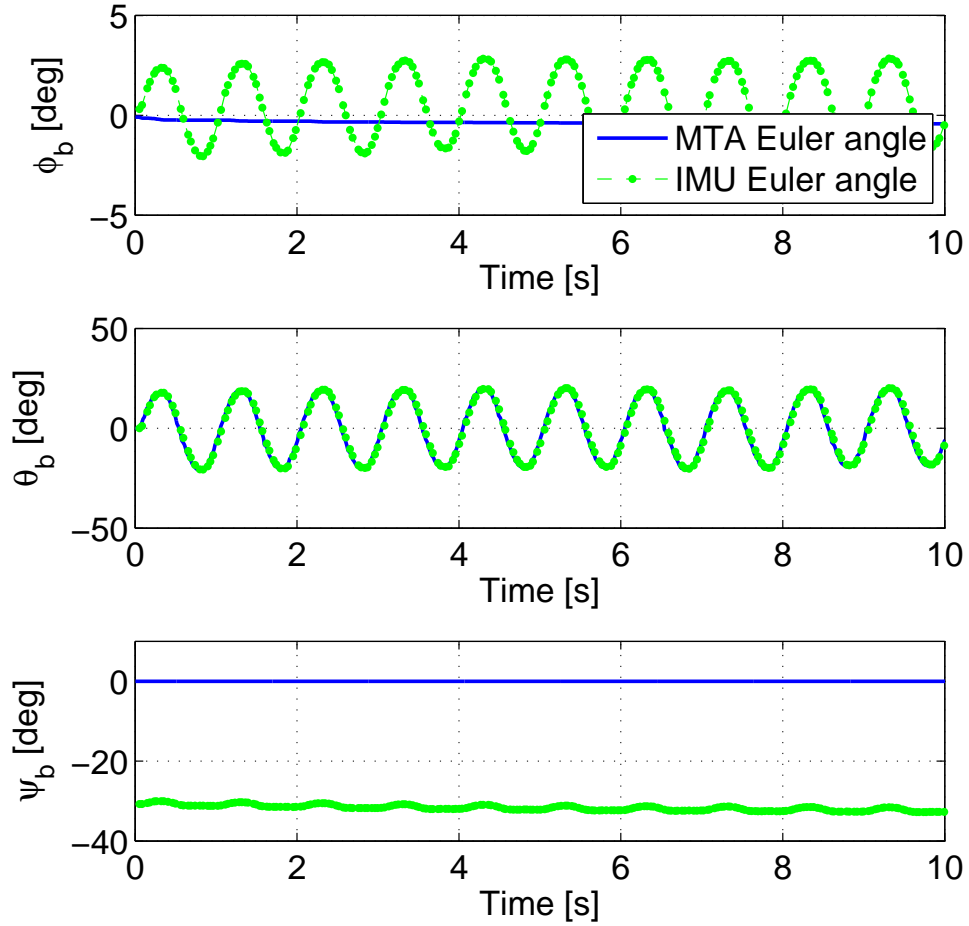
Figure 77. IMU Euler angles are compared to the Euler angles calculated by the MTA during a pitch oscillation $1\,\mathrm{Hz}$, $20°$ **amplitude, and fan speed of 60 mph.**

Finally these dynamic wind tunnel experiments offered an opportunity to study the performance of the MTA's closed-loop system when aerodynamic loads were introduced. Figures 79–81 demonstrate the performance of the MTA's wrist roll system in presence of freestream velocity compared to no freestream velocity. The duration of these tests was $60\,\mathrm{s}$ but only a portion of the outputs were shown in order to examine the details between data sets. In all cases the closed-loop system exhibited consistent behavior.

Even at the higher velocity, Figure 82, the MTA wrist roll system demonstrated consistent behavior with and without freestream velocity. However, while the wrist
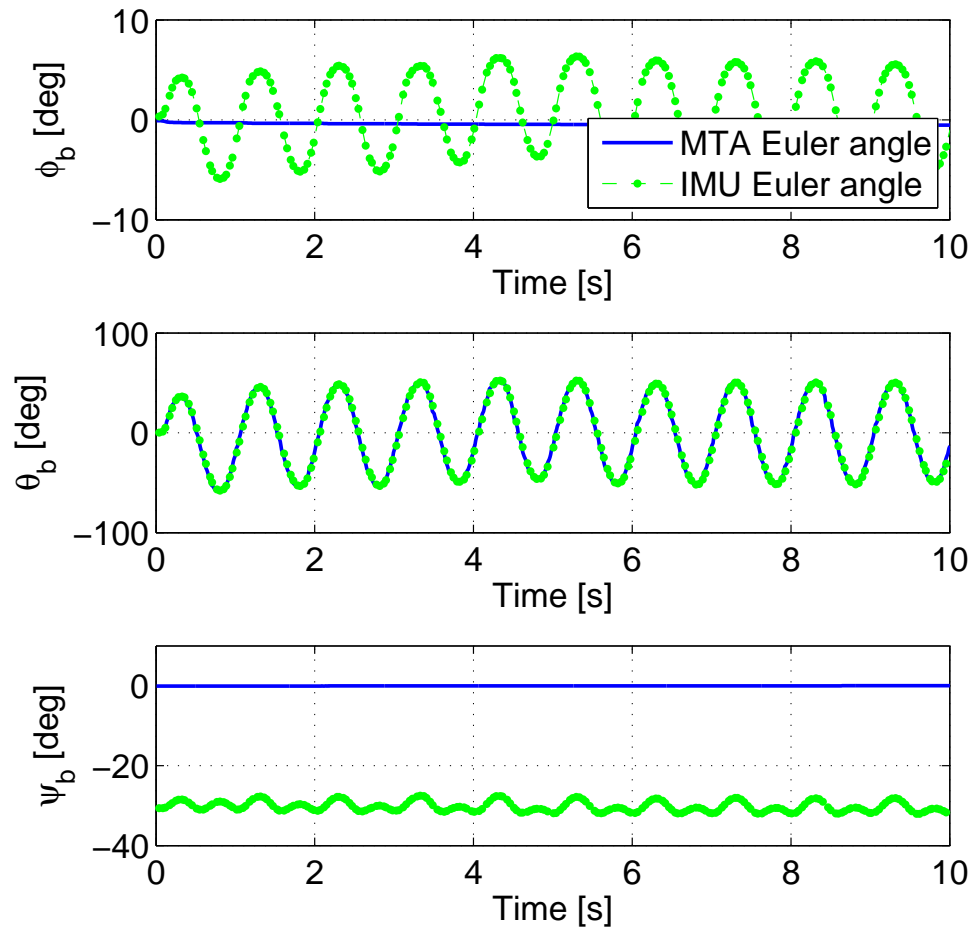
Figure 78. IMU Euler angles are compared to the Euler angles calculated by the MTA during a pitch oscillation $1\,\mathrm{Hz}$, $50°$ amplitude, and fan speed of 60 mph.
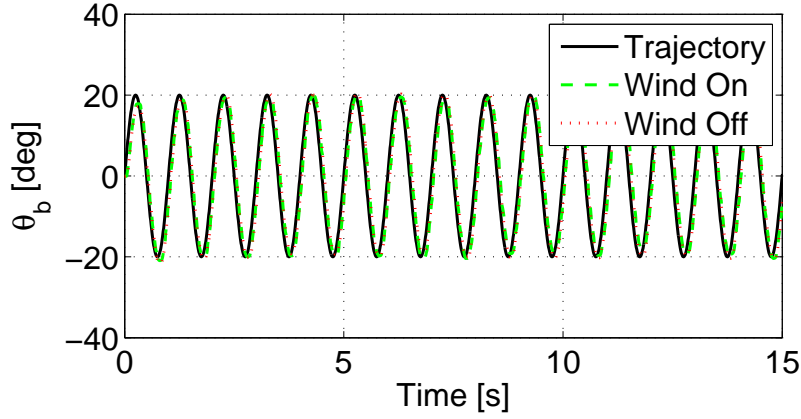
Figure 79. The performance of the wrist roll closed-loop system was compared with and without the presence of freestream velocity (60 mph). The pitch oscillation was 1 Hz, 20° amplitude.
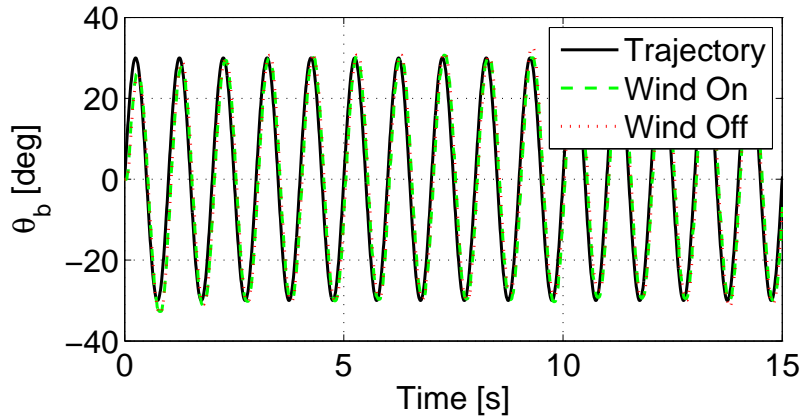
Figure 80. The performance of the wrist roll closed-loop system was compared with and without the presence of freestream velocity (60 mph). The pitch oscillation was 1 Hz, 30° amplitude.

roll system performed well, the other MTA joints could not maintain their static positions under the larger aerodynamic loads. The elbow pitch and wrist pitch began to rotate as the model oscillated. These movement permeated through the inverse kinematics to affect both the model's position and orientation, shown in Figures 83 and 84. The pitch of the model was unaffected because of the manner in which the model's control point was defined. The control point was defined to lie on the axis of rotation of the wrist roll joint. Therefore, even if the other joints do not maintain their positions, the pitch is unaffected. These uncontrolled oscillations likely contaminated

117
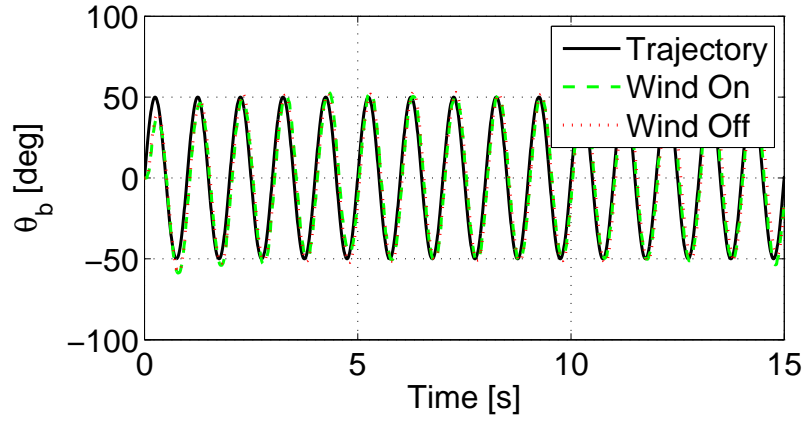
Figure 81. The performance of the wrist roll closed-loop system was compared with and without the presence of freestream velocity (60 mph). The pitch oscillation was 1 Hz, 50° amplitude.

the single-DOF study performed.
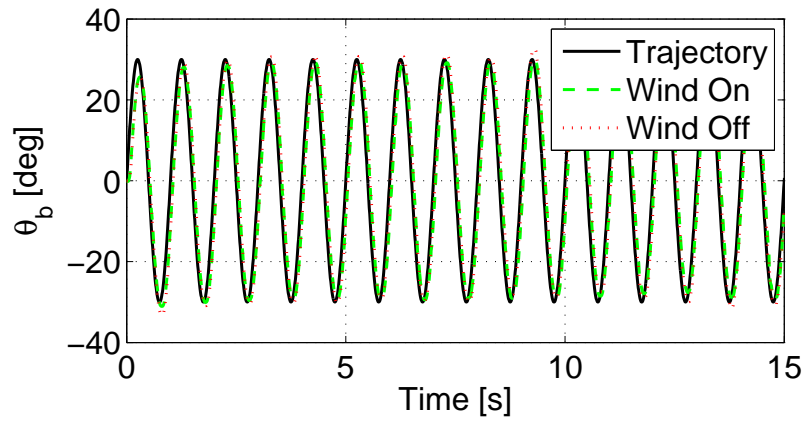
Figure 82. Motor encoders showed the performance of the wrist roll closed-loop system was compared with and without the presence of freestream velocity (120 mph). The pitch oscillation was 1 Hz, 30° amplitude.
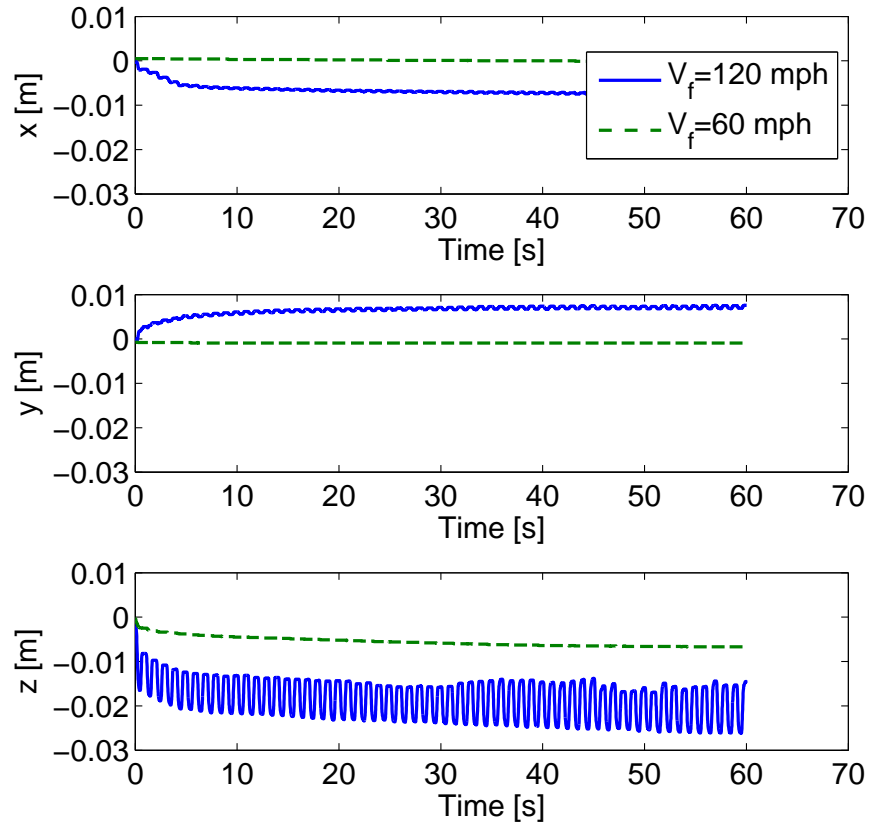
Figure 83. There were large displacements in the other degrees of freedom when the aerodynamic loads increased.

119
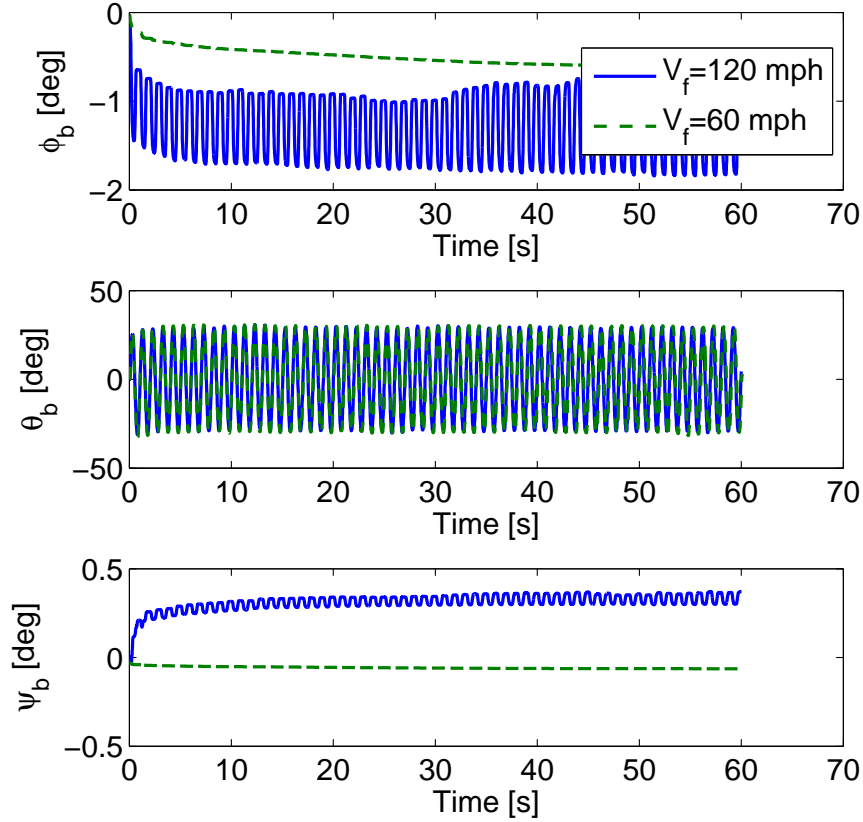
Figure 84. There were large rotations in the other degrees of freedom when the aero-dynamic loads increased. However the pitch, θ_b, showed agreement.

4.8   Chapter Summary

Instead of conducting thousands of tests to acquire a statistical quantify the performance of the MTA wrist roll system at each frequency-amplitude pair, the results of *Chapter IV* revealed that good statistical characterization could be obtained by conducting only 10 experiments at each test point. Each of the 10 output signals were averaged together to determine the response of the system. Since the system was non-linear, the open-loop system was characterized by performing pitch oscillations with seven frequencies at three different amplitudes. These experiments revealed large signal bias and amplitude attenuation which needed to be corrected. Using position feedback, the proportional gain was tuned by improving the worst test points from

the open-loop system. The new closed-loop system was characterized using the same test matrix for evaluating the open-loop system. As shown in the comparisons between the open-loop system and closed-loop system, Figures 64–67, the incorporation of position feedback greatly reduced the signal bias and amplitude attenuation. This chapter also showed that the secondary, independent position and orientation sensor, IMU, validated the pitch angle of the model calculated by the MTA Computer. Magnetic field interference from the environment and motor caused a large bias in the yaw angle recorded by the IMU. Finally dynamic wind tunnel testing revealed evidence of unsteady vortex shedding. These experiments also demonstrated that the MTA had equivalent performance under aerodynamic load. However, when the wind tunnel speed was increased to 120 mph, two joints could not maintain their static positions causing motion to occur in all six degrees of freedom.

V. Conclusion and Recommendations

In order to perform a DOE for testing complex systems such as the "flexible weapon" or micro air vehicles it is important to design a testbed capable of performing these complex experiments. This research was focused on the first efforts to establish the MTA and the supporting systems which could fulfill these requirements. This chapter discusses the significance and reliability of the findings discovered during this research effort. Furthermore, *Chapter V* examines the limitations of these findings and recommendations for future work.

5.1 MTA Performance

When the MTA was initially installed, several complex trajectories were conducted to evaluate the performance of the robotic manipulator. These motions involved the use of several MTA joints. For example, the pitch-plunge oscillation involved the use of the wrist roll, wrist pitch, elbow pitch, and shoulder pitch joints. Simple yet valuable lessons were learned from these motions. First the original position of the MTA was found to be too far away from the wind tunnel. In order to improve the performance of small motions, such as a small plunge oscillation, under inertial loading, the MTA was moved approximately $0.592\,\mathrm{m}$ closer to the wind tunnel. Additionally, both the visual observation and encoder output suggested that further performance enhancements would be needed in order to maximize the potential of the MTA system.

During the course of this research effort, focus was placed on the performance of the MTA wrist roll motor and controller by executing a series of model pitch oscillation experiments. Since the system unexpectedly violated the properties of a time-invariant, linear system, a quasi-linear, time-domain approach was used to sample the behavior of the system. The wrist roll system was characterized using

sine wave, pitch oscillations for a range of frequencies (0.3 Hz–1.5 Hz) and amplitudes (±5°,±15°,±25°). The open-loop system exhibited varying degrees of amplitude attenuation and signal bias.

In order to improve the wrist roll system, position feedback control was implemented using the MTA source code. The proportional gain, K_p, was tuned to provide the best response when multiplied by the position error. The gain was tuned at two test points which exhibited the largest signal bias and largest amplitude attenuation. The sine wave input at 0.3 Hz and 5° amplitude had the largest amplitude attenuation. The second test point was at 1.5 Hz and 25° amplitude; this test point demonstrated the largest signal bias. The proportional gain was finalized at $K_p = 1$. This provided the best improvement for signal bias and amplitude attenuation without greatly amplifying the input at other test points.

Incorporating the position feedback into the wrist roll system improved the performance at all test points previously tested. At the lower amplitude inputs (±5°), the closed-loop system still demonstrated some evidence of amplitude attenuation. With the position feedback, the average normalized amplitude only increased, on average, from 73% to 79%. However, preconditioning the input with the necessary amplitude can be used to compensate for the difference in order to achieve the correct output amplitude. During dynamic wind tunnel experiments at a fan speed of 60 mph, the MTA closed-loop system performed nearly the same as when there was no freestream velocity despite the increased aerodynamic loading. In an experiment performed at a higher fan speed (120 mph), other MTA joints began to deflect from their stationary positions under the increased aerodynamic loads, presumably in part because they remained part of an open-loop control structure. These deflections permeated through the inverse kinematics into all the other Cartesian coordinates except pitch. The pitch was unaffected by the deflection of the wrist pitch and elbow pitch joints

because the control point of the model was defined on the axis of rotation of the wrist roll joint. The closed-loop system of the MTA demonstrated its reliability, even under large aerodynamic loads of a pitch oscillation at 1 Hz and 50° at a 60 mph nominal speed.

Since the system does not behave linearly, these findings are limited by the frequency and amplitude of the input. The closed-loop system performed more consistently at 5° amplitude, 1.5 Hz than it did at 25° amplitude and 1.5 Hz because the performance of the closed-loop system is dependent upon the angular velocities commands given to the system. As the magnitude of the angular acceleration, or the difference between velocity commands divided by the timestep, increases, the closed-loop system behaves more erratically. For example, when the frequency and amplitude of oscillation were 2 Hz and 25°, the output appeared unstable. The wrist roll motor could not execute a change in direction at the extrema fast enough to meet the commanded velocities. While it is difficult to predict angular velocity and acceleration during the trajectory, the angular velocity and angular acceleration limits of the wrist roll motor must be considered when planning pitch oscillations for dynamic wind tunnel experiments.

5.2 Integrating Sensors with the Wind Tunnel

The MTA calculated the Cartesian position of the model using the joint angles and inverse kinematics. Assumptions were made that, regardless of load, the sting and MTA links were infinitely stiff. Realistically, the sting and links will flex a small amount when the load is above a certain threshold. Furthermore, aeroelastic effects may lead to difference in both model position and orientation. To address these concerns, an independent, second position and orientation sensor was used to validate the model orientation. The IMU was attached to the sting in close proximity to the

trailing edge of the wing in order to measure the Euler angles during dynamic wind tunnel tests. First, the IMU and model, which were both attached to the sting, were oscillated at three different frequency-amplitude pairs with no freestream velocity. The IMU data was time-shifted to match the MTA's pitch output (θ_b). Unfortunately, time-shifting the data inhibited pure quantitative analysis of the phase lag between the IMU Euler angles and the MTA Euler angles. The time-shifting involved matching the onset of motion for each of θ_b outputs, and so despite the limitation, a level of qualitative evidence still existed. The pitch Euler angle of the IMU and the MTA did match frequency and amplitude with less than 12% error. When attempting to perform a multi-DOF trajectory, it will be crucial to perform the inertial-value reset in order to align the IMU reference frame with respect to the inertial reference frame approximated for straight-and-level. In this study, the IMU's performance was limited to single-DOF motions about the y_b axis. The IMU proved its reliability to measure θ_b at fan speeds up to 60 mph.

Along with the MTA, Air Force Research Laboratory (AFRL), Munitions Directorate delivered the data acquisition system and computer used for the dynamic wind tunnel. The NI® PXI-6123 was an eight-channel simultaneous sampling DAQ card installed into the delivered system to measure force/torque and pressure analog signals. This DAQ card was acquired because it was able to record up to eight analog signals from either a force balance or pressure transducer signals. The ATI® Nano-25 force/torque balance was purchased in order to measure the forces and moments during dynamic wind tunnel testing.

In initial studies, four, fast-response pressure transducers flush-mounted on the model's wing were used to study the aerodynamics of an oscillatory pitch motion. The transducers were set directly opposite one another on the top and bottom surface at the quarter-chord and three-quarter-chord. The pressure was measured while

125

executing pitch oscillations at 20°, 30°, and 50° at 1 Hz and the wind tunnel's fan speed was 60 mph. Another test was performed with a pitch amplitude of 30° at an increased fan speed of 120 mph. An encouraging result was demonstrating that the pressure signals of the upper and lower surfaces were inversely oscillating. The three-quarter-chord pressure signals resembled a square wave instead of a sine wave. When the amplitude was increased to 50°, the three-quarter-chord signals began to more closely resemble a sinusoidal wave. Another interesting phenomenon appeared during the oscillation. A downward spike occurred at the quarter-chord in the lower pressure half-cycle of the oscillation. The downward spike may have been caused by the flow detaching from the wing as the wing began to pitch-down towards $\theta_b = 0$. The pressure coefficient generally collapsed the pressure data for the 30° amplitude cases at 60 mph and 120 mph, as expected.

5.3 Problem Statement, Refined

Significant progress has been made towards future endeavors such as control systems-in-the-loop wind tunnel testing. By performing a series of moderately complex maneuvers invoking the operation of all the joints on the MTA, the system exhibited easily observed discrepancies in the output. To address this concern the MTA and supporting equipment were configured to perform single-DOF dynamic wind tunnel testing. While this motion is basic for the 6-DOF robotic manipulator to perform, this motion provided a useful benchmark for unsteady aerodynamic data. The problem statement was refined as follows:

1. Quantify the performance of the MTA wrist roll motor and controller using a single-DOF, pitch oscillation. If necessary apply feedback control to enhance performance.

   The MTA wrist roll motor and controller, or open-loop system, was charac-

terized by examining the output of the model's Cartesian position given various frequency and amplitude pitch oscillations. The open-loop system exhibited large signal bias and amplitude attenuation. Using position feedback a proportional gain was tuned to improve the issues of the open-loop system.

2. Quantify the performance of the closed-loop system using a single-DOF, pitch oscillation, MTA wrist roll motor, controller, and position feedback.

   The closed-loop system demonstrated considerable improvements over the open-loop system. Specifically, the signal bias was reduced in some cases up to 95% and the amplitude attenuation was reduced in some cases up to 10%. Furthermore, under lower aerodynamic load, the MTA performed equivalently to the absence of aerodynamic loads, i.e. zero freestream velocity. Although, as the aerodynamic load increased (wind tunnel fan speed of 120 mph, with a 30° oscillation), the other joints of the MTA (e.g. wrist pitch and elbow pitch) did not maintain their static positions.

3. Validate the model orientation with a second in-situ device and compare to the MTA's Cartesian position output using a secondary position sensor.

   The IMU closely matched the range of pitch angles of the MTA for test cases with and without wind. One potential drawback of the IMU as configured in the study is that its maximum sampling rate was limited to 22 Hz. However the principle of operation was sound; perhaps the IMU could be integrated with the NI® DAQ in order to increase the sample rate. If not, a smaller, faster-responding IMU might be a better solution.

4. Incorporate the secondary position sensor and pressure transducers into dynamic wind tunnel experiments using a pitch oscillation

   The IMU and pressure transducers measured the motion and pressure, respec-

tively, during three pitch oscillations at different amplitudes. The IMU validated the pitch angle calculated by the MTA. Meanwhile, the pressure transducers indicated evidence of unsteady aerodynamic effects including dynamic stall during oscillation.

5.4 Future Work

With MTA wrist roll system characterized for single-DOF dynamic wind tunnel testing, the next logical research effort is to characterize the wrist pitch system using the established procedure. The wrist pitch system should be characterized using a trajectory designed to isolate the wrist pitch joint. This oscillatory motion will move the wind tunnel model and sting along an arc in the y_i-z_i plane. Once the system is characterized, improvements can be made to enhance the performance of the motor and controller system. This process can be extended to characterizing the other joints as well.

While pressure measurements are useful for studying unsteady aerodynamics, incorporating a force balance, such as the Nano25, will provide valuable aerodynamic data. Using the hardware acquired, the force balance should be interfaced with the NI$^{®}$ DAQ system. Tests will should be performed which calibrate the force balance. Once the force balance is integrated with the MTA, experiments should be performed to determine the procedure for dynamic taring. Experiments may include the use of a helium or vacuum container to isolate the time-history of the dynamic-inertial loads. Next, the trigger needs to be establish in order to corroborate the aerodynamic data with the motion. The MTA source code has an established executable file which can test the functionality of the trigger.

Currently the secondary position and orientation sensor, the IMU, only outputs the Euler angles, but the Matlab$^{®}$ program can be modified to report its position as

well. The position of the IMU is calculated using the axial accelerations and angular rates which are acquired during operation. In order to synchronize the IMU with the motion of the MTA, the IMU can be connected to the DAQ system. With the trigger synchronizing the motion, aerodynamic data, and IMU data, improved correlations can be made. Connecting the IMU to the DAQ system also may increase the IMU's sample rate because the IMU can be operated in "continuous mode." These research objectives will further the effort towards performing complex dynamic wind tunnel tests, such as the design of experiments for the flexible weapon.

Appendix A. Remaining Experimental Data

This appendix entails the remianing data gathered during this research effort. Each section is labeled with the corresponding title from *Chapter IV*.

Wrist Roll System Model

The figures below are samples of the data collected to characterize the wrist roll motor and controller.
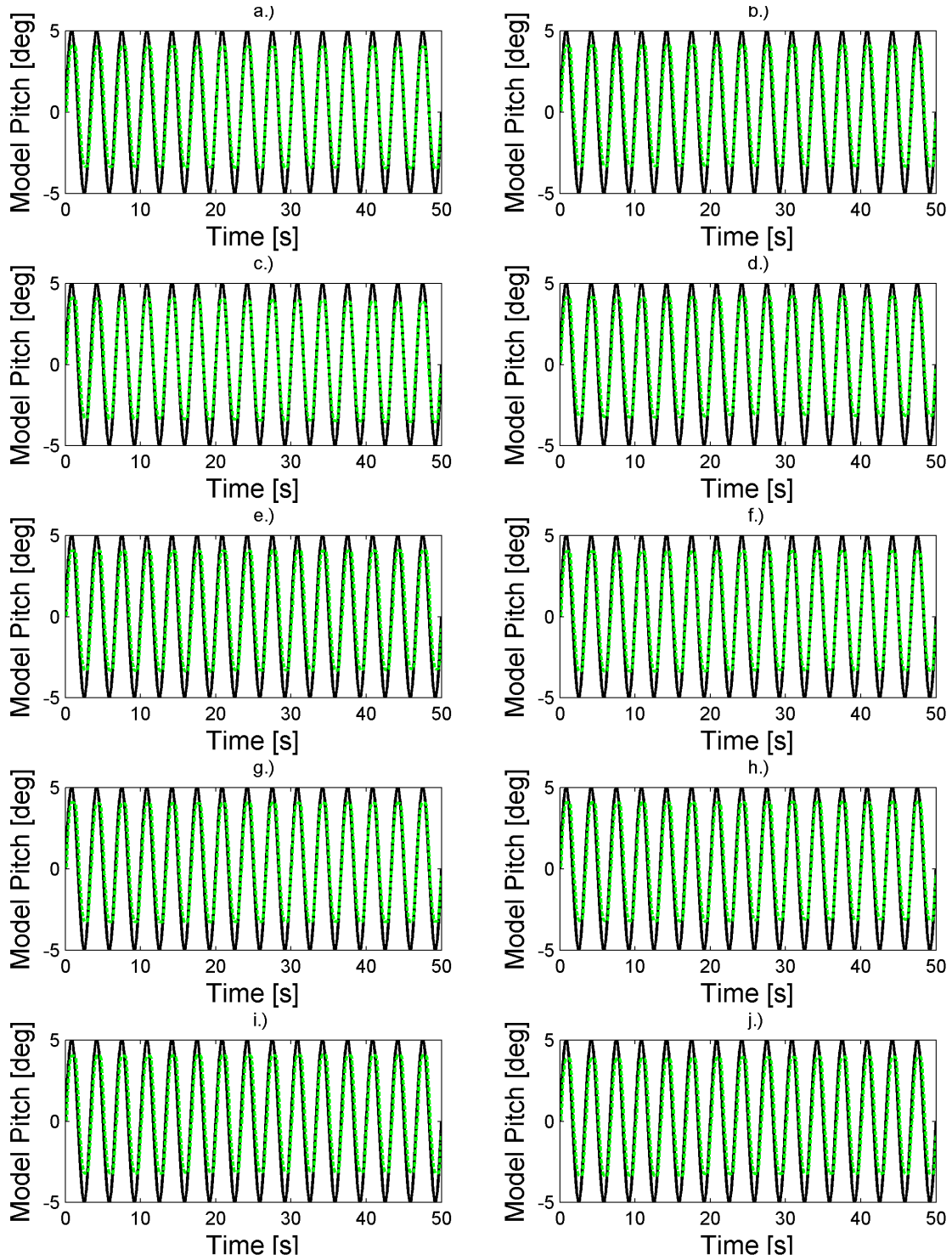
Figure 85. The input-to-output (solid, black line and dashed, green line respectively) relationship for the 10 tests conducted at $0.3\,\mathrm{Hz}$ and $5°$.
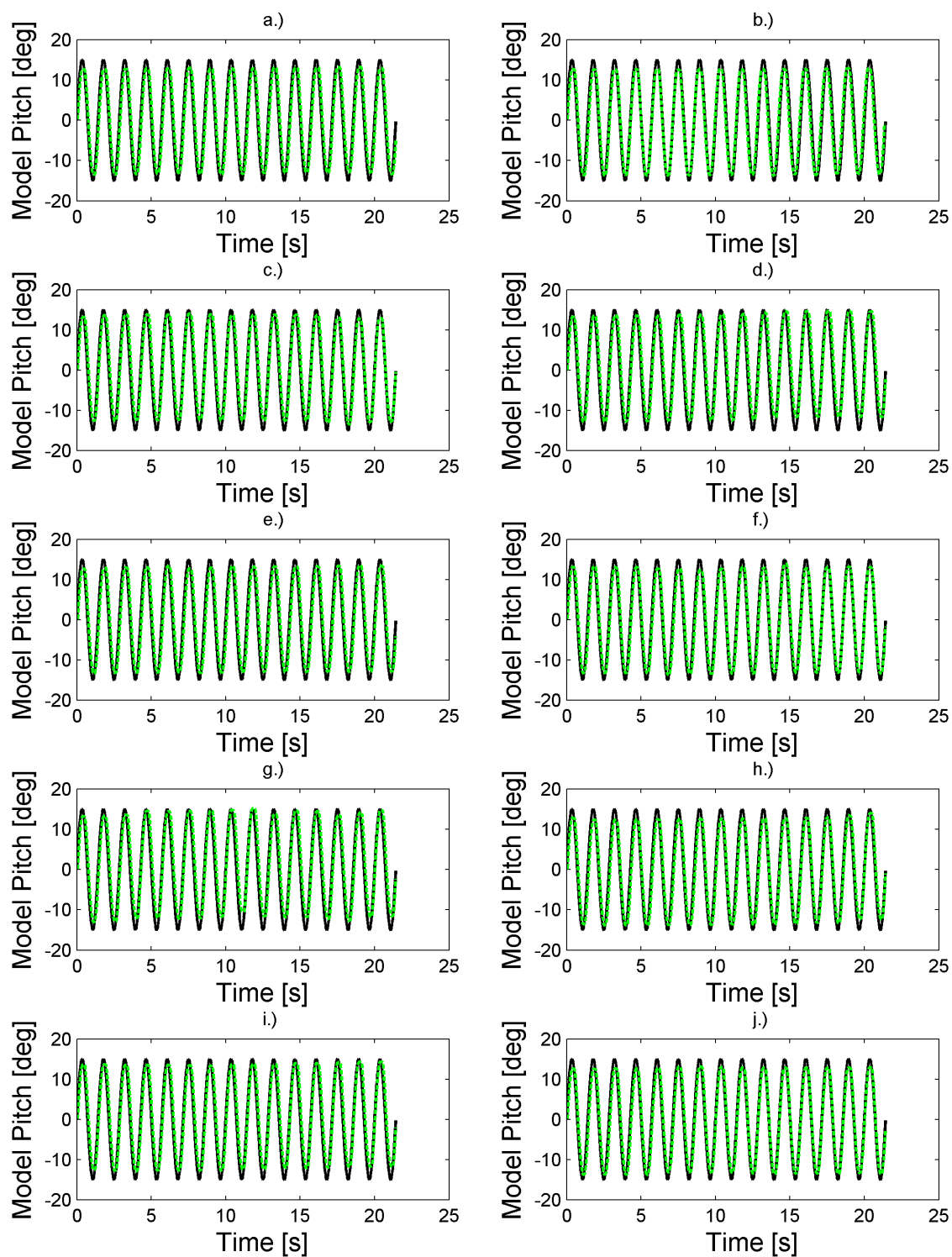
Figure 86. The input-to-output (solid, black line and dashed, green line respectively) relationship for the 10 tests conducted at $0.7\,\mathrm{Hz}$ and $15°$.
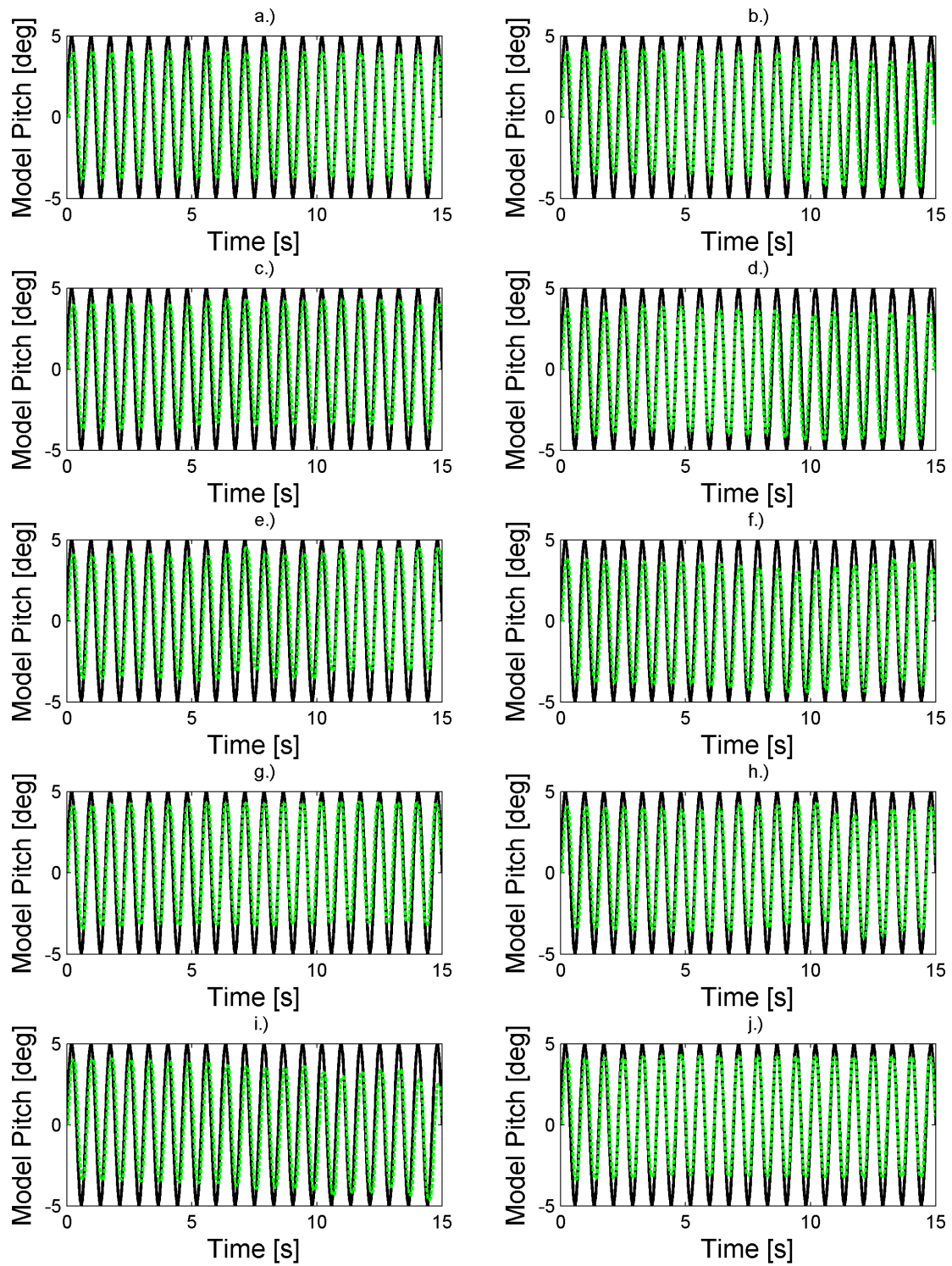
Figure 87. The input-to-output (solid, black line and dashed, green line respectively) relationship for the 10 tests conducted at $1.3\,\mathrm{Hz}$ and $5°$.

133
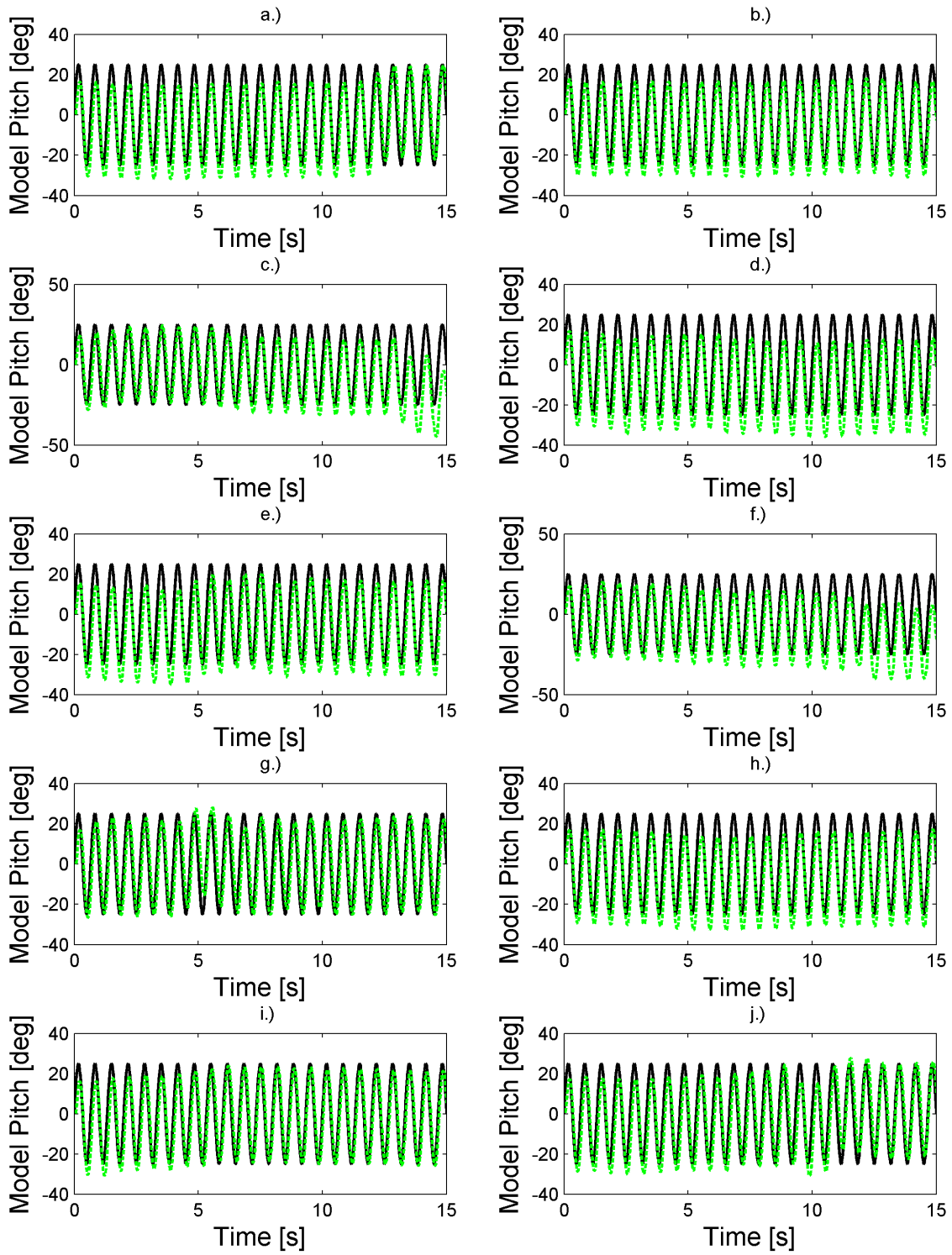
Figure 88. The input-to-output (solid, black line and dashed, green line respectively) relationship for the 10 tests conducted at $1.5\,\mathrm{Hz}$ and $25°$.

134

Evaluation of the Closed Loop System

The figures below are samples of the data collected to characterize the closed loop system for $K_p = 1$.
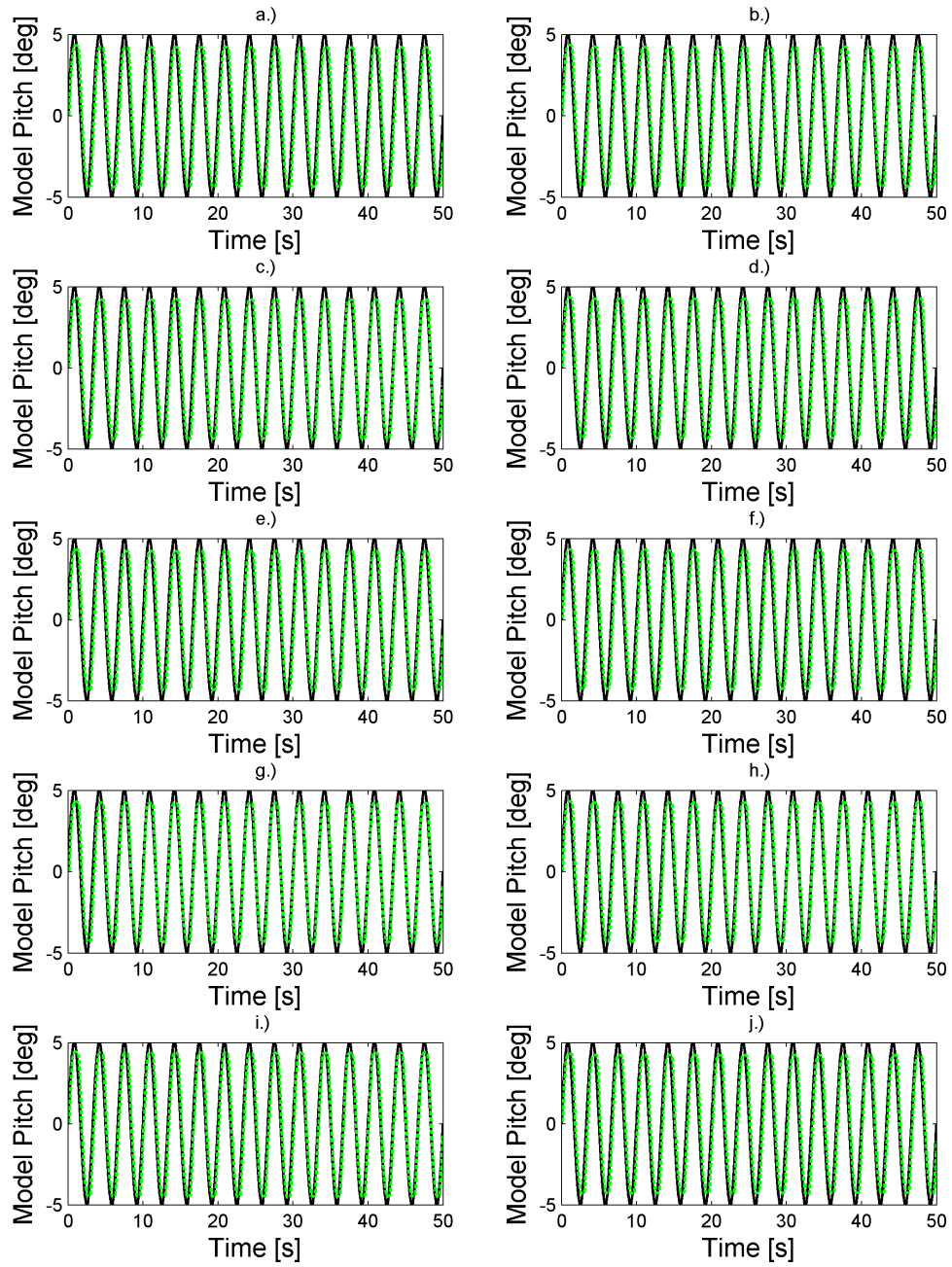
Figure 89. The input-to-output relationship for 3 of the 10 tests conducted at $0.3\,\mathrm{Hz}$ **and** $5°$ **for** $K_p = 1$**.**

136
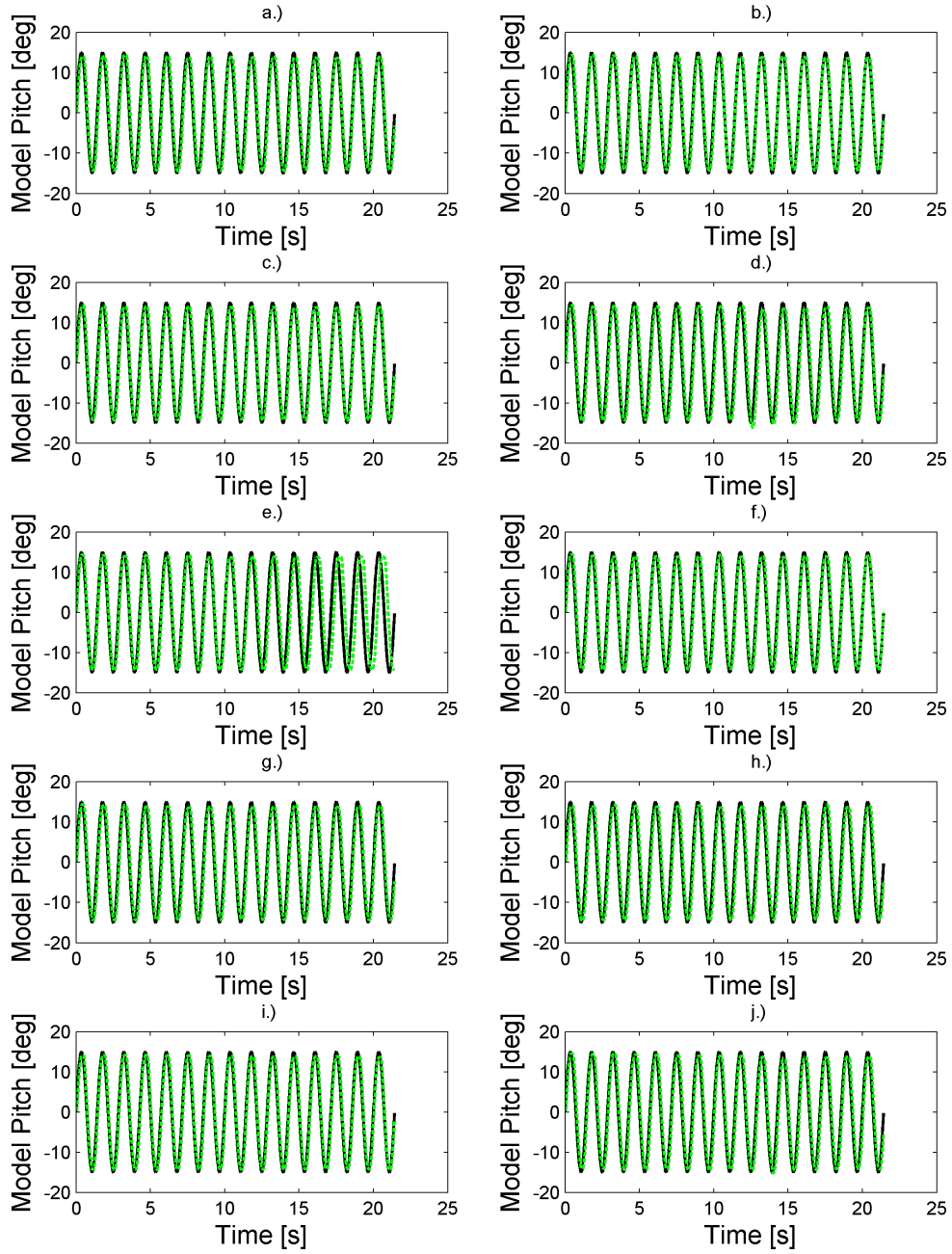
Figure 90. The input-to-output relationship for 3 of the 10 tests conducted at $0.7\,\text{Hz}$ and $15°$ for $K_p = 1$.

137
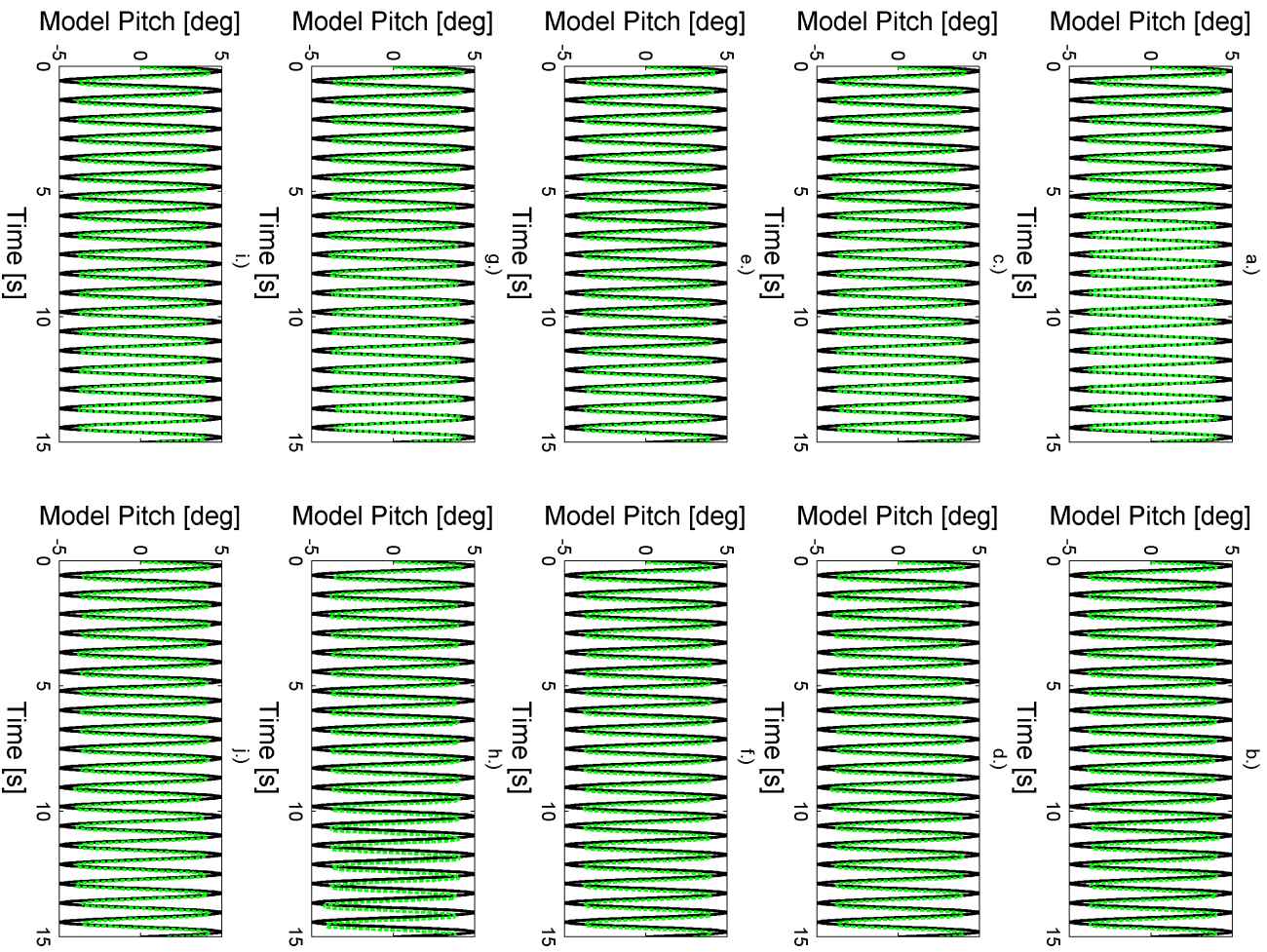
Figure 91. The input-to-output relationship for 3 of the 10 tests conducted at 1.3 Hz and 5° for $K_p = 1$.

138
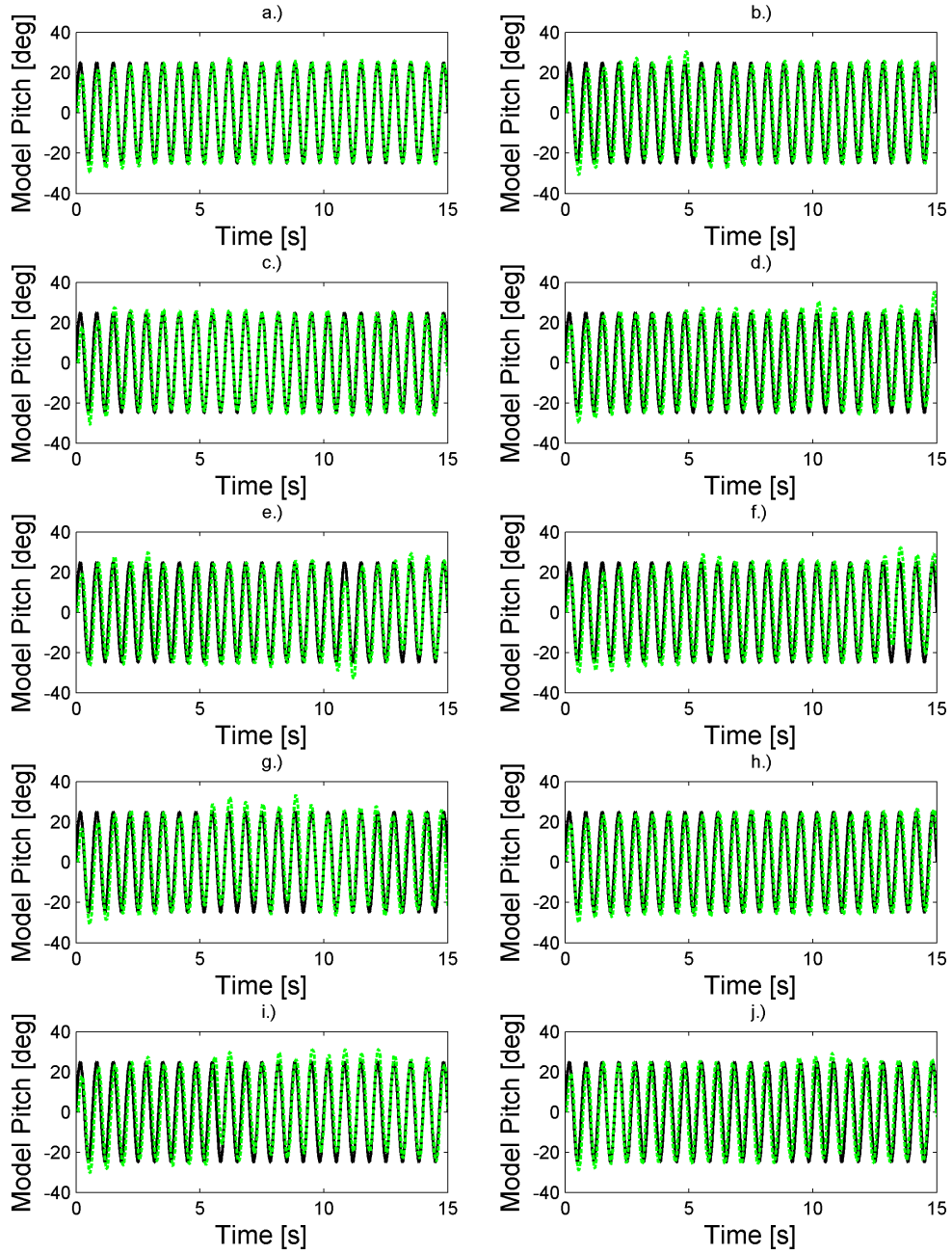
Figure 92. The input-to-output relationship for **3 of the 10 tests conducted at** $1.5\,\mathrm{Hz}$ and $25°$ for $K_p = 1$.

139

IMU Validation of Sting Rigidity and MTA Output

The figure below presents the agreement between the IMU and MTA Euler angles while perfoming a pitch oscillation at $1.1\,\text{Hz}$ and $15°$ amplitude.
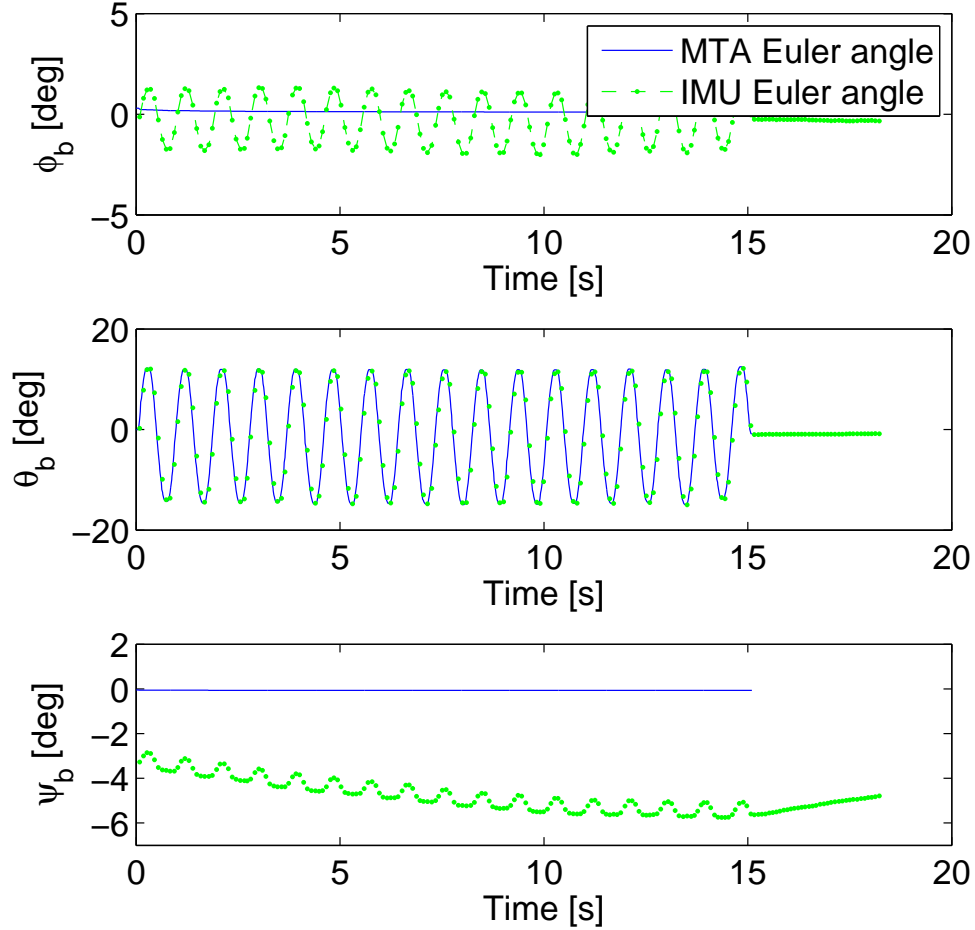
Figure 93. The time-shifted IMU Euler angle, θ_b demonstrated good agreement with the MTA Cartesian positions. However the IMU detects a small oscillations for ϕ_b and ψ_b during a pitch oscillation at $1.1\,\text{Hz}$ and $15°$ amplitude.

Incorporation of Dynamic Pressure Measurements

The figure below presents the agreement between the IMU and MTA Euler angles while perfoming a pitch oscillation at $1\,\text{Hz}$ and $30°$ amplitude at a nominal speed of 60 mph.
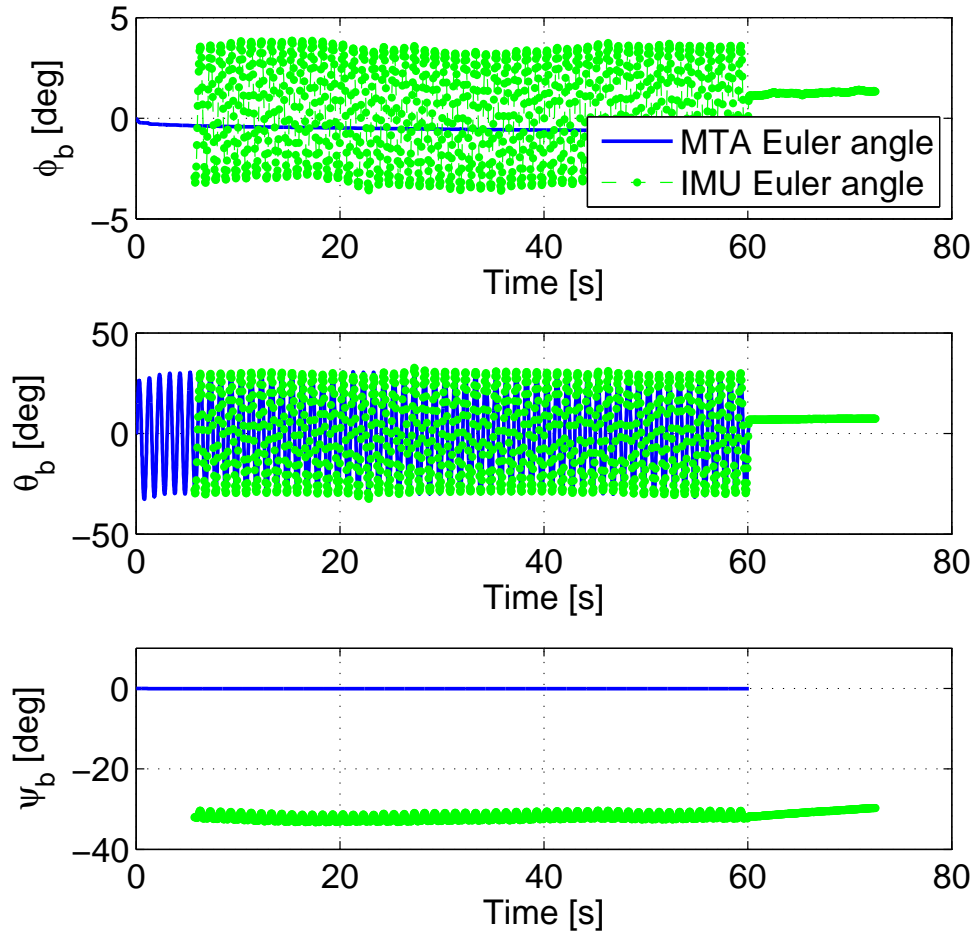
Figure 94. IMU Euler angles are compared to the Euler angles calculated by the MTA during a pitch oscillation $1\,\mathrm{Hz}$, $30°$ amplitude, and nominal speed of 60 mph.

Appendix B. Matlab Code

Coordinate Transformation Program GUI

```matlab
function Trajectory_Coord_Trans
%%   Set up some varables
%   First clear everything
        clear all
        clc

%   Set Number of tabs and tab labels.  Make sure the number of tab labels
%   match the HumberOfTabs setting.
        NumberOfTabs = 3;                    % Number of tabs to be generated
        TabLabels = {'Coordinate Transformation'; 'Operating Conditions';'Trajectory Cre
        if size(TabLabels,1) ~= NumberOfTabs
            errordlg('Number of tabs and tab labels must be the same','Setup Error');
            return
        end

%   Get user screen size
        SC = get(0, 'ScreenSize');
        MaxMonitorX = SC(3);
        MaxMonitorY = SC(4);

 %   Set the figure window size values
        MainFigScale = .6;              % Change this value to adjust the figure size
        MaxWindowX = round(MaxMonitorX*MainFigScale);
        MaxWindowY = round(MaxMonitorY*MainFigScale);
        XBorder = (MaxMonitorX-MaxWindowX)/2;
        YBorder = (MaxMonitorY-MaxWindowY)/2;
        TabOffset = 0;                  % This value offsets the tabs inside the figure.
        ButtonHeight = 35;
        PanelWidth = MaxWindowX-2*TabOffset+4;
        PanelHeight = MaxWindowY-ButtonHeight-2*TabOffset;
        ButtonWidth = round((PanelWidth-NumberOfTabs)/NumberOfTabs);

 %   Set the color varables.
        White = [1  1  1];              % White - Selected tab color
        BGColor = .9*White;            % Light Grey - Background color

%%   Create a figure for the tabs
        hTabFig = figure(...
            'Units', 'pixels',...
            'Toolbar', 'none',...
            'Position',[ XBorder, YBorder, MaxWindowX, MaxWindowY ],...
            'NumberTitle', 'off',...
            'Name', 'Trajectory Coordinate Transformation',...
            'MenuBar', 'none',...
            'Resize', 'off',...
```

```matlab
            'DockControls', 'off',...
            'Color', White);
%%  Define a cell array for panel and pushbutton handles, pushbuttons labels and other
    %   rows are for each tab + two additional rows for other data
    %   columns are uipanel handles, selection pushbutton handles, and tab label strings
            TabHandles = cell(NumberOfTabs,3);
            TabHandles(:,3) = TabLabels(:,1);
    %   Add additional rows for other data
            TabHandles{NumberOfTabs+1,1} = hTabFig;          % Main figure handle
            TabHandles{NumberOfTabs+1,2} = PanelWidth;       % Width of tab panel
            TabHandles{NumberOfTabs+1,3} = PanelHeight;      % Height of tab panel
            TabHandles{NumberOfTabs+2,1} = 0;                % Handle to default tab 2 co
            TabHandles{NumberOfTabs+2,2} = White;            % Selected tab Color
            TabHandles{NumberOfTabs+2,3} = BGColor;          % Background color
%%  Build the Tabs
        for TabNumber = 1:NumberOfTabs
        % create a UIPanel
            TabHandles{TabNumber,1} = uipanel('Units', 'pixels', ...
                'Visible', 'off', ...
                'Backgroundcolor', White, ...
                'BorderWidth',1, ...
                'Position', [TabOffset TabOffset ...
                PanelWidth PanelHeight]);

        % create a selection pushbutton
            TabHandles{TabNumber,2} = uicontrol('Style', 'pushbutton',...
                'Units', 'pixels', ...
                'BackgroundColor', BGColor, ...
                'Position', [TabOffset+(TabNumber-1)*ButtonWidth PanelHeight+TabOffset.
                    ButtonWidth ButtonHeight], ...
                'String', TabHandles{TabNumber,3},...
                'HorizontalAlignment', 'center',...
                'FontName', 'arial',...
                'FontWeight', 'bold',...
                'FontSize', 10);

        end
%%  Define the callbacks for the Tab Buttons
%   All callbacks go to the same function with the additional argument being the Tab num
        for CountTabs = 1:NumberOfTabs
            set(TabHandles{CountTabs,2}, 'Callback', ...
                {@TabSellectCallback, CountTabs});
        end
%%  Define content for the --Model to MTA Tab--
        %   Build the text for the first tab
        Intro = {'This tab will perform a';'coordinate tranfromation'};
        InputTxt={'Browse for your input trajectory file:'};
        UnitTxt={'What are the units (Model to MTA) or'; ' desired units (MTA to Model)
        PosTxt={'Position:'};
        AngTxt={'Angle:'};
        OutputTxt={'Desired Output filename (with extension):',' ';...
            '(Note: this file will be placed in the same directory',...
```

143

```matlab
            ' as the model trajectory and will overwrite the file'};
%    Display "Intro"
     uicontrol('Style', 'text',...
         'Position', [ round(PanelWidth/4) round(PanelHeight*.8) ...
             round(PanelWidth/2) round(PanelHeight/6) ],...
         'Parent', TabHandles{1,1}, ...
         'string', Intro,...
         'BackgroundColor', White,...
         'HorizontalAlignment', 'center',...
         'FontName', 'arial',...
         'FontWeight', 'bold',...
         'FontSize', 16);
%     Coordinate Transformation Type PopMenu
      h(1)=uicontrol('Parent', TabHandles{1,1}, ...
         'Units', 'pixels', ...
         'Position', [round(PanelWidth/6) round(PanelHeight*.75)...
         160 ButtonHeight], ...
         'String', 'Model to MTA|MTA to Model', ...
         'Style', 'popupmenu',...
         'HorizontalAlignment', 'center',...
         'FontName', 'arial',...
         'FontWeight', 'normal',...
         'FontSize', 14,...
         'Tag','Function');
%    Display "InputTxt"
     uicontrol('Style', 'text',...
         'Position', [ round(PanelWidth/6) round(PanelHeight*(2/3)) ...
             300 35 ],...
         'Parent', TabHandles{1,1}, ...
         'string', InputTxt,...
         'BackgroundColor', White,...
         'HorizontalAlignment', 'left',...
         'FontName', 'arial',...
         'FontWeight', 'normal',...
         'FontSize', 12);
StaticTxtWidth=425;
%    "Input Filename" Static Text
     uicontrol('Parent',TabHandles{1,1},'Tag','InputFilename',...
         'Units','pixels',...
         'String','(Input Filename)','Style','text',...
         'HorizontalAlignment','center',...
         'Position',[round(PanelWidth/6) ...
         round(PanelHeight*(2/3))-35 StaticTxtWidth ButtonHeight],...
         'FontName','arial','FontWeight','normal','FontSize',12);
%    "Get Input file"  Pushbutton
     uicontrol('Parent', TabHandles{1,1}, ...
         'Units', 'pixels', ...
         'Position', [round(PanelWidth/6)+StaticTxtWidth+10 ...
         round(PanelHeight*(2/3))-35 85 ButtonHeight], ...
         'String', 'Browse', ...
         'Callback', @GetInputCallback , ...
         'Style', 'pushbutton',...
```

```matlab
            'HorizontalAlignment', 'center',...
            'FontName', 'arial',...
            'FontWeight', 'normal',...
            'FontSize', 12);
Offset=round(PanelHeight*(2/3))-35;
UnitTxtWidth=290;
%    Display "UnitTxt"
    uicontrol('Style', 'text',...
        'Position', [ round(PanelWidth/6) Offset-ButtonHeight-30 ...
            UnitTxtWidth 35 ],...
        'Parent', TabHandles{1,1}, ...
        'string', UnitTxt,...
        'BackgroundColor', White,...
        'HorizontalAlignment', 'left',...
        'FontName', 'arial',...
        'FontWeight', 'normal',...
        'FontSize', 12);
Offset=Offset-ButtonHeight-30;
PopupWidth=120;
%    Display "PosTxt"
    uicontrol('Style', 'text',...
        'Position', [ round(PanelWidth/6)+UnitTxtWidth+5 Offset ...
            PopupWidth 35 ],...
        'Parent', TabHandles{1,1}, ...
        'string', PosTxt,...
        'BackgroundColor', White,...
        'HorizontalAlignment', 'left',...
        'FontName', 'arial',...
        'FontWeight', 'normal',...
        'FontSize', 12);
Leftset=round(PanelWidth/6)+UnitTxtWidth+5;
%    Display "AngTxt"
    uicontrol('Style', 'text',...
        'Position', [ Leftset+PopupWidth+20 Offset PopupWidth 35 ],...
        'Parent', TabHandles{1,1}, ...
        'string', AngTxt,...
        'BackgroundColor', White,...
        'HorizontalAlignment', 'left',...
        'FontName', 'arial',...
        'FontWeight', 'normal',...
        'FontSize', 12);
%    Position Unit PopMenu
    h(1)=uicontrol('Parent', TabHandles{1,1}, ...
        'Units', 'pixels', ...
        'Position', [Leftset Offset-30 120 ButtonHeight], ...
        'String', 'm|cm|mm|ft|in', ...
        'Style', 'popupmenu',...
        'HorizontalAlignment', 'center',...
        'FontName', 'arial',...
        'FontWeight', 'normal',...
        'FontSize', 12,...
        'Tag','PositionUnit');
```

```matlab
%     Angle Unit PopMenu
      h(2)=uicontrol('Parent', TabHandles{1,1}, ...
          'Units', 'pixels', ...
          'Position', [Leftset+PopupWidth+25 Offset-30 120 ...
          ButtonHeight], ...
          'String', 'rad|deg', ...
          'Style', 'popupmenu',...
          'HorizontalAlignment', 'center',...
          'FontName', 'arial',...
          'FontWeight', 'normal',...
          'FontSize', 12,...
          'Tag','AngleUnit');
Offset=Offset-35;
%     Display "OutputTxt"
      uicontrol('Style', 'text',...
          'Position', [ round(PanelWidth/6) Offset-ButtonHeight-25 500 35 ],...
          'Parent', TabHandles{1,1}, ...
          'string', OutputTxt,...
          'BackgroundColor', White,...
          'HorizontalAlignment', 'left',...
          'FontName', 'arial',...
          'FontWeight', 'normal',...
          'FontSize', 12);
Offset=Offset-ButtonHeight-25;
OutputTxtWidth=450;
%    "Output Filename" Edit Textbox
      uicontrol('Style','edit',...
          'Parent',TabHandles{1,1},...
          'Units','pixels',...
          'Position',[ round(PanelWidth/6) Offset-ButtonHeight...
          OutputTxtWidth ButtonHeight],...
          'HorizontalAlignment','left',...
          'FontName','arial',...
          'FontWeight','normal',...
          'FontSize',12,...
          'Tag','OutputFilename');
%    "Convert file"  Pushbutton
      uicontrol('Parent', TabHandles{1,1}, ...
          'Units', 'pixels', ...
          'Position', [round(PanelWidth/6)+OutputTxtWidth+25 ...
          Offset-ButtonHeight 85 ButtonHeight],...
          'String', 'Convert', ...
          'Callback', @ConvertCallback , ...
          'Style', 'pushbutton',...
          'HorizontalAlignment', 'center',...
          'FontName', 'arial',...
          'FontWeight', 'normal',...
          'FontSize', 12);

%%  Define content for the --Operating Conditions Tab--
    TxtHeight=30;
    % Center Tetbox
```

```matlab
uicontrol('Parent', TabHandles{2,1},...
'Units','pixels',...
'Position',[round(PanelWidth/5)-30 round(PanelHeight*.875) ...
    620 TxtHeight],...
'Style','text',...
'String','Location of MTA-model origin relative to MTA-inertial ref. frame',...
'HorizontalAlignment','left',...
'BackgroundColor','white',...
'FontName','arial',...
'FontWeight','bold',...
'FontSize', 14);
% Straight & Level Tetbox
%    uicontrol('Parent', TabHandles{2,1},...
%    'Units','pixels',...
%    'Position',[round(PanelWidth*(2/3))-30 round(PanelHeight*.875) ...
%        220 TxtHeight],...
%    'Style','text',...
%    'String','Straight & Level',...
%    'HorizontalAlignment','left',...
%    'BackgroundColor','white',...
%    'FontName','arial',...
%    'FontWeight','bold',...
%    'FontSize', 14);
Center={'Xc [m]';'Yc [m]';'Zc [m]';'Roll [rad]';...
        'Pitch [rad]';'Yaw [rad]'};
CenterValues={'-0.064';'-2.551';'-1.793';'0.00';'0.00';'-1.67182'};
Leftset=round(PanelWidth/8);
Offset=round(PanelHeight*.8)-TxtHeight-10;
for cnt=1:length(Center)
    %    "_ Center" Static Textbox
        uicontrol('Parent', TabHandles{2,1},...
            'Units','pixels',...
            'Position',[Leftset round(PanelHeight*.8) ...
                100 TxtHeight],...
            'Style','text',...
            'String',Center{cnt},...
            'HorizontalAlignment','left',...
            'BackgroundColor','white',...
            'FontName','arial',...
            'FontWeight','normal',...
            'FontSize', 12);
    %    "_ Center" Edit Textbox
        h(cnt+10)=uicontrol('Parent', TabHandles{2,1},...
            'Units','pixels',...
            'Position',[Leftset Offset ...
                75 ButtonHeight],...
            'Style','edit',...
            'String',CenterValues{cnt},...
            'HorizontalAlignment','left',...
            'FontName','arial',...
            'FontWeight','normal',...
            'FontSize', 12);
```

147

```matlab
                Leftset=Leftset+115;
        end

    MaxDist={'Max in x-dir [m]';'Max in y-dir [m]';...
            'Max in z-dir [m]'};
    MaxDistValues={'0';'0.1143';'0.1143'};
    Leftset=round(PanelWidth/8);
    Offset=round(PanelHeight*.8)-TxtHeight-ButtonHeight-20;
    for cnt=1:length(MaxDist)
        %   "_ Operating Space" Static Textbox
            uicontrol('Parent', TabHandles{2,1},...
                'Units','pixels',...
                'Position',[Leftset Offset ...
                    150 TxtHeight],...
                'Style','text',...
                'String',MaxDist{cnt},...
                'HorizontalAlignment','left',...
                'BackgroundColor','white',...
                'FontName','arial',...
                'FontWeight','normal',...
                'FontSize', 12);
        %   "_ Operating Space" Edit Textbox
            h(cnt+20)=uicontrol('Parent', TabHandles{2,1},...
                'Units','pixels',...
                'Position',[Leftset Offset-10-TxtHeight ...
                    75 ButtonHeight],...
                'Style','edit',...
                'String',MaxDistValues{cnt},...
                'HorizontalAlignment','left',...
                'FontName','arial',...
                'FontWeight','normal',...
                'FontSize', 12);
        Leftset=Leftset+165;
    end
%% Saves the handles to UserData
    set(hTabFig,'UserData',h )
%%  Save the TabHandles in guidata
        guidata(hTabFig,TabHandles);


%%  Make Tab 1 active
        TabSellectCallback(0,0,1);



end
%%  Callback for Tab Selection
function TabSellectCallback(~,~,SelectedTab)
%   All tab selection pushbuttons are greyed out and uipanels are set to
%   visible off, then the selected panel is made visible and it's selection
%   pushbutton is highlighted.

    %   Set up some varables
        TabHandles = guidata(gcf);
```

```matlab
        NumberOfTabs = size(TabHandles,1)-2;
        White = TabHandles{NumberOfTabs+2,2};             % White
        BGColor = TabHandles{NumberOfTabs+2,3};           % Light Grey

%   Turn all tabs off
        for TabCount = 1:NumberOfTabs
            set(TabHandles{TabCount,1}, 'Visible', 'off');
            set(TabHandles{TabCount,2}, 'BackgroundColor', BGColor);
        end

%   Enable the selected tab
        set(TabHandles{SelectedTab,1}, 'Visible', 'on');
        set(TabHandles{SelectedTab,2}, 'BackgroundColor', White);

end

%%  Get Input File Callback
    function GetInputCallback(~,~)
    global chosenfile chosendir
%     %   Get TabHandles from guidata and set some varables
%         TabHandles = guidata(gcf);
%         NumberOfTabs = size(TabHandles,1)-2;
%         PanelWidth = TabHandles{NumberOfTabs+1,2};
%         PanelHeight = TabHandles{NumberOfTabs+1,3};

%   Get the file name from the user
        [chosenfile,chosendir]=uigetfile('*.txt;*.csv','Input File');
        set(findobj('Tag','InputFilename'),'String',[chosendir,chosenfile]);
        [~,~,ext]=fileparts([chosendir,chosenfile]);

        if chosenfile == 0,
            %   If User cancels then display error message
            errordlg('Please select a either *.txt or *.csv');
            return
        elseif ~strcmp(ext,'.csv')&& ~strcmp(ext,'.txt')
            errordlg('Please select a either *.txt or *.csv');
            return
        end

%   Build path to file
%         PicFilePath = strcat(PicDirectory,PicNameWithTag);
    end


%% Convert file Callback
    function ConvertCallback(~,~)
    global chosenfile chosendir
    h=get(gcf,'UserData');
    Center=zeros(1,6);
    Max=Center;
    for cnt=1:6
        Center(cnt)=str2double(get(h(cnt+10),'String'));
```

```
        end
        for cnt=1:3
            Max(cnt)=str2double(get(h(cnt+20),'String'));
        end
        Func=get(findobj('Tag','Function'),'Value');
        Units(1)=get(findobj('Tag','PositionUnit'),'Value');
        Units(2)=get(findobj('Tag','AngleUnit'),'Value');
        Output_Filename=get(findobj('Tag','OutputFilename'),'String');
        switch Func
            case 1
                ModeltoMTA_Transform(chosenfile,chosendir,Output_Filename,Units,Center,Max)
            case 2
                MTAtoModel_Transform(chosenfile,chosendir,Output_Filename,Units,Center,Max)
        end
        str='Coordinate transformation is complete.';
        %msgbox('Message','Title of Window')
        END=msgbox(str,'Coordinate Transformation');
        end
```

ModeltoMTA.m

```
function ModeltoMTA_Transform(File,Dir,OutputFilename,in_units,Cent,MxDist)

%----------WIND TUNNERL MODEL-ROBOT ARM COORDINATE TRANSFORMATION----------
%This file reads your input file and outputs a trajectory file with respect
%to the Robot Arm reference frame.
%-------------------------------------------------------------------------
%%This program assumes that the model offset is accounted for in
%%"MtaParameters.txt"
%*************************************************************************
%----Acronyms----
%MTA -> Motion Test Aparatus
%RPY -> Roll, Pitch Yaw
%mod_* -> Model (or Wind Tunnel) Reference Frame
%mta_* -> Robot Reference Frame


%----Wind Tunnel constants (written in wind tunnel reference frame)----
%%Wind Tunnel center point
x_c=Cent(1);
y_c=Cent(2);
z_c=Cent(3);
%%Wind Tunnel straight-and-level
roll_c=Cent(4);
pitch_c=Cent(5);
yaw_c=Cent(6);
%%Wind Tunnel entrance tolerances; maximum distances off-center
x_max=MxDist(1);
y_max=MxDist(2);
```

150

```matlab
z_max=MxDist(3);
%%Tolerance from wall
%%%This is how close you are willing to get to the max off-center distances
esp_x=0.05; %[m], x tolerance away from wall (or object)
esp_y=0.05; %[m], y tolerance away from wall (or object)
esp_z=0.05; %[m], z tolerance away from wall (or object)
%%This is the figurative window in which you can build a trajectory in
%%%Traj_Window=[Xmin,Xmax;Ymin,Ymax;Zmin,Zmax]
Traj_Window=[x_c-x_max+esp_x, x_c+x_max-esp_x;
    y_c-y_max+esp_y, y_c+y_max-esp_y;
    z_c-z_max+esp_z, z_c+z_max-esp_z];

%----General Information----
%%The input file should be written as a trajectory file for the model with
%%respect to the wind tunnel reference frame. The columns of the input file
%%should be as follows:
%%Time [sec] | X [m] | Y [m] | Z [m] | Roll [rad] | Pitch [rad] | Yaw [rad]
%%*********************************************************************

%----Read Input file----
In_fID=fopen([Dir,File],'r');
FirstValue=fscanf(In_fID,'%f',1);
[~,~,ext]=fileparts([Dir,File]);

if strcmp(ext,'.csv')
    if isempty(FirstValue) %There is a header line
        mod_data=csvread([Dir,File],1,0);
    else %There is no Header line
        mod_data=csvread([Dir,File]);
    end
else %The file is *.txt
    if isempty(FirstValue) %There is a header line
        Headers=textscan(In_fID,'%s %s %s %s %s %s %s',1);
    else %There is no Header line
        fseek(In_fID,0,'bof');
    end
    mod_data=textscan(In_fID,'%f %f %f %f %f %f %f ');
    mod_data=cell2mat(mod_data);
end


Time=mod_data(:,1);
mod_xyz=mod_data(:,2:4);
mod_rqp=mod_data(:,5:end);
fclose(In_fID);

%----Unit Conversion---
%%Converts units of the input file to meters and radians

[mod_xyz,mod_rqp]=UnitsIn(in_units,mod_xyz,mod_rqp);

%----Time step check----
```

```matlab
%%Ensures that the time step is 0.008 sec. If not the code will adjust
%%your file and interpolate data points if necessary.
del_t=0.008;

del_T=diff(Time);
del_T=mean(del_T);
if del_T==del_t
    check_t=1;
else
    check_t=0;
end


if check_t==0
    time=[0:del_t:Time(end)]';
    model=[mod_xyz,mod_rqp];
    model_new=zeros(length(time),6);
    disp('Your time-step does not equal 0.008 sec and was corrected')
    figure()
    for m=1:6
        model_new(:,m)=spline(Time,model(:,m),time);
        subplot(3,2,m)
        plot(Time,model(:,m),time,model_new(:,m),'--')
        legend('Original Trajectory','Time-Step Corrected Trajectory')
    end
    Time=time;
    mod_xyz=model_new(:,1:3);
    mod_rqp=model_new(:,4:6);
end

%----Coordinate Transformation----
%%Converts x-y-z translation
rot_xyz=[0 1 0; -1 0 0; 0 0 1]; %Rotation Matrix XYZ
rot_rpy=[0 1 0; -1 0 0; 0 0 1]; %Rotation Matrix RPY
mta_xyz=zeros(size(mod_xyz));
mta_rqp=zeros(size(mod_rqp));
for cnt=1:length(Time)
    %%Transforms the position coordinate system
    mta_xyz(cnt,:)=rot_xyz*mod_xyz(cnt,:)';
    %%Transforms the anglular position coordinate system
    mta_rqp(cnt,:)=rot_rpy*mod_rqp(cnt,:)';

end
%%Centers the trajectory based on the Wind Tunnel Constraints
mta_xyz(:,1)=mta_xyz(:,1)+x_c;
mta_xyz(:,2)=mta_xyz(:,2)+y_c;
mta_xyz(:,3)=mta_xyz(:,3)+z_c;
%%Straight-and-levels the trajectory based on the Wind Tunnel Constraints
mta_rqp(:,1)=mta_rqp(:,1)+roll_c;
mta_rqp(:,2)=mta_rqp(:,2)+pitch_c;
mta_rqp(:,3)=mta_rqp(:,3)+yaw_c;
```

152

```matlab
%----Trajectory Collision Check----
%%Performs wind tunnel-robot arm violation checks
C=[x_c,y_c,z_c];
Tol=[x_max,y_max,z_max];
esp=[esp_x,esp_y,esp_z];

del=[0 0 0; 0 0 0];%row 1-max height difference; row 2-min height difference
del_2=[0 0 0; 0 0 0];%used for recheck

%%%Traj_Window=[Xmin,Xmax;Ymin,Ymax;Zmin,Zmax]
for m=1:3
        del(1,m)=max(mta_xyz(:,m))-Traj_Window(m,2);%del>=0 is a violation
        del(2,m)=Traj_Window(m,1)-min(mta_xyz(:,m));%del>=0 is a violation
        if del(1,m)>=0 && del(2,m)>=0
            fprintf('The maximum and minimum amplitude of your trajectory violate the %i
            fprintf('Please ensure your trajectory stays with these bounds:\n')
            fprintf('X->[%5.3f, %5.3f], Y->[%5.3f, %5.3f], and Z->[%5.3f, %5.3f]\n',...
                -x_max+esp_x,x_max-esp_x,-y_max+esp_y,y_max-esp_y,-z_max+esp_z,z_max-esp
            exit
        elseif del(1,m)>=0
            fprintf('The maximum apmplitude is violating the boundary in the %f directio
            fprintf('Attempting to fix the violation...\n')
            mta_xyz(:,m)=mta_xyz(:,m)-del(1,m);
        elseif del(2,m)>=0
            fprintf('The minimum apmplitude is violating the boundary in the %f directio
            fprintf('Attempting to fix the violation...\n')
            mta_xyz(:,m)=mta_xyz(:,m)+del(1,m);
        end
        %%%Rechecking that the max/min amplitude is not violated
        del_2(1,m)=max(mta_xyz(:,m))-Traj_Window(m,2);%del>=0 is a violation
        del_2(2,m)=Traj_Window(m,1)-min(mta_xyz(:,m));%del>=0 is a violation
        if del_2(1,m)>=0 %&& del(2,m)>=0
            fprintf('The program was unable to fix the amplitude violations\n')
            fprintf('The maximum and minimum amplitude of your trajectory violate the %i
            fprintf('Please ensure your trajectory stays with these bounds:\n')
            fprintf('X->[%5.3f, %5.3f], Y->[%5.3f, %5.3f], and Z->[%5.3f, %5.3f]',...
                Traj_Window(1,1),Traj_Window(1,2),Traj_Window(2,1),...
                Traj_Window(2,2),Traj_Window(3,1),Traj_Window(3,2))
            exit
        elseif del_2(2,m)>=0 %&& del(1,m)>=0
            fprintf('The program was unable to fix the amplitude violations\n')
            fprintf('The maximum and minimum amplitude of your trajectory violate the %i
            fprintf('Please ensure your trajectory stays with these bounds:\n')
            fprintf('X->[%5.3f, %5.3f], Y->[%5.3f, %5.3f], and Z->[%5.3f, %5.3f]',...
                -x_max+esp_x,x_max-esp_x,-y_max+esp_y,y_max-esp_y,-z_max+esp_z,z_max-esp
            exit
        end
end


%----Output to File----
%%Prints output to text file
```

153

```
OUTPUT=[Time mta_xyz mta_rqp];
% OUTPUT(1,:)
Out_fID=fopen([Dir,OutputFilename], 'w');
for cnt=1:length(Time)
    fprintf(Out_fID,'%f %f %f %f %f %f %f\n',OUTPUT(cnt,:));
end
fclose(Out_fID);
end
```

MTAtoModel.m

```
function MTAtoModel_Transform(File,Dir,OutputFilename,out_units,Cent,MxDist)
%----------WIND TUNNERL MODEL-ROBOT ARM COORDINATE TRANSFORMATION----------
%This file reads your output file and outputs a file with respect
%to the body-fixed Arm reference frame.
%-------------------------------------------------------------------------
%%This program assumes that the model offset is accounted for in
%%"MtaParameters.txt"
%*************************************************************************
%----Acronyms----
%MTA -> Motion Test Aparatus
%RPY -> Roll, Pitch Yaw
%mod_* -> Model (or Wind Tunnel) Reference Frame
%mta_* -> Robot Reference Frame


%----Wind Tunnel constants (written in wind tunnel reference frame)----
%%Wind Tunnel center point
x_c=Cent(1);
y_c=Cent(2);
z_c=Cent(3);
%%Wind Tunnel straight-and-level
roll_c=rad2deg(Cent(4));%the output of the MTA Computer is degrees
pitch_c=rad2deg(Cent(5));
yaw_c=rad2deg(Cent(6));
%%Wind Tunnel entrance tolerances; maximum distances off-center
x_max=MxDist(1);
y_max=MxDist(2);
z_max=MxDist(3);
%%Tolerance from wall
%%%This is how close you are willing to get to the max off-center distances
esp_x=0.05; %[m], x tolerance away from wall (or object)
esp_y=0.05; %[m], y tolerance away from wall (or object)
esp_z=0.05; %[m], z tolerance away from wall (or object)
%%This is the figurative window in which you can build a trajectory in
%%%Traj_Window=[Xmin,Xmax;Ymin,Ymax;Zmin,Zmax]
Traj_Window=[x_c-x_max+esp_x, x_c+x_max-esp_x;
    y_c-y_max+esp_y, y_c+y_max-esp_y;
    z_c-z_max+esp_z, z_c+z_max-esp_z];
```

154

```matlab
%----General Information----
%%The input file should be written as a trajectory file for the model with
%%respect to the wind tunnel reference frame. The columns of the input file
%%should be as follows:
%%Time [sec] | X [m] | Y [m] | Z [m] | Roll [rad] | Pitch [rad] | Yaw [rad]
%%***********************************************************************

%----Read Input file----

In_fID=fopen([Dir,File],'r');
FirstValue=fscanf(In_fID,'%f',1);
[~,~,ext]=fileparts([Dir,File]);

if strcmp(ext,'.csv')
    if isempty(FirstValue) %There is a header line
        mta_data=csvread([Dir,File],1,0);
    else %There is no Header line
        mta_data=csvread([Dir,File]);
    end
else %The file is *.txt
    if isempty(FirstValue) %There is a header line
        Headers=textscan(In_fID,'%s %s %s %s %s %s %s',1);
    else %There is no Header line
        fseek(In_fID,0,'bof');
    end
    mta_data=textscan(In_fID,'%f %f %f %f %f %f %f ');
    mta_data=cell2mat(mta_data);
end


Time=mta_data(:,1);
mta_xyz=mta_data(:,2:4);
mta_rqp=mta_data(:,5:end);
fclose(In_fID);

%----Bias Removal----
%%Centers the trajectory based on the Wind Tunnel Constraints
mta_xyz(:,1)=mta_xyz(:,1)-x_c;
mta_xyz(:,2)=mta_xyz(:,2)-y_c;
mta_xyz(:,3)=mta_xyz(:,3)-z_c;
%%Straight-and-levels the trajectory based on the Wind Tunnel Constraints
mta_rqp(:,1)=mta_rqp(:,1)-roll_c;
mta_rqp(:,2)=mta_rqp(:,2)-pitch_c;
mta_rqp(:,3)=mta_rqp(:,3)-yaw_c;

%----Coordinate Transformation----
%%Converts x-y-z translation
rot_xyz=[0 1 0; -1 0 0; 0 0 1]; %Rotation Matrix XYZ
rot_rpy=[0 1 0; -1 0 0; 0 0 1]; %Rotation Matrix RPY
mod_xyz=zeros(size(mta_xyz));
mod_rqp=zeros(size(mta_rqp));
```

```matlab
for cnt=1:length(Time)
    %%Transforms the position coordinate system
    mod_xyz(cnt,:)=rot_xyz\mta_xyz(cnt,:)';
    %%Transforms the anglular position coordinate system
    mod_rqp(cnt,:)=rot_rpy\mta_rqp(cnt,:)';

end

%----Unit Conversion---
%%Converts units of the input file to meters and radians
%**********For Debuging Purpose***************

%********************************************
if out_units(1)==1 && out_units(2)==2
else
    [mod_xyz,mod_rqp]=UnitsOut(out_units,mod_xyz,mod_rqp);
end

%----Output to File----
%%Prints output to text file
OUTPUT=[Time mod_xyz mod_rqp];
Out_fID=fopen([Dir,OutputFilename], 'w');
for cnt=1:length(Time)
    fprintf(Out_fID,'%f %f %f %f %f %f %f\n',OUTPUT(cnt,:));
end
fclose(Out_fID);
end
```

Bibliography

1. "MicroStrain - Inertial Sensors, 3DM-GX1". URL `http://www.microstrain.com/inertial/3DM-GX1`.

2. Albertani, Roberto, Parvez Khambatta, Adam Hart, Lawrence Ukeiley, Matias Oyarzun, Louis Cattafesta, Gregg Abate, et al. "Validation of a Low Reynolds Number Aerodynamic Characterization Facility". *47th AIAA aerospace sciences meeting*, volume 35, 455–506. AIAA 2003-1726, 2009.

3. Carr, Lawrence W, Kenneth W McAlister, and William J McCroskey. "Analysis of the development of dynamic stall based on oscillating airfoil experiments". 1977.

4. Cobb, Richard. "Conversation: Acquiring data from the Microstrain IMU", October 2014.

5. Dally, James W., William F. Riley, and Kenneth G. McConnell. *Instrumentation for Engineering Measurements*. John Wiley and Sons, 1984.

6. DeLuca, Anthony M. *Aerdyanmic Performance and Particle Image Velocimetery of Piezo Acuated Biometric Manduca Sexta Engineered Wings Towards Design and Application of a Flapping Wing Flight Vehicle*. Technical report, DTIC Document, AFIT-ENY-DS-13-D-01, 2013.

7. Dickinson, M. "The effects of wing rotation on unsteady aerodynamic performance at low Reynolds numbers". *Journal of experimental biology*, 192(1):179–206, 1994.

8. Dickinson, Michael H and Karl G Gotz. "Unsteady aerodynamic performance

of model wings at low Reynolds numbers". *Journal of Experimental Biology*, 174(1):45–64, 1993.

9. Dunn, William C. *Fundamentals of Industrial Instrumentation and Process Control*. McGraw-Hill Companies, 2005.

10. Eldredge, Jeff D, Chengjie Wang, and MV Ol. "A computational study of a canonical pitch-up, pitch-down wing maneuver". *AIAA paper*, 3687:2009, 2009.

11. Ellington, Charles P. "The novel aerodynamics of insect flight: applications to micro-air vehicles". *Journal of Experimental Biology*, 202(23):3439–3448, 1999.

12. Ellington, CP. "The aerodynamics of hovering insect flight. VI. Lift and power requirements". *Philosophical Transactions of the Royal Society of London. B, Biological Sciences*, 305(1122):145–181, 1984.

13. Gieles, ACM and GHJ Somers. "Miniature pressure transducers with a silicon diaphragm". *Philips technical review*, 33(1):14–20, 1973.

14. Gray, Lewis and Jaan Liiva. *Wind Tunnel Tests of Thin Airfoils Oscillating Near Stall. Volume Ii. Data Report*. Technical report, DTIC Document, 1969.

15. Hall, Christopher D. "Space Attitude Dynamics and Control". 2011.

16. Hart, Adam and Lawrence Ukeiley. "Low Reynolds Number Unsteady Aerodynamics over a Pitching-Plunging Flat Plate". *48th AIAA Aerospace Sciences Meeting Including the New Horizons Forum and Aerospace Exposition*. 2010.

17. Hart, Adam and Lawrence Ukeiley. "Leading Edge Vortex Development on a Pitching Flat Plate at Low Reynolds number". *42nd AIAA Fluid Dynamics Conference and Exhibit*. 2012.

18. Jenkins, Jerry E. "The Care, Feeding, and Measurement of Dynamic Stability Derivatives", 2007.

19. Jensen, Martin. "Biology and physics of locust flight. III. The aerodynamics of locust flight". *Philosophical Transactions of the Royal Society of London. Series B, Biological Sciences*, 239(667):511–552, 1956.

20. Liiva, Jaan, Franklyn J Davenport, Lewis Gray, and Ivor C Walton. *Two-dimensional Tests of Airfoils Oscillating Near Stall. Volume I. Sumary and Evaluation of Results.* Technical report, DTIC Document, 1968.

21. McCroskey, WJ. *The phenomenon of dynamic stall.* Technical report, NASA, USAAVRADCOM TR 81-A-6, 1981.

22. Mehta, Aaron. "USAF Eyes Flexible Weapons to Lower Costs, Increase Capability", 2013. URL `http://archive.defensenews.com/article/20130903/DEFREG02/309030016/USAF-Eyes-Flexible-Weapons-Lower-Costs-Increase-Capability`.

23. Newland, D. E. *A Introduction to Random Vibrations, Spectral and Wavelet Analysis.* Peason Education, 1993.

24. Ogata, Katsuhiko. *Mondern Control Engineering.* Prentice Hall, 5 edition, 2010.

25. Okamoto, Masato and Akira Azuma. "Experimental study on aerodynamic characteristics of unsteady wings at low Reynolds number". *AIAA journal*, 43(12):2526–2536, 2005.

26. Ol, Michael V., Haibo Dong, and Charles Webb. "Motion Kinematics vs. Angle of Attack Effects in High-Frequency Airfoil Pitch-Plunge". *38th Fluid Dynamics Conference and Exhibit.* 2008.

27. Pattinson, J, MH Lowenberg, and MG Goman. "Multi-Degree-of-Freedom Wind-Tunnel Maneuver Rig for Dynamic Simulation and Aerodynamic Model Identification". *Journal of Aircraft*, 50(2):551–566, 2012.

28. Poirel, D, Y Harris, and A Benaissa. "Self-sustained aeroelastic oscillations of a NACA0012 airfoil at low-to-moderate Reynolds numbers". *Journal of Fluids and Structures*, 24(5):700–719, 2008.

29. Poirel, D and F Mendes. "Experimental Small-Amplitude Self-Sustained Pitch–Heave Oscillations at Transitional Reynolds Numbers". *AIAA Journal*, 52(8):1581–1590, 2014.

30. Puri, N. N. *Fundamentals of Linear Systems for Physical Scientists and Engineers*. CRC Press, Taylor and Francis Group, 2010.

31. Rowe, Patrick. "Motion Test Apparatus (MTA) Manipulator User Manual", 2014.

32. Sane, Sanjay P and Michael H Dickinson. "The control of flight force by a flapping wing: lift and drag production". *Journal of experimental biology*, 204(15):2607–2626, 2001.

33. Sytsma, Michael. *6-DOF Motion Test Apparatus for Characterizing the Dynamic Properties of Micro Air Vehicles*. Sbir, DTIC Document, 2013.

34. Sytsma, Michael J. *Effects of turbulence on fixed wing small unmanned aerial systems*. Ph.D. thesis, University of Florida, 2013.

35. Titterton, David and John Weston. *Strapdown Inertial Navigation Technology*. Radar, Sonar, and Navigation Series 17. Institute of Electrical Engineers, 2 edition, 2004.

36. Von Ellenrieder, KD, Kamalluddien Parker, and Julio Soria. "Flow structures behind a heaving and pitching finite-span wing". *Journal of Fluid Mechanics*, 490:129–138, 2003.

37. Weis-Fogh, Torkel. "Quick estimates of flight fitness in hovering animals, including novel mechanisms for lift production". *Journal of Experimental Biology*, 59(1):169–230, 1973.

38. Williams, Robert L. II. "Robot Mechanics Notes", 2015.

39. Windsor, Richard I. *Measurement of Aerodynamic Forces on an Oscillating Airfoil.* Technical report, DTIC Document, 1970.

40. Wright, Jan R. and Jonathan E. Cooper. *Introduction to Aircraft Aeroelasticity and Loads.* AIAA Education Series. John Wiley and Sons, 1 edition, 2007.

41. Wright, Nick. "Taking Adaptive Measurements". *FFJournal*, 2014.

List of Acronyms

AFRL Air Force Research Laboratory

AFIT Air Force Institute of Technology

CAD Computer Aided Design

CAN Contoller Area Network

DAQ Data Acquisition

DOE Design of Experiments

DOF Degree-of-Freedom

IMU Inertial Measurement Unit

IUT Item Under Test

LEV leading edge vortex

MAV Micro Air Vehicle

MAVs Micro Air Vehicles

MTA Motion Test Apparatus

P2P Peak-to-Peak

PIV Particle Image Velocimetry

REEF Research and Engineering Education Faciility

ssh Secure Shell

VI Virtual Instrument

REPORT DOCUMENTATION PAGE

1. REPORT DATE (DD–MM–YYYY)	2. REPORT TYPE	3. DATES COVERED (From — To)
03–26–2015	Master's Thesis	Sept 2013 — Mar 2015

4. TITLE AND SUBTITLE

Characterization of a Robotic Manipulator for Dynamic Wind Tunnel Applications

5a. CONTRACT NUMBER

5b. GRANT NUMBER

5c. PROGRAM ELEMENT NUMBER

6. AUTHOR(S)

Lancaster, James C. Capt, USAF

5d. PROJECT NUMBER

5e. TASK NUMBER

5f. WORK UNIT NUMBER

7. PERFORMING ORGANIZATION NAME(S) AND ADDRESS(ES)

Air Force Institute of Technology
Graduate School of Engineering and Management (AFIT/EN)
2950 Hobson Way
WPAFB OH 45433-7765

8. PERFORMING ORGANIZATION REPORT NUMBER

AFIT-ENY-15-M-227

9. SPONSORING / MONITORING AGENCY NAME(S) AND ADDRESS(ES)

Air Force Institute of Technology
2950 Hobson Way
WPAFB OH 45433-7765
DSN 785-3636x4530, COMM 937-255-3636x4530
Email: mark.reeder@afit.edu

10. SPONSOR/MONITOR'S ACRONYM(S)

AFRL/RW

11. SPONSOR/MONITOR'S REPORT NUMBER(S)

12. DISTRIBUTION / AVAILABILITY STATEMENT

DISTRIBUTION STATEMENT A:
APPROVED FOR PUBLIC RELEASE; DISTRIBUTION UNLIMITED.

13. SUPPLEMENTARY NOTES

This material is declared a work of the U.S. Government and is not subject to copyright protection in the United States.

14. ABSTRACT

The newly acquired 6-DOF Motion Test Apparatus (MTA) was installed to perform dynamic wind tunnel testing in the AFIT Low Speed Wind Tunnel. Several complex motions revealed that the overall performance of the test rig needed improvement especially during small motions. The motions exposed that further enhancements would need to be performed individually for each joint. This research effort focused on the improvement of the MTA wrist roll motor and controller using a pitch oscillation. The controller software was improved using position feedback because the MTA wrist roll motor and controller exhibited reduced signal bias and amplitude attenuation. The enhanced system was then utilized for wind tunnel experiments along with supporting systems. A secondary position and orientation sensor, an Inertial Measurement Unit (IMU), was used to validate the Euler angle output calculated by the MTA Computer using forward kinematics. Four, fast-response pressure transducers were flush-mounted to the wing of the model in order to record aerodynamic data during pitch oscillations. The acquired pressure signals demonstrated signs of unsteady aerodynamic effects such as dynamic stall. The MTA performed equally well under aerodynamic loads at tunnel speeds of 60 mph, when compared to tests performed with no freestream velocity.

15. SUBJECT TERMS

Robotic Manipulator, Dynamic Wind Tunnel, Pitch Oscillation, Statistical Control

16. SECURITY CLASSIFICATION OF:			17. LIMITATION OF ABSTRACT	18. NUMBER OF PAGES	19a. NAME OF RESPONSIBLE PERSON
a. REPORT	b. ABSTRACT	c. THIS PAGE			Dr. Mark Reeder, AFIT/ENY
U	U	U	U	181	19b. TELEPHONE NUMBER (include area code) (937) 255-3636, x4530; mark.reeder@afit.edu